VARIABLE X-RAY FLUXES FROM CELESTIAL OBJECTS

by

John Robathan Harries, B. Sc., (Adel.) M. Sc., (Minn.)

Department of Physics

A thesis

presented for the degree of

Doctor of Philosophy

in the

University of Adelaide

October 1968

TABLE OF CONTENTS

SUMMARY

This thesis discusses two independent experiments, a celestial
X-ray experiment that was flown on two Skylark rockets from Woomera,
South Australia, and a proportional counter flown on the United States
IMP-F satellite.

Two identical X-ray experiments were flown on Skylark rockets
from Woomera, South Australia, at 00h 32m, 4 April 1967 and 22h 36m,
20 April 1967. The X-rays were detected by proportional counters
which were caused to scan the sky by the motion of the rocket.
Sco XR-1 was observed on both flights and served as a reference to
compare the flux from a new source Cen XR-2. This source was found
to have a softer spectrum on the second flight and its intensity
(2 to 8 keV) had decreased by 33%. Several possible models of
sources that could show this variability are presented.

An X-ray albedo from the earth was observed on both flights.
This flux peaked at the horizon closest to the sun and was due to the
scattering of the incident solar X-rays by the electrons in the
atmospheric gas molecules. Fluorescent K X-rays from Argon, were
excited by solar X-rays greater than 3.2 keV and also contributed to

the albedo flux. The change in the countrate as the rocket passed through the X-ray absorption layer of the atmosphere was used to determine the diffuse celestial X-ray flux.

A small proportional counter was carried on the IMP-F satellite and provided continuous temporal data on galactic and solar X-rays. Data on the possible variability in the intensity of Sco XR-1 are presented. The solar X-ray flux was composed of bursts with durations between ten minutes and several hours that were superimposed on a slowly varying flux with a time scale of many days. The intensity of the X-ray bursts was found to have a maximum correlation with the intensity of 4000 MHz radio bursts and to decrease away from this frequency. Eighteen percent of the X-ray bursts occurred without associated Hα flares, and these occurred at times of maximum Hα limb activity. The results can be understood if the mean height of the X-ray burst emission region was $(4 \pm 2) \times 10^4$ km above the photosphere.

PREFACE

This thesis contains no material that has been accepted for the award of any other degree or diploma in any University, and to the best of the candidate's knowledge and belief contains no material previously published or written by another person, except when due reference is made in the text of the thesis.

John R. Harries

ACKNOWLEDGEMENTS

Finally, the author thanks his wife for her constant moral support and for typing this thesis.

CHAPTER 1

INTRODUCTION TO X-RAY ASTRONOMY

Solar X-rays were first observed in 1948 when rockets began to carry experiments above the atmosphere. Even before this, it was suspected that solar X-ray emission played an important part in the formation of the ionosphere. The solar X-ray flux is very variable, changing over the sunspot cycle and showing short time scale bursts associated with flares and will be discussed in detail in Section 1.2.

1.1 Galactic X-rays

Although the solar X-ray flux can be very large during a flare, it would be unobservable if the sun was at the distance of the nearest star. Consequently no experiments were carried out to look for X-ray stars until Giacconi et al. (1962) observed galactic X-rays during an experiment to measure albedo X-rays from the moon. Since then the development of X-ray astronomy has been very rapid. Numerous reviews of the field have been written, the most important being those of Giacconi and Gursky (1965), Hayakawa et al. (1966), Friedman (1967), Giacconi (1967), Gould (1967), and Morrison (1967); theoretical reviews by Hayakawa and Matsuoka (1964),

Ginzburg and Syrovatsky (1965), and Burbidge (1966) and reviews by
Boyd (1965) and Giacconi et al. (1966) covering the experimental
techniques. In view of the number and quality of the review papers in
the literature, only the principle developments in the field will be
discussed here.

In order to observe celestial X-rays it is necessary to carry the
experiments above the bulk of the earth's atmosphere which is an efficient
absorber of X-rays. Most of the results to date have been obtained by
rocket-borne proportional or geiger counters sensitive in the energy
range 2 to 8 keV. Balloon-borne experiments have made an important
contribution to the field; they can only observe X-rays greater than
20 keV due to atmospheric attenuation, but compensate for this by their
very much longer observing times.

The celestial X-ray flux consists of discrete sources superimposed
on a diffuse background flux. At the present time almost 40 sources have
been named, but only about 20 can be considered to have been reliably
observed. Unfortunately different groups have tended to use a different
nomenclature for the sources. There are two main systems, the first
uses the form Sco XR-1 or Sco X-1 to denote the first X-ray source in
the constellation Scorpius and subsequently discovered sources are
denoted Sco XR-2, Sco XR-3 etc. Usually the position of X-ray sources
is not known very accurately and the error circle can include more than

one constellation. The second system avoids this problem and uses the
form GX9+1 where 9° is the galactic longitude and +1.0° is the galactic
latitude.

Most of the known sources are located close to the galactic plane
in two groups, one close to the galactic centre and the other in the
direction of Cygnus (Friedman et al. 1967a; Gursky et al. 1967; Bradt
et al. 1968; Fisher et al. 1968). The latter grouping is probably
associated with the Cygnus-Orion spiral arm of the galaxy.

The strongest source is Sco XR-1 and this lies well off the galactic
plane which is indicative of its relative proximity to the solar system.
Apart from the variable source Cen XR-2 which is the subject of part
of this thesis, all of the other sources are at least an order of
magnitude weaker than Sco XR-1. The location of Sco XR-1 has been
measured with a precision of about 1 arc min by Gursky et al. (1966)
and has been identified with a variable blue nova by Sandage et al.
(1966) and radio emission detected (Andrews and Purton 1968). Tau XR-1
has been identified with the Crab nebula by lunar occultation (Bowyer
et al. 1964) and by using slit collimators (Oda et al. 1967). Tentative
optical identifications have been made for Cyg XR-1 (Giacconi et al. 1967b),
GX3+1 (Blanco et al. 1968a), and two different identifications for
Cen XR-2 by Blanco et al. (1968b) and Eggen et al. (1968). In all cases
there were many objects in the error circles and one was picked out as

being the most likely candidate. It must be emphasised that these
identifications are tentative, and have been made on the basis of
extrapolation of the X-ray spectrum to optical wavelengths or by
similarity to the Sco XR-1 object. The only extragalactic object that
appears to have been observed in X-rays is M87 (Bradt et al. 1967;
Friedman et al. 1967b). Observations of X-rays from other unusual
astronomical objects have been claimed but they are not conclusive when
the quality of the attitude solution or pointing control of the rocket
is considered together with the statistical accuracy of the data.

Besides the discrete sources there is a large diffuse celestial
X-ray flux. It has been shown to be isotropic at 2 to 8 keV but becomes
anisotropic at lower energies (Seward et al. 1967; Bowyer et al. 1968;
Henry et al. 1968). It is not known at present if the flux is due to
unresolved extragalactic point sources or if it is produced in the
interstellar and intergalactic medium by the inverse compton effect
between energetic electrons and the universal blackbody radiation
photons (Bergamini et al. 1967; Brecher and Morrison 1967; Gould 1967;
Maraschi et al. 1968; Silk 1968; Verma 1968).

The possible variability of galactic X-ray sources has been postulated
by many of the theoretical models which associate the celestial X-ray
emission with novae, supernovae, and the accretion of matter between
the components of a binary system. As might be expected for such a

young science different experiments have observed different fluxes from
the same source, however this might not necessarily imply a variable
source, it could be indicative of the errors inherent in the experimental
method.

The first source that was claimed to be variable was Cyg XR-1
(Byram et al. 1966). The geiger counter countrate from this source was
observed to have decreased by a factor of 4 between June 1964, and April
1965 while that due to Cyg XR-2 was constant. However, the counters
used on the two flights had very different characteristics, those on
the latter flight being more sensitive at higher energies. In addition
the sources were observed on very few scans, leading to difficulties in
correcting for the collimator response. A subsequent rocket experiment
in October 1966 showed that the sources had not changed significantly
in the 18 months since April 1965 (Gorenstein et al. 1967).

The possible variability of Cyg XR-1 has been pursued at balloon
energies by Overbeck and Tananbaum (1968a, b) who claim a significant
variation using the same instruments on different flights. However
their equipment was subject to some coronal discharges on the flight in
which they observed the biggest variation. Chodil et al. (1968a) take
the opposite view, that the differences between the various experiments
and experimenters was an indication of the experimental accuracy and did
not represent a real variation.

Friedman et al. (1967a) attempted to show variability of the sources near the galactic centre using data from the flights in June 1964 and April 1965 as mentioned in the Cyg XR-1 discussion. In this case, as well as the different detector responses on the two flights some of the sources were only observed on one scan and the very complexity of the region meant that 'subjective judgements' were necessary in order to separate the responses due to the various sources and to interpolate between scans. A more accurate survey of the galactic centre region by Bradt et al. (1968) on July 7, 1967 with much narrower, crossed collimators and using proportional counters, yielded 'no clear evidence for time variations' when the results were compared with earlier experiments. It is worth noting the excellent agreement between their source positions and those of Fisher et al. (1966) obtained in September 1965. Such positional agreement allows for the valid comparison of source strengths.

The Sco XR-1 spectrum has been measured many times by proportional counters. Experiments in June 1965 (Chodil et al. 1965), July 1965 (Hayakawa et al. 1966b) and October 1965 (Grader et al. 1966) were remarkably consistent; however results from later experiments in July 1966 and May 1967 indicated a decrease in flux by about 50% (Chodil et al. 1967ab). Even though most of these experiments were performed by the group at Lawrence Radiation Laboratory, the experimenters did not claim variability, which suggests that this change was perhaps instrumental.

The results presented in this thesis and those of Cooke et al (1967) agreed with the later Chodil spectrum. Chodil et al. (1968) have attempted to relate a change in spectral shape observed on two flights in 1967 with the optical variations of the source. The observed change was not large and although the IMP results discussed in Chapter 10 tend to support the variation in the spectrum between their two flights the result is not conclusive. Lewin et al. (1968b) claim to have seen an X-ray flare from Sco XR-1 with a balloon experiment. Also in the balloon region Overbeck and Tananbaum (1968b) have plotted the long term variations in the balloon flux from Sco XR-1, but a constant strength source is only just outside their error bars.

Finally, there is one source for which variability has been proved, and this is Cen XR-2. This source was observed on the Skylark experiments and will be discussed in detail in the first part of this thesis. It was observed by three different experimental groups, each experiment also observed Sco XR-1 which could be used as a reference. The flux was observed to change by more than an order of magnitude, and the source was observed on many scans in each experiment.

Admittedly, this discussion has been written from a skeptical point of view. Nevertheless, it is unfortunate that variability of X-ray sources is fashionable and so discrepancies between experiments tend to be explained in terms of variability rather than limitations in

experimental method. This is not to say that variations in X-ray emission have not occurred, but if so, they have only been of the order of, or smaller than, the inherent accuracy of the experiments. The conclusions the author would derive from this study of the literature are that most sources have varied by less than 30% in two years; one source, Sco XR-1, has shown a possible high energy flare, and one source, Cen XR-2, has shown large variations over a time scale of about a month.

1.2 Solar X-rays

The solar X-ray emission can be divided into three components; (1) X-rays from the quiet corona which are always present, (2) a slowly varying component emitted from coronal condensations above long lived active regions and (3) impulsive emission associated with solar flares. One of the main characteristics of the solar X-ray emission is its variability which becomes greater at higher photon energies and provides a very sensitive measure of the solar activity. The X-ray flux above 1.5 keV (0 - 8 A) in the absence of flares decreased from about 10^{-3} erg cm^{-2} sec^{-1} at solar maximum to 5×10^{-6} erg cm^{-2} sec^{-1} at solar minimum whereas the flux at 0.25 keV (44 - 60 A) only decreased from 5×10^{-2} to 10^{-2} erg cm^{-2} sec^{-1} (Mandelstam 1965). In addition, flares can cause the 0 - 8 A flux to increase by more than an order of magnitude within ten minutes.

An excellent review of solar X-ray emission has been given by Mandelstam (1965b); other good reviews of the subject are those by Friedman (1963), de Jager (1964), Kundu (1965), Goldberg (1967), and Underwood (1968). In view of these numerous reviews the present discussion will be limited to a brief description of the types of experiments performed, followed by a summary of the present knowledge of solar X-rays.

1.2.1 Solar X-Ray Experiments

The solar X-ray flux up to 4 keV and its variation with time have been measured by ionisation chambers and geiger counters on the NRL SOLRAD satellites which have provided continuous data observations since 1960 (Kreplin et al. 1962; Acton et al. 1963; Thomas et al. 1965; Kreplin and Gregory 1966; Gregory and Kreplin 1967; Landini et al. 1967ab; Acton 1968). Similar experiments have been flown on OSO-1 (White 1964), the Vela satellite (Conner et al. 1965), Injun-1 (Van Allen et al. 1965), and the Electron-II station (Mandelstam 1965b). These experiments have enabled the variation of the slowly varying component of the solar X-rays to be investigated, and correlated with other measures of solar activity. Although they observed many X-ray bursts these experiments suffered from very wide spectral channels leading to uncertainties in the spectral shape. In addition, the short periods of data reception prevented the observation of the complete time development of the bursts. Better

spectral resolution was obtained by the proportional counters on Ariel 1
(Bowen et al. 1964; Culhane et al. 1964; Pound 1965) and on sounding
rockets (Chubb et al. 1966). They showed a hardening of the X-ray
spectrum during the bursts.

Several experimenters have looked at the X-ray flux at higher photon
energies. A scintillator on OSO-1 (Frost 1965) monitored the solar
X-rays in the energy interval 20 to 100 keV and although the quiet sun
flux was below the threshold of the instrument, eight energetic X-ray
flares were observed. Arnoldy et al. (1968) measured the 10 to 50 keV
X-ray flux using an ionisation chamber on OGO-1 and OGO-3, and observed
many flares. Cline et al. (1968) observed X-rays up to 500 keV from one
flare, and suggested a nonthermal bremsstrahlung origin. Hudson et al.
(1968) measured the spectra from 8 keV to 210 keV and showed the
softening of the spectrum as the burst decayed.

The best spectral data have been obtained by making use of the
wave like character of X-rays as opposed to the photon detectors already
discussed. Blake et al. (1965) used a Bragg crystal spectrometer over
the wavelength interval 25 to 13 A (0.5 to 1.0 keV) and showed that most
of the X-ray flux was concentrated in emission lines. This method has
been developed by Rugge and Walker (1968) and Evans and Pounds (1968),
and extended to 1.9 A (6.5 keV) by Fritz et al. (1967) and to 1.3 A
(9.5 keV) by a spectrometer on OSO-3 (Neupert et al. 1967, 1968). The

latter instrument took a spectrum every 5 minutes with a resolution of

0.01 A and showed that most of the burst X-rays less than 6 keV were

emitted in line spectra. A grazing incidence spectrometer using a

diffraction grating has also been used to measure the spectrum down to

9.5 A by Zhitnik et al. (1967).

Most of the experiments discussed so far, observed the X-rays

from the whole disc. The spatial distribution of the X-ray emitting

regions was first determined by pinhole cameras flown on stabilised

rockets by a number of experimenters (Blake et al. 1963; Blake et al.

1965; Russell 1965; Pounds and Russell 1966; Russell and Pounds 1966;

Broadfoot 1967; Fritz et al. 1967; and Zhitnik et al. 1967). Various

thin filters over the pinhole enabled the camera sensitivity to be

adjusted to different energy intervals. Although this technique has

given valuable results, grazing incidence telescopes have a higher

sensitivity than the pinhole cameras and resolutions of 20 arc seconds

have been achieved (Giacconi et al. 1965; Underwood and Muney 1967;

and Reidy et al. 1968).

The spatial distribution of X-ray emitting areas has also been

obtained, although less accurately, from the width and position of the

emission lines in the Bragg spectrometers (Blake et al. 1965; Broadfoot

1967; and Fritz et al. 1967) and by slit collimator scans across the

solar disc (Blake et al. 1965). The size of the emitting regions has

been determined by measuring the change in flux as the regions were
obscured by the moon during solar eclipses (Friedman 1963; Mandelstam
1965; and Landini et al. 1966).

1.2.2 X-rays from the Quiet Corona

The solar corona is a hot thin plasma above the chromosphere with
a temperature of about 10^6 °K. The electron density is about 10^9 cm^{-3}
at 2×10^4 km above the solar limb and has decreased to 1.6×10^8 cm^{-3}
by 5×10^4 km. The corona is optically thin to X-rays and the total
flux is proportional to the integral of the square of the electron
          line of sight. This results in a limb brightening
with a latitude dependence that has been observed by Underwood and
Muney (1967) and Reidy et al. (1968). The theoretical thermal emission
of X-rays by the corona has been calculated by Elwert (1961) and his
results agree with the observed spectrum and limb brightening at solar
minimum. The emission processes that occur in a hot plasma are
discussed in Section 1.3.

In order to measure the spectrum of X-rays from the quiet corona
it is essential to be sure that there are no active regions contributing
as these produce a greatly enhanced X-ray emission. This is difficult
to achieve with whole sun instruments because it is extremely rare that
the sun is completely quiet.

1.2.3 Emission from Active Regions

Most of the solar X-ray emission occurs from areas in the corona overlying active regions on the photosphere. The magnetic fields associated with the active regions result in an increased electron density and temperature in the corona producing an enhancement of the coronal X-ray emission. The thermal emission from such a hot, thin plasma is discussed in more detail in Section 1.3. The early calculations for the solar corona and the coronal condensations were performed by Kawabata (1960) and Elwert (1961), however they omitted the effects of dielectronic recombination which can be important. This has been rectified and the calculations extended to higher energies by Mandelstam (1965a), Tucker and Gould (1966) and Tucker (1967a). These calculations have shown that the importance of the different emission processes is very dependent on the relative abundances of the elements and the electron temperature. They show for example that for the interval 2 to 8 A, at 5×10^6 °K, and for the abundance of elements observed in the photosphere emission occurs equally by radiative recombination and by line emission.

The Bragg spectrometer results have shown that most of the emission less than 4 keV consists of line spectra. Lines have been observed from Si XIII indicating a temperature greater than 7×10^6 °K (Fritz et al. 1967), however it would not be the same for all

condensations but would depend on the activity of the underlying photospheric region. The intensity of the lines provided information on the abundances of the elements in the X-ray emitting region and showed that iron is much more common than in the photosphere (Evans and Pounds 1968).

X-ray photographs of the sun have shown that at 0.2 keV X-ray energies every active centre on the disk has an associated enhancement in the X-ray emission of the overlying corona (Underwood and Muney 1967). At 1 keV the emission regions are small and located directly above the most active plage regions. That is, all active regions cause an enhancement of the coronal X-ray emission, but the highest temperature and density occur immediately above the most active regions to produce the highest intensity and hardest X-ray spectra. Emission has been observed associated with a plage region around the limb, enabling the height of emission to be estimated as $(2.2 \pm 0.3) \times 10^4$ km (Broadfoot 1967).

Fritz et al. (1967) favoured a nonthermal source mechanism because of variations that they observed in the line intensities during their rocket flight. If this was a real variation, it would be hard to explain by thermal emission from long lived coronal condensations.

The total emission from all the active regions changes slowly as

active regions develop and die away, and as they move across the visible
face of the sun. The slow variation of the X-ray flux greater than
1.5 keV shows a good correlation with the slowly varying component of
the 2800 MHz flux (White 1964; Mandelstam 1965b; Landini et al. 1967b).
The spatial distribution of the X-ray emitting regions agrees with the
map of the 9.1 centimeter emitting regions of the sun (Blake et al.
1963; Pounds and Russell 1966; and Underwood and Muney 1967). However
the difference in radio emission between active regions and the quiet
corona are not as marked as for X-rays.

1.2.4 Solar X-ray Bursts

Many X-ray bursts have been observed but the precise mechanism by
which emission occurs is still not properly understood. The rise time,
decay time and duration of the bursts is variable, but on the average
at 2 keV the duration is about 10 minutes. The time scales can, however,
be much longer for a large flare while at higher photon energies the
bursts have shorter durations.

Proportional counter experiments have measured an increased
X-ray intensity and a hardening of the spectrum during flares (Pounds
1965; and Chubb et al. 1966). Neupert et al. (1967, 1968) have
measured the line spectra during a flare, and observed a strong line
at 6.5 keV corresponding to the $1s^2 - 1s2p$ transition in Fe XXV, i.e.

an iron nucleus with only two electrons and weaker lines corresponding to other heavy elements, nickel, calcium and chromium. Their data was consistent with the hypothesis that the initial ionisation was predominantly Fe XXV and that subsequent recombination produced successively lower stages of ionisation whose spectra could be excited by electron collision, or alternatively, recombination into the excited states was followed by a cascade into the ground state. The presence of Fe XXV indicated very high energy electrons; in the laboratory a 19 kV arc was necessary to excite its spectrum (Feldman and Cohen 1968).

High energy X-rays have been observed up to 500 keV during an importance 3 Hα flare (Cline et al. 1968). The duration of the burst for energies greater than 80 keV was less than five minutes, whereas the duration for X-rays greater than 1.5 keV from the same flare was at least 90 minutes (Van Allen 1967). Hudson et al. (1968) have also observed this effect, where the duration of the flare is much longer at lower energies ($<$ 10 keV) than at high photon energies.

The intensity of the X-ray bursts is not directly related to the importance of an accompanying Hα flare, and in fact some X-ray bursts occur without an observed Hα flare (Culhane et al. 1964; White 1964; Connor et al. 1965). The results of Chapter 9 show that this is probably due to flares occurring around the limb obscuring the Hα emission. Hence it is likely that all X-ray bursts are in fact

accompanied by some Hα activity. A good correlation exists between
the X-ray and the centimeter radio bursts, often even the subsidiary
peaks in the radio burst are related to peaks in the X-ray data
(Frost 1965; Kundu 1965; Pounds 1965; Kawabata 1966; Acton 1968;
Arnoldy et al. 1968; Cline et al. 1968; and Neupert 1968).

There are several theories for the emission of X-ray bursts
(Kundu 1965). In the first, high energy nonthermal electrons are
produced in the flare probably by a Fermi-type acceleration. The
electrons emit centimeter radiation by synchrotron emission and X-rays
by bremsstrahlung either in the corona or when they penetrate into the
chromosphere. Some X-rays would also be emitted by the synchrotron
and the inverse compton processes. In the second theory, (Chubb et al.
1966) the flare causes local heating of the corona to produce a small
volume high density, high temperature plasma which emits both X-ray
and centimeter radiation by thermal processes. In fact both processes
are likely to occur although the relative importance could vary from
flare to flare. Most of the high energy X-rays are emitted promptly
and are produced by nonthermal bremsstrahlung. On the other hand,
the low energy photons are predominantly produced by thermal processes
in a region of the corona and the change in intensity results from the
cooling of the plasma. The two processes would probably become
equally important in the range 2 to 8 keV. Acton (1968) has pointed

out that even the variation in the low energy photon intensity might be due to the variation in the energetic electron source. A real understanding of the processes involved is likely to come from a detailed study of the variation in the high resolution spectra from many bursts.

1.3 Emission Mechanisms for X-Rays

Apart from the sun, the mechanisms of X-ray emission that occur in celestial X-ray sources are not known. This section will briefly review the processes which could produce X-rays in the celestial environment, and the results of investigations to apply these processes to the known X-ray sources.

1.3.1 Thermal Radiation from a Hot Thin Plasma

The most complete treatment of low density plasmas has been given by Tucker and Gould (1966) and Tucker (1967a). A plasma is considered in which the ionising radiation field is weak, so that ionisation is only by electron collision and, in the equilibrium condition, is balanced by radiative and dielectronic recombination. Since both the ionisation and recombination are proportional to the electron density, the ionisation equilibrium is then independent of density and only depends on the temperature.

Earlier calculations by Kawabata (1960), Elwert (1961), and Mandelstam (1965) omitted the effects of dielectronic recombination which can be important (Burgess 1964). In dielectronic recombination an electron recombines with an ion, but instead of emitting a photon which carries away the excess energy as in radiative recombination, the energy is used to raise one of the already bound electrons to a higher energy level. The resulting ion is hence doubly excited and can either emit an Auger electron or one of the excited electrons can undergo a radiative transition to a lower level. Since the incident electron has to supply energy to the ion, the process is very energy dependent, and is most important at about 10^6 or 10^7 $^\circ$K. Such temperatures are conceivable in a celestial X-ray source.

A hot plasma emits photons by three distinct processes, (1) bremsstrahlung, (2) radiative recombination and (3) line emission. Bremsstrahlung or free-free radiation, occurs during the coulomb scattering of the electrons by the ions in the plasma. For a Maxwellian distribution of electrons at temperature T encountering ions of charge Z the emission spectrum is given by

$$\frac{dN}{dtdVdE} = 1.033 \times 10^{-11} \, n_e T^{-\frac{1}{2}} \left[\sum_z Z^2 n_z g(Z,T,E) \right] \exp(-E/kT)/E$$

$$\text{photons cm}^{-3} \text{ sec}^{-1} \text{ keV}^{-1} \quad (1.1)$$

where g is the average Gaunt factor, E is in keV and T is in degrees Kelvin.

In radiative recombination an electron of energy E_e recombines with an ion of atomic number Z in the state n and emits a photon of energy

$$\hbar\omega = E_e + I_{z,n} \qquad\qquad (1.2)$$

where $I_{z,n}$ is the ionisation potential of state n. The resulting spectrum is a continuum but as photons with energies less than $I_{z,n}$ cannot be produced by recombination to the state n, there is an edge in the emission spectrum whenever the energy is equal to the ionisation potential of an atomic state. The resulting singly excited ion decays by radiative transitions to the ground state, as does the doubly excited ion produced by dielectronic recombination.

Line emissions are excited by inelastic electron collisions. One electron is raised to a higher level by the collision and then emits a photon during the transitions to lower levels.

For a hot gas exhibiting the cosmic abundances of the elements, line emission dominates the cooling at temperatures of less than 5×10^6 $^\circ$K, but above this temperature bremsstrahlung is the most important process. The total X-ray production in the interval 2 to 8 A (1.5 to 6 keV) has been calculated by Tucker (1967a) and is mainly radiative recombination below 8×10^6 $^\circ$K, and then bremsstrahlung above this temperature. However the relative proportions were

extremely dependent on the abundances, and he showed that line emission
caused the greatest emission in the 2 to 8 A range at 10^7 ^{o}K for the
abundances found in the outer shells of supernovae.

The corona of the sun is the best example of a thin hot plasma
that emits X-rays and is discussed in detail in Section 1.2. Tucker
(1967a) considered the possibility of observing the X-rays from the
coronas of other stars and concluded that the emission from some of
the bright, nearby stars could be within the present limit of detectability
during large flares. Bless et al. (1968) and Wallerstein (1968) have
suggested that as Wolf-Rayet stars are thought to have extensive hot
coronas they are very likely to be strong X-ray emitters. Their
distribution in the galaxy matches that of the observed X-ray sources.

Hot plasmas could also be produced by the shock heating of the
envelope around novae or supernovae or might occur in the ejecta from
supernova (Tucker 1967a). Sartori and Morrison (1967) investigated
the possibility that the X-rays from the Crab nebula are produced by
thermal bremsstrahlung instead of the synchrotron emission that occurs
at radio and optical wavelengths.

Thermal bremsstrahlung from a thin hot plasma is consistent with
the observed X-ray spectrum from Sco XR-1 over the range 2 to 8 keV.
Johnson (1966, 1967) and Tucker (1967b) have proposed models for the
optical and X-ray observations that require the coexistence of a 10^5 ^{o}K

plasma with a much larger amount of 10^7 °K plasma. Shklovsky (1967) suggested, alternatively, that Sco XR-1 might be a member of a close binary which was rapidly accreting plasma from its companion. The gravitational potential energy released would heat the plasma which would then emit thermal X-rays. This accretion theory has been investigated further by Cameron and Mock (1967), Sofia (1967), and Prendergast and Burbidge (1968).

1.3.2 Neutron Stars

Significant X-rays can be produced by blackbody radiation if the temperature is high enough. The flux emitted by blackbody at temperature T is given by

$$\frac{dN}{dtdSdE} = 9.88 \times 10^{31} E^2 \left[\exp(E/kT) - 1 \right]^{-1}$$

$$\text{photons cm}^{-2} \text{ sec}^{-1} \text{ keV}^{-1} \qquad (1.3)$$

where E is in keV.

To explain the galactic X-ray sources it is necessary to postulate an object which is a strong emitter of X-rays, but with negligible emission at optical and radio wavelengths. Chiu and Salpeter (1964) suggested that a neutron star with a radius of about 10 km and a surface temperature about 10^7 °K would satisfy these requirements. A neutron star is an end product of stellar evolution, and is proposed to be

formed from the collapsing stellar core that triggers a supernova
(Colgate and White 1966). The density of a neutron star would be
approximately nuclear density; the protons and electrons having
combined to form neutrons which exist in a degenerate state. A neutron
star has a mass limit of about two solar masses (Tsuruta and Cameron
1966b, Cazzola et al. 1967); above this mass the close range repulsive
nuclear forces cannot support the gravitational attraction of the star.
It should be noted that these stars have been theoretically proposed
but have not been actually observed.

The average properties of a neutron star are expected to be

radius $\sim$ 10 km

mass $\sim$ 1 $M_\odot$ = 2 x 10^{33} gms

density $\sim$ 4 x 10^{14} gm cm^{-3} (1.4)

If the neutron star is formed in a catastrophic process, it will
initially have a high temperature. Bahcall and Wolf (1965), Finzi
(1965), Tsuruta and Cameron (1966a), and Wolf (1966), have calculated
the cooling rate due to neutrino emission and have shown that the
neutron star would cool very rapidly by the reaction

$$n + n \longrightarrow n + p + e^- + \overline{\nu}_e \qquad (1.5)$$

and its related muon producing and inverse reactions. The opacity of
the neutron star to the neutrinos is negligible, and so they very

efficiently carry off energy. It must be assumed that there are no quasifree pions present otherwise the star would cool within a few days to a temperature too low for X-ray emission (Bahcall and Wolf 1965). The rate of cooling by neutrino emission is

$$T = (6.7 \times 10^{-12}) \, 1/18 \, t^{1/6} \; {}^{o}K \qquad (1.6)$$

where t seconds is the time for cooling from a very high temperature ($> 10^{10} \; {}^{o}K$) to T ${}^{o}K$, (Wolf 1966).

Photon emission occurs from the surface of the star which is considerably cooler than the interior. Morton (1964) and Tsuruta and Cameron (1966a) have investigated the properties of the neutron star atmosphere to obtain the surface temperature as a function of the core temperature. The ratio of the core temperature T to the effective surface temperature T_e was

$$T/T_e \sim 165 \qquad (1.7)$$

at $T_e = 10^7 \; {}^{o}K$ and it was a slowly increasing function of temperature. Table 1 shows the rate of cooling of the neutron star due to (1) neutrino emission and (2) photon emission.

Neutrino cooling is very efficient at high temperatures and no matter how hot the neutron star was when it was formed, it would cool down to $T_e \doteq 2 \times 10^7 \; {}^{o}K$ in less than a day. However, it takes 10^4 years for the star to cool down to $T_e = 2 \times 10^6 \; {}^{o}K$ and then photon emission from the surface becomes the dominant means of cooling.

TABLE 1

AGE OF NEUTRON STAR

T_e surface $10^6 \, ^\circ K$	peak emission (keV)	2 - 8 keV flux ergs cm^{-2} sec^{-1}	T core $10^6 \, ^\circ K$	Age (seconds)	
				neutrino emission	photon emission
20.0	8.6	5.9×10^{24}	3800	4.3×10^4	5.2×10^{10}
10.0	4.3	4.2×10^{23}	1600	5.4×10^6	1.5×10^{11}
8.0	3.4	1.4×10^{23}	1300	3.0×10^7	2.2×10^{11}
6.0	2.6	3.1×10^{22}	950	1.8×10^8	3.9×10^{11}
4.0	1.7	2.3×10^{21}	610	2.7×10^9	8.1×10^{11}
3.0	1.3	2.2×10^{20}	440	1.8×10^{10}	1.4×10^{12}
2.0	0.86	3.0×10^{18}	280	2.5×10^{11}	2.7×10^{12}
1.0	0.43	9.1×10^{12}	110	8.0×10^{13}	6.7×10^{12}

1 year = 3.15×10^7 seconds

1 day = 8.46×10^4 seconds

1 keV = 1.602×10^{-9} ergs

It must be emphasised that the cooling rate due to neutrino
emission is difficult to calculate since we have no experience of such
processes. Meltzer and Thorne (1966) and Chiu (1966) have pointed out

uncertainties in the calculations, nevertheless, the ages calculated above should be accurate to at least an order of magnitude (see also Hansen and Tsuruta 1967).

The majority of galactic X-ray sources appear to be relatively time invariant (age greater than two years) and hence are not neutron stars because their X-ray spectrum cannot be fitted by a blackbody spectrum for a surface temperature of less than 8×10^6 °K, (i.e. age > 1 year). Clearly, however, the fact that none of the known sources are neutron stars does not imply that neutron stars cannot be X-ray sources. Thus, a neutron star model for Cen XR-2 will be discussed in Chapter 7.

1.3.3 Synchrotron Radiation

When relativistic electrons spiral in a magnetic field they emit synchrotron radiation (magnetic bremsstrahlung). Two difficulties associated with this mechanism are (1) the extremely high energy electrons required to produce X-rays in a magnetic field at 10^{-3} gauss and (2) the radiative lifetimes of these electrons is of the order of a year.

A relativistic electron with energy E_e keV in a field H oersteds produces a wide spectrum of photon energies but with a peak at photon energies of

$$E_p = 1.9 \times 10^{-17} H_{\perp} (E_o)^2 \qquad (1.8)$$

The spectrum of photons from a source will further depend on the spectrum of the electrons, and the range of magnetic fields within the object.

For the case where the directions of the magnetic field are random, and the electron density distribution is isotropic and has the power law spectrum in energy:

$$\frac{dN_e}{dVdE} = kE^{-\gamma} \text{ electrons cm}^{-3} \text{ keV}^{-1} \qquad (1.9)$$

then the spectrum of photons emitted by the synchrotron process is

$$\frac{dN}{dVdEdt} = 3.85 \times 10^{21} \, a(\gamma)k\left[\frac{6.64 \times 10^{-17}H}{E}\right]^{(\gamma + 1)/2}$$

$$\text{photons cm}^{-3} \text{ sec}^{-1} \text{ keV}^{-1} \qquad (1.10)$$

where H is the magnetic field in oersteds, E is the photon energy in keV and the function $a(\gamma)$ is approximately 0.1 for γ between 1 and 5 (Ginzburg and Syrovatskii 1965b). Equation 1.10 is valid provided that the electron spectrum satisfies equation 1.8 up to $E \sim 10^5$ GeV. Manley (1966) has considered the photon spectrum produced by a flat electron spectrum with a high energy cutoff and found that it was approximately exponential at high energies.

In any X-ray source the electron spectrum would not stay constant unless there was a continuous injection or acceleration of higher

energy electrons. The synchrotron emission causes the electron to lose energy at the rate

$$\frac{dE}{dt} = 0.98 \times 10^{-6} \; H_{\perp}^2 \left(\frac{E}{mc^2} \right)^2 \;\; keV/sec \qquad (1.11)$$

where $H_{\perp}$ is the magnetic field at right angles to the electron velocity measured in oersteds. The time for the electron to lose half of its energy is

$$T = \frac{5 \times 10^8}{H_{\perp}^2} \left(\frac{mc^2}{E} \right) \;\; seconds \qquad (1.12)$$

Synchrotron emission is very important at radio wavelengths in the Crab nebula, Tau XR-1, and Tucker (1967a) has investigated the possibility of synchrotron emission in the X-ray region. The Crab nebula is the remnant from the supernova of 1054 A.D. and so the biggest problem for the synchrotron theory is the short lifetime of high energy electrons due to synchrotron losses. Tucker was able to fit the X-ray, optical and radio observations with several models using different initial electron spectra and acceleration mechanisms. Only one of these models did not require any acceleration or injection of electrons since the initial outburst, but it required a very hard electron spectrum extending to very high energies, and a low energy cutoff at 10^3 GeV which is rather difficult.

Manley (1966) proposed a synchrotron model for Sco XR-1 using an

electron spectrum with a high energy cutoff. The radio flux from this source observed by Andrews and Purton (1968) is in good agreement with Manley's predicted spectrum. The contribution of synchrotron emission from galactic electrons to the diffuse X-ray flux has been discussed by Verma (1968) but was found to be small.

1.3.4 Compton Effect

One of the theories of the diffuse X-ray flux suggests that compton interactions between high energy electrons and low energy photons in interstellar and intergalactic space produce the X-rays. The effect is often called an "inverse" compton effect as the energy of the photon is increased in the interaction. An electron of energy E_e colliding with thermal photons of average energy E_p (= 2.7 kT) will produce scattered photons with an average energy $\bar{E}$ where (Ginzburg and Syrovatskii 1964)

$$\bar{E} = 1.33 \, E_p (E_e/mc^2)^2 \qquad (1.13)$$

Numerous calculations have been performed to determine the diffuse X-ray flux produced by the interactions of the high energy electrons with the photons of the 3° K universal blackbody radiation (Fazio et al. 1966; Felten and Morrison 1966; Bergamini et al. 1967; Brecker and Morrison 1967; Cheng 1967; Felten 1967; and Maraschi et al. 1968). The results are very dependent on the intensity and shape of

the galactic and intergalactic electron spectra, but making the most
reasonable estimates, the X-ray flux produced is less than the
observed diffuse flux. The discrepancy would disappear if there were
more electrons than expected or if there were more electrons in the
past, both of which are possible. Alternatively, the major component
of the diffuse flux could be unresolved extragalactic sources (Silk
1968).

PART A

SKYLARK EXPERIMENT TO OBSERVE CELESTIAL X-RAYS

CHAPTER 2

DESCRIPTION OF THE EXPERIMENT

Two identical X-ray astronomy experiments were flown on Skylark
rockets from Woomera, South Australia: SL426 (Flight I) at 0032 U.T.
on 4 April and SL425 (Flight II) at 2236 U.T. on 20 April 1967,
(Figure 1). These experiments were conducted jointly by the
Universities of Adelaide and Tasmania (UAT) and were flown as ancillary
experiments on rockets carrying ionospheric experiments of the
University College of Wales, Aberystwyth, U.K.

The prime purpose of these experiments was to survey the southern
sky, in particular, the Magellanic clouds and the galactic disk south
of the galactic centre, for sources of X-rays in the energy range
2 to 8 keV. These X-rays can only be observed from a rocket or
satellite as they are absorbed in the atmosphere at about 80 km
altitude.

The Skylark rocket is a solid fuel, unguided vehicle and on both

Figure 1. The launch of the Skylark rocket (Flight II)

from Woomera, South Australia.
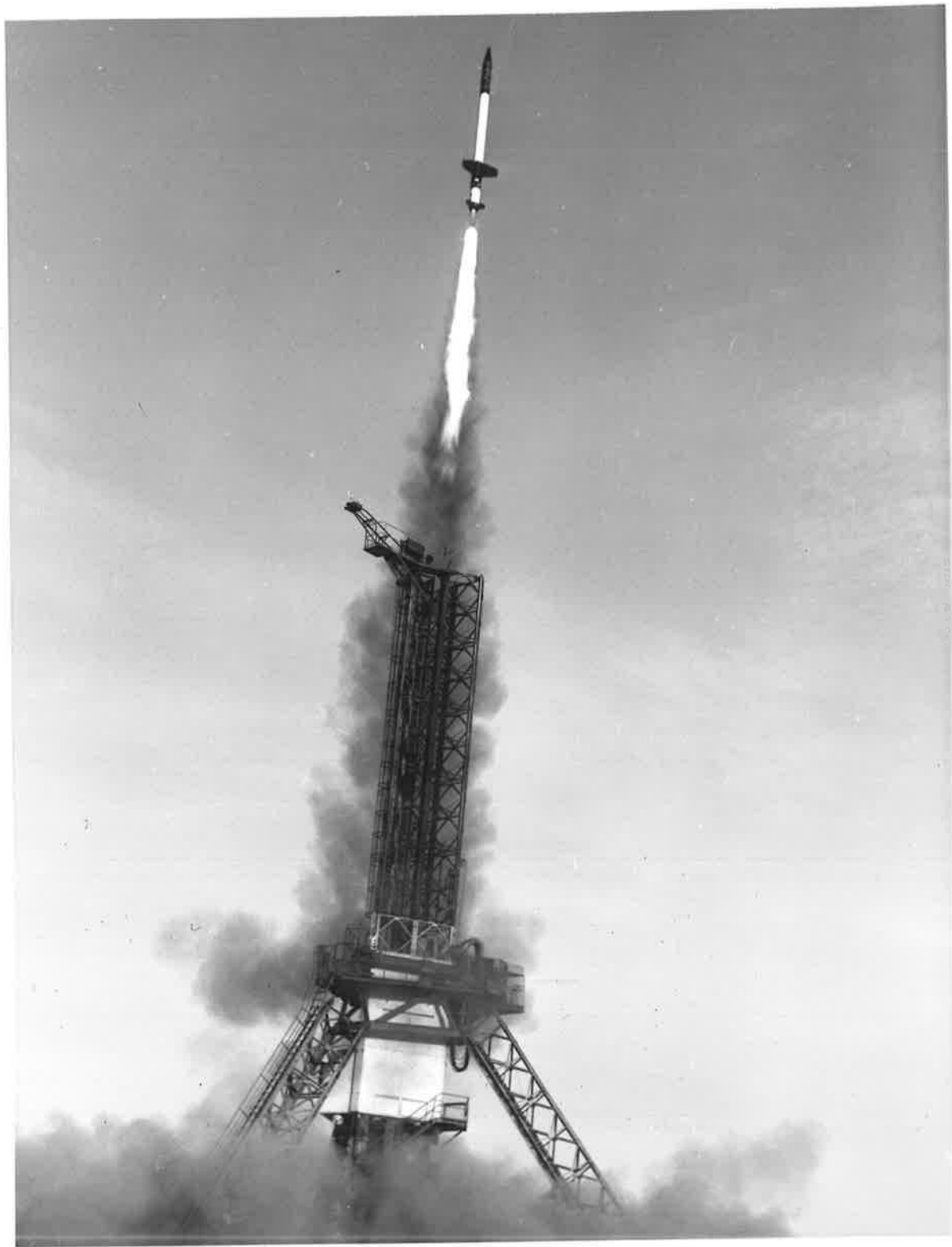
flights gave 350 seconds of observing time above 80 km. The head of the rocket consists of a series of cylindrical sections called "rings" which are mounted one above the other, culminating in the nose cone. The standard skylark instrumentation includes three orthogonal fluxgate magnetometers, three orthogonal accelerometers, two orthogonal rate gyroscopes, and four pairs of crossed sunslits. The data from these instruments enabled the attitude of the rocket to be determined at all times through the flight.

The X-rays were detected by a set of four proportional counters mounted in pairs around the circumference of the rocket, so that the two pairs looked in opposite directions. Aluminium collimators in front of the counters restricted the field of view to 70° x 20° (full angles) with the long axis parallel with the spin axis of the rocket. The motion of the rocket above the atmosphere consisted of a spin about the longitudinal axis and precession of this axis around a cone. The spin caused the counters to scan across the sky while the precession motion varied the scan paths from one revolution to the next. As a result, at the end of the flight the counters had scanned most of the celestial sphere above the horizon in an orderly manner.

The output from each pair of detectors was analysed by a two channel pulse height analyser with the channels set to accept pulses corresponding to 2 to 5 keV and 5 to 8 keV deposited in the counter.

The output from these channels was telemetered in real time to the ground.

The experiments were housed in a multipurpose ring (B16-01-1005), Figure 2, and holes were milled in the side for the proportional counters. The electronics were mounted on a pressure bulkhead which was attached to the base of the ring. The UCW experiment and the sunslits were mounted above the UAT ring while the telemetry, battery box, and other standard instrumentation was located below. This necessitated interconnect cables passing through the UAT ring, and these can be seen in Figure 2. The head was hermetically sealed so that the electronics only needed to operate at one atmosphere pressure.

The experiment power was supplied by a set of silver-zinc batteries in the rocket battery pack. The voltage from these batteries during a normal flight was between 32 and 26 volts, although voltages up to 37 volts could be expected under light load conditions. Consequently, the power converter had to be capable of operating over this range of voltages and yet supply the various regulated voltages required for the experiment. The input current to the power converter was 0.25 amp.

The block diagram, Figure 3, and the photograph of the ring, Figure 2, show the relation between the various components of the experiment. Where possible, connection was made via the master terminal trip for ease in checking the operation of the system. The interface
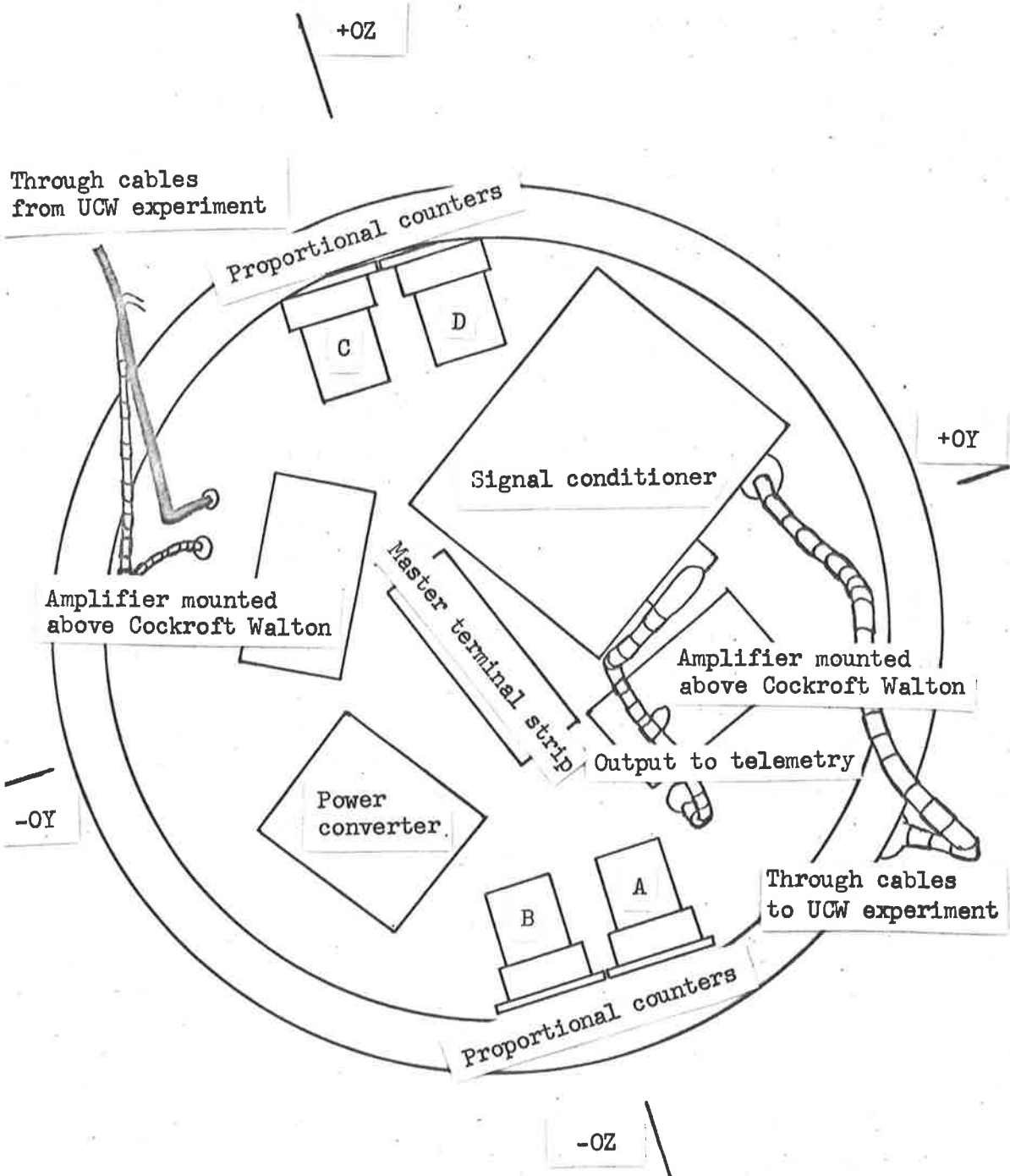
Figure 2. The UAT experiment mounted in the cylindrical 'ring' of the rocket. The sketch above shows the location of the various components.
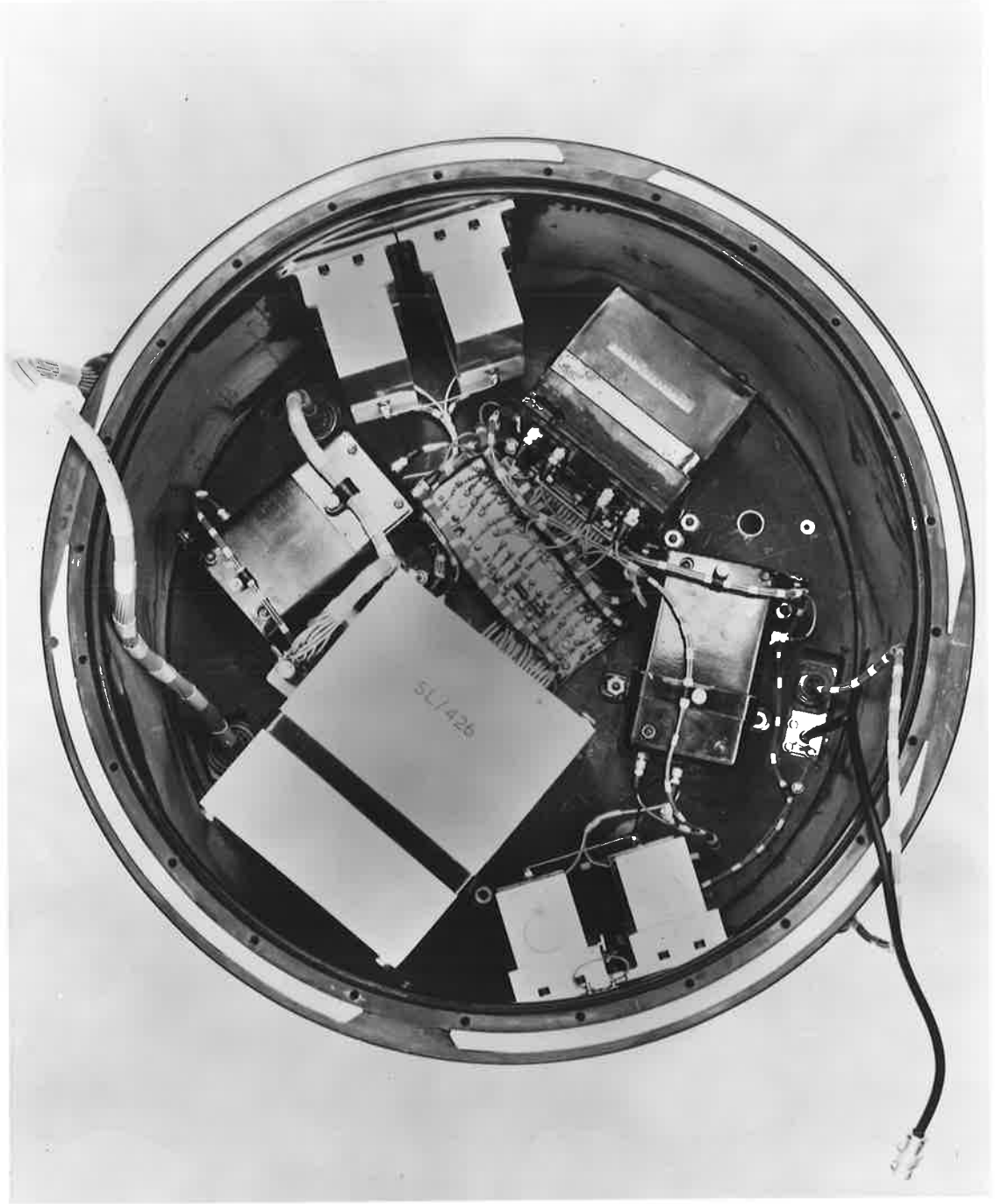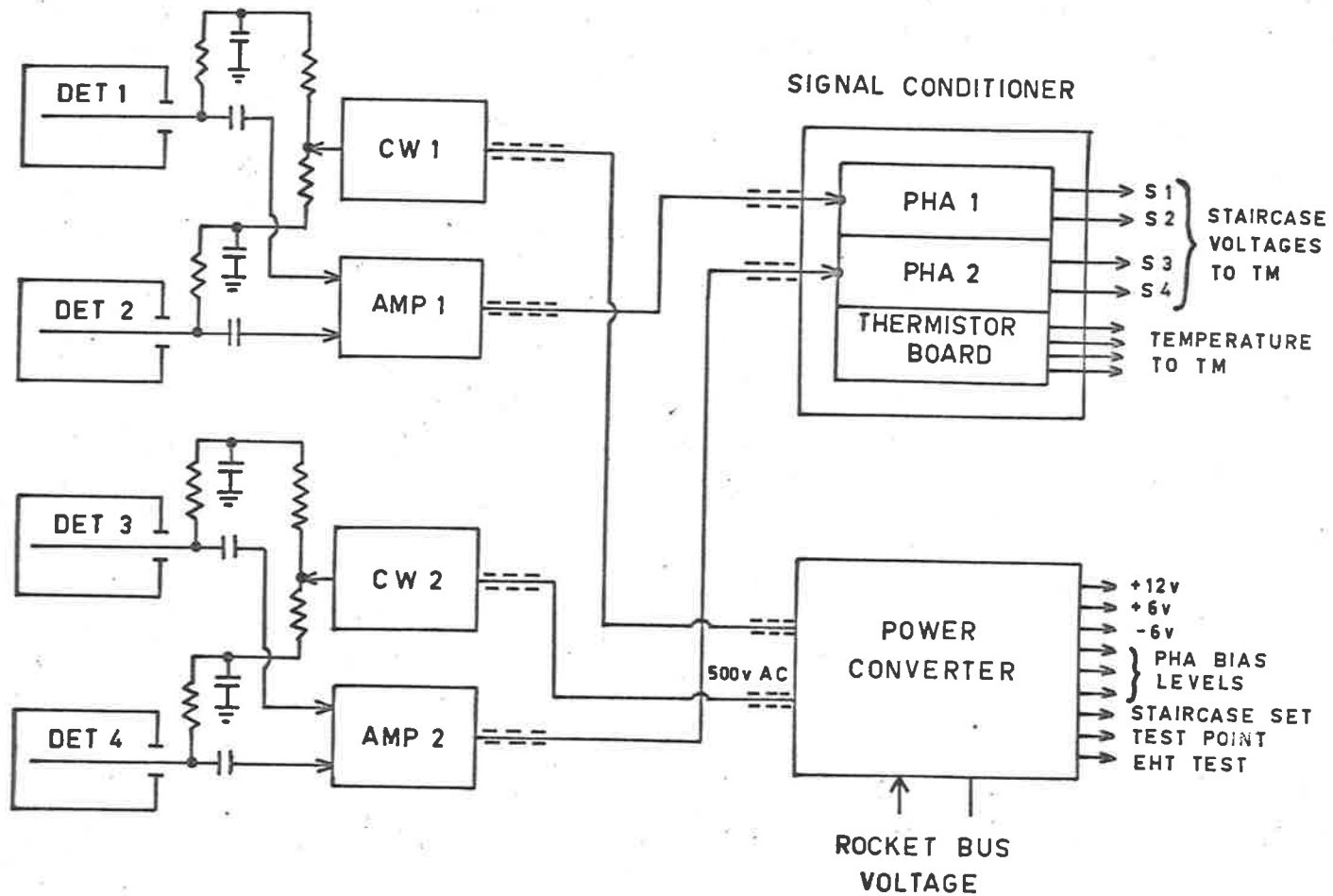
Figure 3. Block diagram of the UAT experiment showing the electrical connection between the various components.

with the rocket power supplies, telemetry and monitor lines was via
a 24 pin amphenol plug which for bench tests could be connected into
the ground checkout unit. There were two independent detection systems,
each consisting of:

(1) a Cockroft Walton voltage multiplier which supplied 2400 volts
for the proportional counters.

(2) Two proportional counters which detected the X-rays and
produced voltage pulses whose amplitude was proportional to
the X-ray photon energy.

(3) An amplifier which amplified the voltage pulses corresponding
to a photon energy of 6 keV to a pulse amplitude of 3 volts.

(4) A signal conditioner which analysed the spectrum of pulses
using a two channel pulse height analyser and generated two
(16 step) staircase voltages each corresponding to one channel,
and each step of the staircase corresponding to one count.
The staircase voltages were telemetered to the ground.

A set of four thermistors mounted at various points throughout
the experiment monitored the temperature during the flight. The
experiment was subjected to aerodynamic heating during launch and so
it was important to be able to determine whether the more temperature
sensitive items (counters, EHT supplies, etc.) were subject to
significant temperature changes. All of the electronics were constructed
from discrete components mounted on printed circuit boards.

2.1 Proportional Counters

The output pulse from a proportional counter is proportional to the energy deposited in the counter gas. This, together with the internal amplification of about 1000, and a high efficiency, (approx. 100%), means that a proportional counter is an ideal detector of X-rays in the energy range 2 to 8 keV.

Basically an X-ray is absorbed in the counter gas and produces a number of ion pairs proportional to the energy deposited in the counter (for xenon the mean energy per ion pair is 22 eV, Jesse and Sadaukis 1957). The counter configuration is usually cylindrical with an anode wire down the axis of the counter so that the electric field becomes intense close to the wire. The electrons are attracted towards the anode; as they get close to the wire they gain sufficient energy in one mean free path to cause ionisation. In this way an avalanche of electrons is built up and provided the counter is properly designed the amplification factor is independent of the initial number of electrons or where they were formed. A full discussion of proportional counters, and their mode of operation is given by Rossi and Staub (1949), Wilkinson (1950), Williams and Sara (1962), Curran and Wilson (1965), and Charles and Cooke (1968).

The proportional counters are shown in Figure 2 and were filled with a xenon-methane gas mixture (90% - 10% by volume) at one

atmosphere pressure. The entrance windows were beryllium foil and their thicknesses were measured subsequent to the rocket flight and found to average 14 mg/cm^2 (effectively 0.003 inch). The measurements were made both with a micrometer calibrated with standard shims and also by weighing known areas of foil. The effective window area of each detector was 11 cm^2 after the struts and collimators had been taken into account. The counters and collimators were made of aluminium which produces fluorescent X-rays of 1.5 keV, well below the lower channel at 2 keV. The counters are shown in the photographs of the experiment before launch, Figure 2, and after launch, Figure 8. The counters were manufactured by LND Inc., Oceanside, N.Y., to specifications drawn up for this experiment.

The experiment was initially designed to fit into a smaller section of the rocket which placed tighter restrictions on the window area and the length of the counter than the "multipurpose" ring that the experiment was actually flown in. Since the counter window occupied an appreciable part of the total length of the counter, difficulties were experienced with end effects. The gain decreased and the resolution worsened for X-rays incident on the end windows of the counter. The first set of counters ordered were flown on Flight II and suitable corrections were made to the results. For the second set of counters a grid of field forming electrodes corrected the poor field configuration towards the end of the counter. Although

this corrected for the gain variations along the length of the counter
the overall resolution was still rather poor. This was probably due
to the proximity of the guard wires to the anode wire which made the
uniform tensioning of all of the wires very critical. Any variation
in the distances between the wires through slackness of the wire
would produce large changes in the multiplication factor.

The counter anode voltage was 2400 V which was regulated by a
corona tube. The field forming electrodes operated at 500 V.
Sufficient filtering was mounted at the detector to remove any transients
from the 2400 V line and a 1 Megohm load resistor was used between the
last capacitor and the anode. The current pulse from the proportional
counter caused a voltage drop across the load resistor and the
resulting voltage pulse was fed to the amplifiers through a coupling
capacitor and a short coaxial cable.

The resolution of the proportional counters is defined as the
full width at half maximum (FWHM) of the distribution of pulses
produced by a monoenergetic source of X-rays, and is expressed
as a percentage of the pulse height. Most of the testing of these
counters was done with 5.9 keV manganese K X-rays from an iron 55
source. The theoretical resolution at this energy is about 16%
which is caused by the statistical processes involved in the
absorption of the photon and the amplification process. All of the
present counters were worse than this and ranged from 20% to 100%.
The characteristics of the counters when flown are shown on Table 2.

TABLE 2

CONDITION OF PROPORTIONAL COUNTERS WHEN FLOWN

Flight	Counter	Position in Expt.	Resolution at 5.9 keV	Voltage of Peak
I(426)	3115	A	52%	3.0
	3116	B	81%	3.0
	3114	C	100%	2.8
	3117	D	25%	2.0
II(425)	2420	A	34%	3.0
	2009	B	28%	3.0
	2025	C	100%	1.0
	2027	D	20%	2.5

Xenon was used as the counter gas because it has a higher cross section for the absorption of X-rays and causes a higher ionisation energy loss by charged particles than any other noble gas. Hence the counter has a greater efficiency for X-rays and at the same time, charged particles tend to deposit more than 8 keV in the counter

and be excluded by the pulse height analyser. Minimum ionising charged particles will deposit about 18 keV per inch (Barkas and Berger 1964) and calculation showed that if minimum ionising charged particles are incident from random directions about 75% of them would be rejected. The proportion will increase at lower energies as the energy loss increases. Methane was necessary to absorb the ultraviolet photons produced in the avalanche before they could eject electrons from the counter walls.

The efficiency of the counter is the probability of detecting a photon of a given energy that is incident on the counter window. It is the product of two factors, the probability of transmission of the photon through the window and the probability of absorption in the gas, i.e.

$$\mathcal{E}(E) = \exp(-\mu_w \rho_w x_w)\left[1 - \exp(-\mu_g \rho_g x_g)\right] \qquad (2.1)$$

where μ is the mass absorption coefficient in grams cm^{-2}, ρ is the density, x the thickness, and the subscripts w and g refer to the window material and the counter gas. The mass absorption coefficients for energies above the K edge are given by Victoreen (1949), while at lower energies empirical relations (Compton and Allison 1935) were used to extrapolate the Victoreen values. The calculated efficiency is shown on Figure 4. The low energy limit is due to absorption in the beryllium windows while the high energy limit is due to the lack of opacity of the xenon. The K absorption
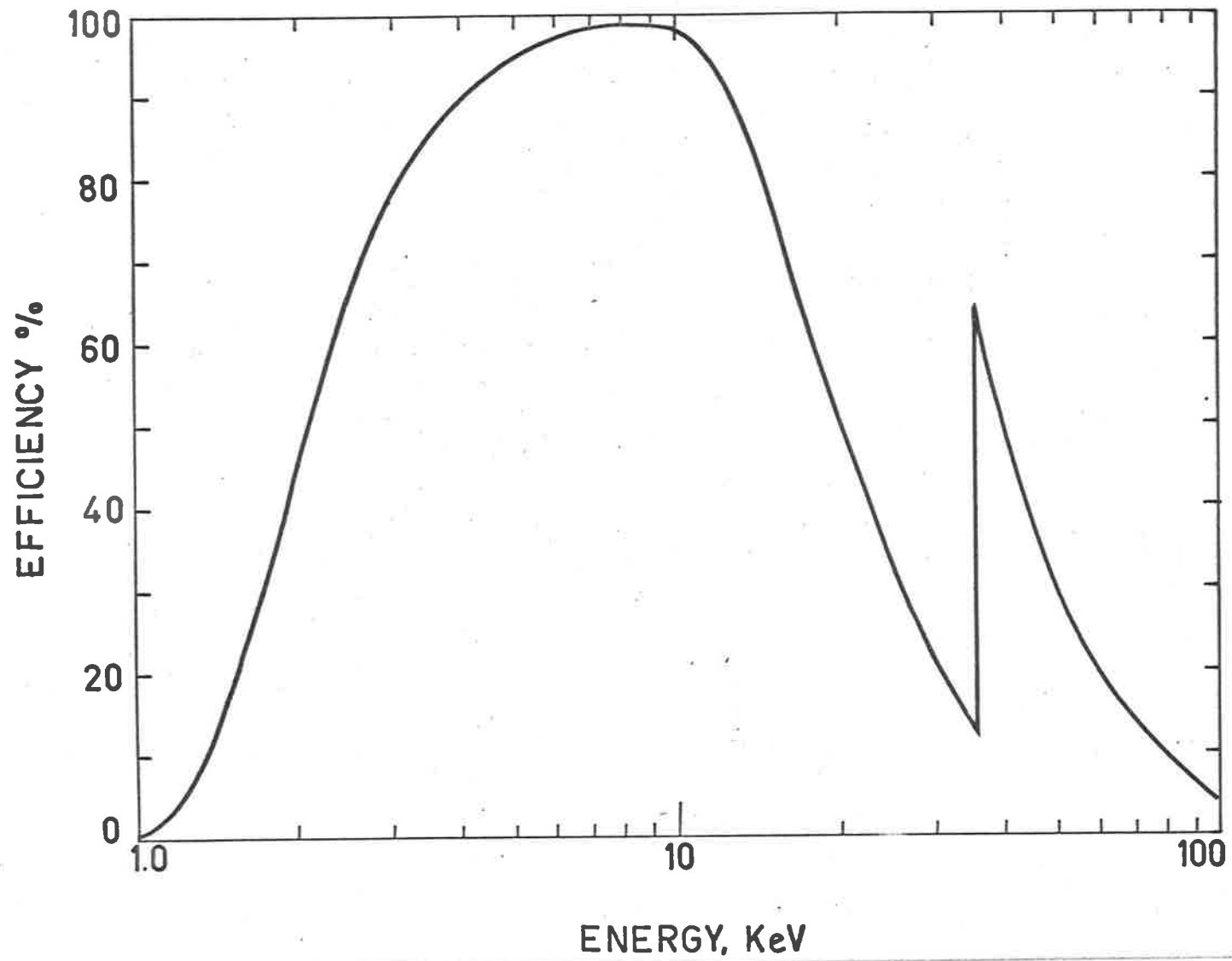
Figure 4. The X-ray efficiency of the Skylark proportional counter.

edge of the xenon can be seen at 34.6 keV and the L edge is at about
5 keV but has a negligible effect.

Although a photon of energy E is absorbed in the counter, this
does not necessarily mean that all of the energy is deposited in the
counter. The photoelectric absorptions of the incident X-rays by the
xenon is followed in 87% of the cases for the K level and 21% for the
L level by the emission of a K or L X-ray (Fink et al. 1966). These
X-rays can then escape from the counter and carry away energy. The
probability of escape for the K X-ray at 29.5 keV is about 90%,
hence if 36 keV X-rays were being detected most of them would produce
pulses corresponding to 6.5 keV deposited in the counter. The
probability of escape for the L X-ray is low but it is very dependent
on the proximity of the walls of the counter to the location of the
original absorption. For example, only 2.5% of normally incident
6 keV X-rays produce an escaping L X-ray of 4 keV. This means that
in the pulse height distribution of pulses from the counter, the
escape peak at 2 keV has only 2.5% of the counts that were observed
in the photopeak at 6 keV.

The detection system is relatively insensitive to low energy
charged particles as it only accepts particles with enough energy
to penetrate the beryllium window but which will at the same time
emerge with less than 8 keV. This requirement is equivalent to
specifying an energy interval of about 1 keV at about 90 keV for

electrons, or less than 1 keV at 2.1 MeV for protons. The calculation of the electron transmission coefficients will be discussed in Section 8.2.

2.2 The Power Converter

The various voltages required in the experiment were supplied by the power converter which operated from the rocket batteries. The voltage from these batteries was nominally 26 V but could be as high as 37 V for short periods. The input voltage was series regulated to provide a stable 25 V using a 9.1 V Zener diode as the voltage reference. The regulated voltage could be adjusted by means of a potentiometer to compensate for changes in the load conditions. This "voltage adjust" potentiometer was set before launch so that the "test voltage" from the power converter was -25 V with respect to the positive battery input.

A 7.5 kHz inverter generated square waves with peak to peak voltages close to 6 V, 12 V, and 500 V. The low voltages were rectified by bridge circuits and series regulated to provide +6 V, -6 V and +12 V. Three potentiometers, between ground and +6 V gave the three bias voltages necessary to define the pulse height analyser window edges. A potentiometer between the +12 V and -6 V provided a voltage used to make fine adjustments to the zero of the staircase

voltages. All of the potentiometers were mounted on the front of the power converter for ease of adjustment. The 500 V square wave was supplied directly to the Cockroft Waltons via a coaxial cable and not through the master terminal strip. On Flight I (SL426) the counters had field forming electrodes which used the rectified 500 V after suitable filtering.

The operation of the power converter was monitored right up to launch by the priming unit, (discussed in Section 3.6) which had provision to measure six voltages and six currents from the UAT experiment. The six voltages monitored were the -6 V, +6 V, +12 V, Bias 1, Bias 2, and Bias 3. Only three currents were measured, and these were used to monitor (1) the input current to the power converter, (2) the -25 V test point and (3) the EHT test point that indicated whether the high voltage was being supplied to the Cockroft Waltons. The current drawn by the meter circuit was only about 100 uA so as not to perturb the operation of the converter. Although the lengths of cable and the numerous connectors caused the current at the meter to be less than expected, the measurements were used to indicate any change in the operating conditions during the countdown.

2.3 The Cockroft Walton Voltage Multiplier

The 2400 V DC required for the proportional counter anode volts
was supplied by a Cockroft Walton voltage multiplier. The 500 V
square wave was applied to one side of a diode capacitor "ladder",
causing the capacitors to be alternately 250 V above and below the
corresponding capacitor on the other side. The diodes allow positive
charge to accumulate up the chain until there is a 250 V increment
across each diode, i.e. 500 V across each capacitor. The net result
is that about 3000 V was generated at the top of the "ladder" which
was filtered and regulated to 2400 V by a corona tube, GV4S - 2400.
The current through the corona tube was about 50 uA and its temperature
coefficient at this current was 0.13 V/$^{\circ}$C.

The proportional counters draw very little current and so further
RC filtering circuits were employed to minimise the A.C. and transient
voltage variations. Each Cockroft Walton supplied a pair of counters
which were isolated by 10 Megohm, 0.01 uF filter. The load resistor,
a coupling capacitor and the filter were potted on the end of the
individual counters. The 500 V DC required for the field forming
electrodes of the counter on SL426 (Flight I) were supplied by coaxial
cable directly from the power converter. A filter on this line was
also potted on the end of each counter.

2.4 The Amplifiers

The pulses from two proportional counters were "equalised" by feeding the output from the counter with the larger gain through a series resistor and then the two outputs were fed into the same amplifier. The input pulses were negative with an amplitude of about 5 mV, and were amplified to 3 V by the amplifier. The amplifier was protected against large pulses, e.g. a discharge in the high voltage line, by two diodes, while a field effect transistor provided a high impedance, low noise input. The gain of the amplifier was constant to within 5% for supply voltages over the range 7 to 15 volts. The output pulses were positive and had a rise time of 8 usec and saturated at 6 volts. The slow rise time was due to the long integration time used to minimise electronic noise. The gain of the two stages of the amplifier could be adjusted by changing the feed back resistors of each stage. For flight the gain was set so that the 5.9 keV X-rays from an iron 55 source in the counter produced 3 V output pulses from the amplifier.

2.5 Signal Conditioner

Pulses from each amplifier were analysed by a two channel pulse height analyser with channels set to 2 to 5 keV and 5 to 8 keV. The output from each channel was a 16 step staircase voltage with each

step corresponding to one count in the channel.

The signal conditioner consisted of two printed circuit boards each containing the electronics of one pulse height analyser and its associated staircase generators. The logic is shown Figure 5, and the time sequence of the various pulses is shown on Figure 6. The output from the amplifier was fed into three discriminators which gave an output, Q, if the pulse was above the respective bias level. The three bias levels were obtained from the power converter and were set to 1 V, 2.5 V and 4 V before launch. The lower channel of the pulse height analyser consisted of all pulses that fired Disc-1 but not Disc-2. Similarly, the upper channel corresponded to pulses that fired Disc-2 but not Disc-3. In order to avoid any sneak pulses due to the finite rise time of an input pulse firing one discriminator before another, a strobe pulse was generated 7 usec after Disc-1 fired, Figure 6. The strobe pulse was a short positive pulse and fixed the time when the NAND gates interrogated the discriminator outputs to determine the amplitude of the input pulse. This was timed to occur after the maximum of the pulse had been reached, i.e. after all discriminators would have fired. The minimum length of the discriminator output pulse was 12 usec so that there was no danger of it ending before the strobe pulse. The gate NAND-1 only gave an output when the peak amplitude of the input pulse was between Bias 1 and Bias 2; similarly a NAND-2 output occurred when the input pulse was between Bias 2 and Bias 3.
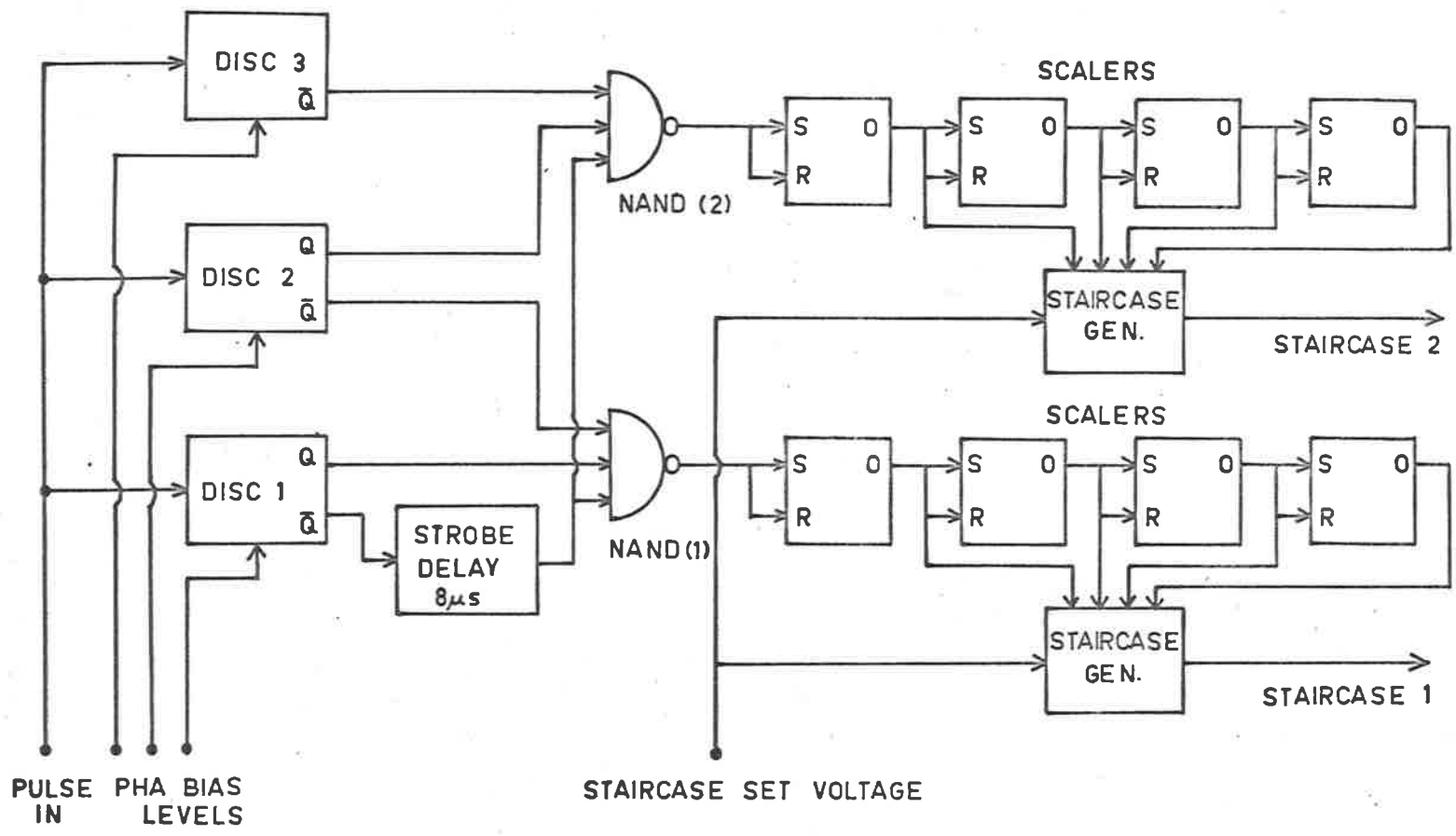
Figure 5.   Signal conditioner logic.

INPUT
— Bias 3 – 4v
— Bias 2 – 2.5v
— Bias 1 – 1v

10μs |20μs   30μs

Q1

Q̄2

Duration of Q pulses
is 10μs or length of
time input is above bias
level – whichever is the longer

Q2

STROBE ←8μs→

NAND 1 OUTPUT

NAND 2 OUTPUT

SCALER OUTPUT
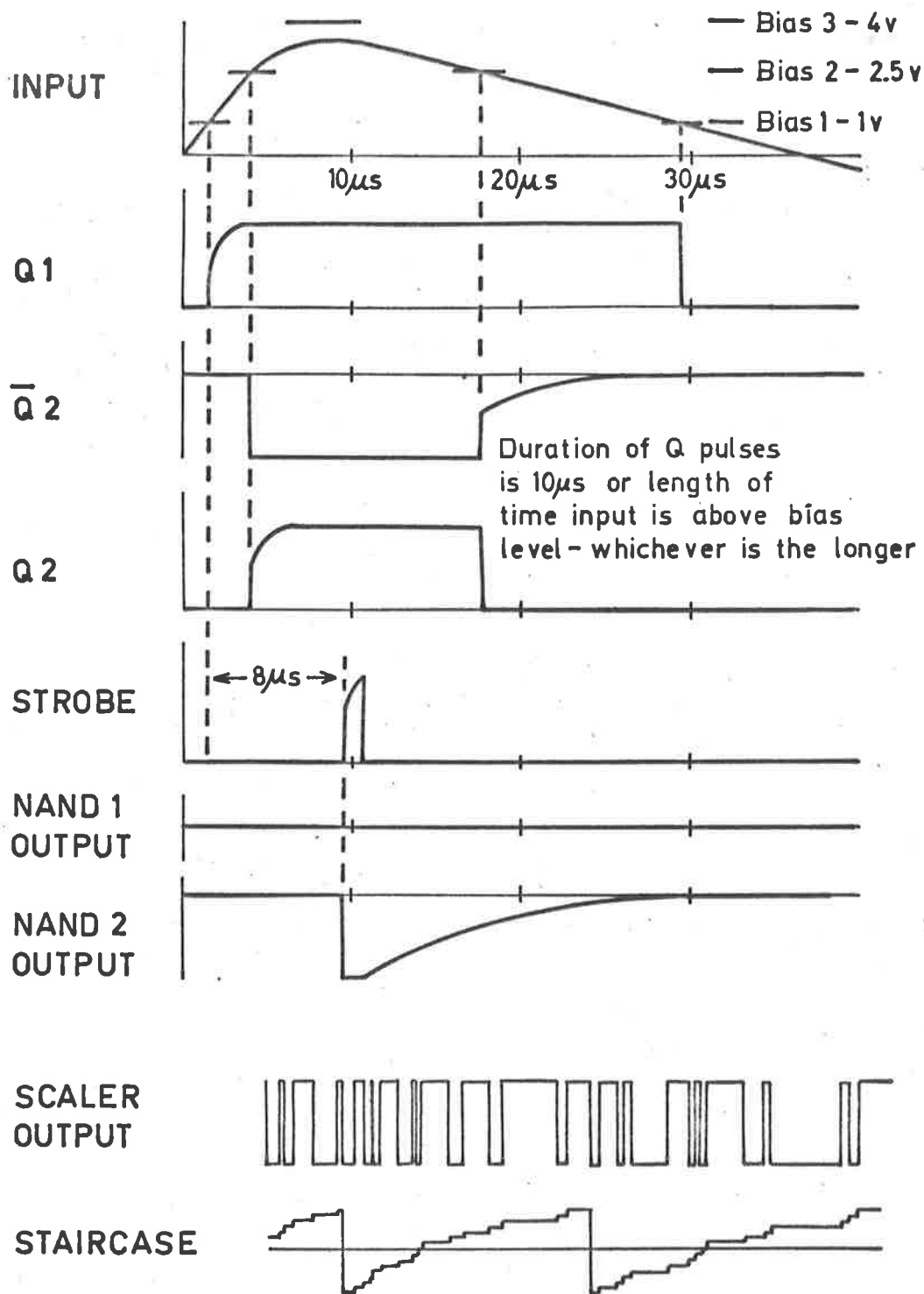
STAIRCASE

Figure 6. The time relation between various pulses in the signal
conditioner. Note that the scaler and the staircase outputs
are on a different time scale than the other pulses.

The output from each NAND gate was fed to a series of bistable
multivibrators forming a four bit scaler. The outputs from all of
the stages were fed to a resistance network that generated a staircase
voltage with 16 steps between -3 V and +3 V corresponding to the 16
states of the scaler. A 'staircase set voltage' enabled small
adjustments to be made to the mean voltage of the staircase so that
it was in the correct range for the telemetry input. A 3 V Zener
diode would have been removed if the telemetry had required signals
in the range 0 to +6 V (as sometimes occurs in the Skylark programme).

The Skylark uses an FM/AM telemetry system with Time Division
Multiplexing to give 24 analogue channels, each of an accuracy of
about 2% and each channel being sampled 80 times per second. Each
of the four staircase voltages from the signal conditioner was
transmitted on a whole channel. The staircase voltage was an efficient
method of transmitting the digital information, i.e. the number of
counts observed in the 1/80 second, on the analogue telemetry channel.
The combination of the sampling rate and the 16 steps in the staircase
puts an effective upper limit of 1280 counts/sec that can be measured
from any pulse height analyser channel. Some of the telemetry
channels could be subswitched to produce quarter channels which were
sampled 20 times per second. The temperature measurements, to be
discussed next, each used two quarter channels.

2.6   Thermistors

Four thermistors were located at various points through the
experiment to monitor the temperature changes during the flight.   One
thermistor which was calibrated in the range 0 to 200 ^{o}C was mounted
in the wall of the ring near to the counters.   The other three
thermistors operated over the range 0 to 100 ^{o}C and were located in
the power converter, in the signal conditioner box, and on the corona
tube of a Cockroft Walton respectively.   Each thermistor had an
associated DC amplifier consisting of two temperature compensated
emitter followers.   All of the thermistor circuits were mounted on
a printed circuit board located in the signal conditioner box.   As
mentioned previously, each temperature output was sampled 40 times
per second by the telemetry sender.

CHAPTER 3

ENVIRONMENT, MECHANICAL CONSTRUCTION AND LAUNCH

The experiment was designed to operate over the range of
environmental conditions expected during the flight. These are
outlined below.

3.1 Temperature

The aerodynamic heating during launch produces temperatures up
to 200 °C on the outer skin of the parallel section of the payload.
However, due to the large thermal capacity of the payload the maximum
ambient temperature in the UAT ring was not expected to exceed 60 °C.
The experiment was tested at temperatures over the range 10 °C to
70 °C while the voltages and spectra were being monitored. For
temperatures less than 50 °C X-ray pulse heights and the channel
positions changed by less than 5%, over the whole temperature range.
The flight takes only seven minutes and the various components took much
longer than this to warm up, even though the skin of the rocket was
subjected to a 200 °C step increase in temperature. Notwithstanding,
four thermistors were mounted through the experiment to monitor the

TABLE 3

TEMPERATURES DURING FLIGHT II

	Time (seconds)					
	0	100	200	300	400	500
Inside of wall	$25^{\circ}C$	$65^{\circ}C$	$71^{\circ}C$	$72^{\circ}C$	$66^{\circ}C$	$91^{\circ}C$
Power converter	35°	36°	38°	42°	44°	48°
Signal conditioner	25°	26°	27°	28°	29°	32°
Cockroft Walton	27°	28°	29°	30°	32°	34°

temperatures during the flight, producing the results shown in Table 3.
Although all of the heating of the rocket skin occurred between zero and
50 seconds, most of the components did not have time to stabilise during
the duration of the flight. The heating after 400 seconds was due to
reentry. The thermistor in the Cockroft Walton was glued to the corona
tube, but the temperature rise recorded must be taken as an upper limit
as the thermistor could have been heated through its leads. In the
signal conditioner and the power converter the leads should be at the
same temperature as the thermistor.

The preflight temperature calibrations, plus the data indicated
in Table 3, indicate that the energy calibrations of the system were

constant to within ± 5% throughout the duration of the flight.

3.2 Vibration and Acceleration

The Skylark rocket is subject to considerable vibration and to a sustained acceleration of 10 g longitudinally during launch. All components and cables were securely fastened; all screws and potentiometers were locked with "LOCK TIGHT"; electronic components were mounted on the printed circuit board with short leads and were conformal coated to prevent resonances. The assembled experiment was tested by applying accelerations of 6 g longitudinally and 2 g laterally with vibration frequencies over the range 30 Hz to 2000 Hz. At the conclusion of the test the experiment was run and no adverse effects or permanent changes could be detected. Although there was no test to see if the experiment could withstand the sustained longitudinal acceleration it had been tested to 6 g vibrations and all of the components had been mounted so as to withstand such an acceleration.

3.3 Pressure

The UAT ring together with the rest of the head was pressure sealed to a leak rate of less than 1 lb/sq. in. per hour, with one atmosphere differential. It is normal practice for the Skylark

vehicle to be sealed in the launcher, so that it maintained its
pressure at one atmosphere throughout the flight. Consequently the
electronics did not need to operate at low pressures during the
flight. Pressure equalising holes were cut in all bulkheads so that
even if a small leak did develop, the large volume of gas in the
payload would mean only a small pressure change during the seven
minute flight. Nevertheless, the equipment was built to withstand low
pressure so that it would continue to operate even if the pressure
were to drop to zero.

The proportional counters were mounted in solid aluminium collars
with an epoxy resin and attached to flat sections of the inner surface
of the ring. Neoprene gaskets between the collar and the flat provided
pressure sealing between the hole through which the counter looked
and the body of the round.

3.4 Compatibility in the Round

Although the experiment worked well by itself it was important
to ensure that it worked when integrated into the rocket and did not
interfere with the other experiments. Because the proportional counter
output consists of low level signals it was possible that interference
could occur from the telemetry signals, or the UCW experiment.

Integration of the round was accomplished at British Aircraft
Corporation, Bristol, U.K., and Mr. R. J. Francey was present to watch
over the UAT interests. Subsequent tests were conducted at Weapons
Research Establishment, Salisbury, South Australia, and at Woomera.
The only interference occurred at the time of the activation of a
relay in the main experiment, but since this only happened twice in
the flight it was of no consequence. Some difficulty was experienced
with the very long leads (550 feet) from the launcher to the priming
unit causing the 7.5 kHz in the UAT power converter to interfere with
the UCW experiment. This disappeared on switching to internal rocket
supplies and so was not a problem during flight.

3.5 Mechanical Construction

The four proportional counters were mounted at holes cut in the
two flat sections of the ring so that the pairs of counters looked in
the $\pm$ OZ directions. Rocket coordinates have +OX as the forward
direction and the +OY direction is down-range at launch. Figures 2
and 8 are photographs showing the attachment of the counters.

The collimators in front of each counter were constructed of
0.009 inch aluminium slats and, as flown, defined a field of view
10.5° by 35° in the longitudinal axis (full width at half transmission),
Figure 7.

The Cockroft Waltons and the amplifiers were in individual brass boxes to give the best RF shielding. The signal conditioner box contained three printed circuit boards, two of which carried the two pulse height analysers and staircase generators, and the third carried the thermistor amplifiers. The signal conditioner box and the power converter were mounted separately on the pressure bulkhead which was attached to the base of the ring. The amplifier and Cockroft Walton boxes for each system were mounted together on the bulkhead. Most of the interconnections between the components were made via the master terminal strip. Figure 2 is a photograph of the experiment showing the positioning of the various components in the ring.

Power input to the experiment and also the telemetry and priming unit output was through a plug on the side of the signal conditioner box. The positioning and mounting of the components was done under the following restrictions:

(a) The centre of mass had to be close to the rocket axis.

(b) No obstruction of the connectors carrying lines fore or aft of the rocket was permitted.

(c) All holes had to avoid the structural webbing of the bulkhead.

(d) The length of the pulse lines was minimised.

(e) The brass of the component boxes could not be in contact with the magnesium alloy of the ring or bulkhead and so Neoprene gaskets were used under the boxes.

(f) The components had to be securely attached.

(g) The total weight of the ring had to be minimised.

3.6 Testing and Launch Procedure

All connections from the experiment were made via a 24 pin
amphenol plug mounted on the side of the signal conditioner box. In
the rocket, cables from this plug went to the telemetry sender, batteries
and priming unit lines, but for test purposes when the payload was
dismantled, the Ground Checkout Unit could be connected to the plug to
simulate the rocket power and enable a complete test of the experiment's
operation to be made. The Ground Checkout Unit was built at the
University of Tasmania and provided the following facilities:

(a) 24 to 37 volts to power the experiment.

(b) Switching and a meter to measure all of the DC levels in the
ring.

(c) A check on the telemetry channel outputs and interfacing to
enable the telemetry output to be measured by a scaler.

(d) Pulse shaping to make the amplifier pulses acceptable to a
RIDL 400 channel pulse height analyser. This involved a linear
gate to provide a pulse with a fast rise time but with an
amplitude proportional to that of the amplifier output pulses.

(e) A pulse generator to simulate the amplifier output for checking
the signal conditioner logic.

A test X-ray source of iron 55 was mounted a standard distance in front of the counters to check the detection system. Iron 55 undergoes internal conversion to manganese 55 which emits a 5.9 keV K X-ray. Pulse height spectra for each counter were taken using a RIDL 400 channel pulse height analyser. The positions of the discriminator thresholds were obtained with respect to the recognisable features of the X-ray spectrum by gating the amplifier output pulses with the output of the NAND gates (i.e. the channel defining gates). At Woomera a multichannel pulse height analyser was not available and so a portable method of checking the channels was required. This was achieved by using a 'Philips' scaler PW4032 to count the number of staircases from the telemetry for the source in a standard position. The countrate observed from each staircase was calibrated by using it in conjunction with the multichannel pulse height analyser before leaving for Woomera. Other equipment taken to Woomera included a multimeter and a Tetronix oscilliscope.

Before firing, the round was powered and controlled by a priming unit which also monitored the operations and measured voltages and currents at various places within the round. The priming unit cables were connected to the round by two pairs of 24 way butting connectors which could be removed by hand, or by the ejector arms on the launcher. The cables were 19 feet long in the laboratory, but 550 feet at the launcher and so could only be used for DC measurements.

The UAT experiment could be switched on and off from the priming unit and up to six voltages and six currents could be measured on two 0 - 100 uA meters with 1600Ω internal resistence, each with a six way input switch. The voltage meter monitored the +12 V, +6 V, -6 V, Bias 1, Bias 2, and Bias 3, while the current meter monitored the input current, the high voltage and the 25 V test voltage of the power converter. In addition to these monitoring facilities a telemetry receiver showed if the staircase stepping rates were consistent with the background countrate and the presence or absence of the X-ray source.

A special counter test was undertaken during the countdown at 15 minutes before launch. The iron 55 source was held in front of each counter in turn for 10 seconds and the resultant telemetry output was recorded. This enabled an estimate to be made of the state of the system immediately prior to launch, and provided a permanent record of the complete system at the time of flight.

At 0032 UT on 4 April, 1967, SL426 (Flight I) was launched, reaching an apogee of 219.9 km and provided 330 seconds of celestial X-ray data. At 2236 UT on 20 April, 1967, the second flight SL425 (Flight II) was launched, with an apogee of 218.6 km, and giving a similar period of X-ray data. Figure 1 is a photograph of the launch and Figures 7 and 8 are recovery photographs.

The telemetry from the rocket was decommutated into the twenty four channels of data and photographic records produced by using the amplitude
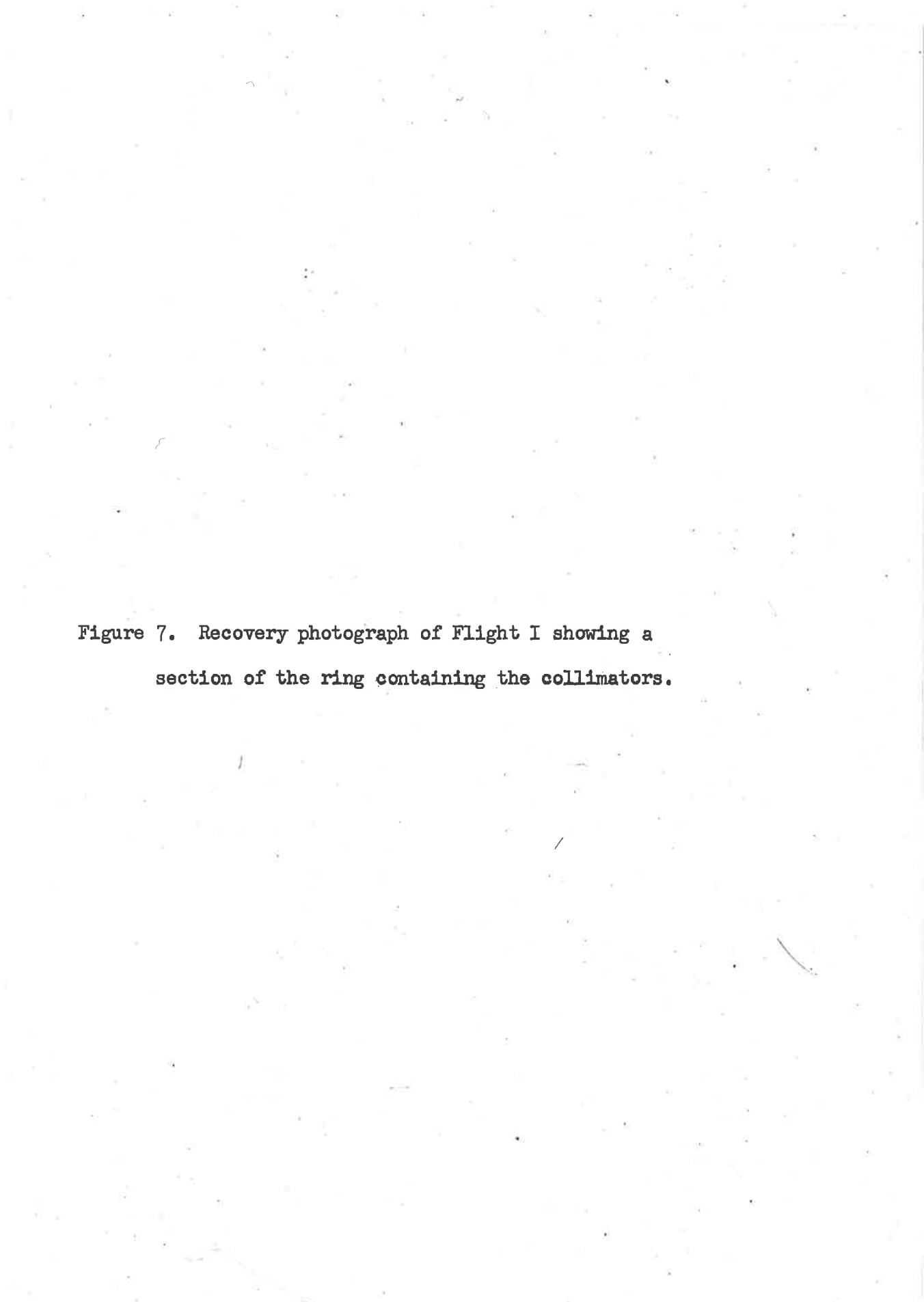
Figure 7. Recovery photograph of Flight I showing a
          section of the ring containing the collimators.

SERIAL 116
TRIAL BS141 1
MISSILE SL426
DATE 4 4 67

Figure 8. An exploded view of the payload of Flight II.
Two proportional counters are mounted on the section
of the ring in front of the tree and the signal
conditioner box can be seen behind the tree.

SERIAL   163
TRIAL   BS141 2
MISSILE   SL425
DATE   21467

of the signal to deflect the beam of a cathode ray tube. The brightness

was controlled so that the signal from a given channel consists of a

series of dots separated by 1/80 second. All tubes displayed the

channel containing the 0%, 50%, 100% and the reference voltage of

+2.68 V from a Mallory cell to calibrate the record. Additional

calibration voltages of 10%, 30%, 70%, and 90% were transmitted and

displayed on some tubes.

Two types of photographic record were generated. A slow speed

24 inch long record containing all of the results for the whole flight

gave an overall view of the flight. For analysis a high speed record

of 2 inches/second, which easily resolved the individual dots, was used.

Four tubes display the attitude information, with one tube

assigned to each of the types of measurement. A sample of these records

is shown Figure 9, and they will be discussed in detail in the next

section. The tubes 5 to 8 display the UAT data and a sample is shown

Figure 10. Each of the four staircases is assigned to a separate tube.

In addition, a temperature channel is displayed on each of the tubes

5 and 6.

Figure 9. Telemetry records of the data from the attitude
instruments.

SL425

Rate Gyroscopes

pitch

spin

0 sec   100 sec   200 sec

Accelerometers

x

Magnetometers

x

y   z

Sunslits
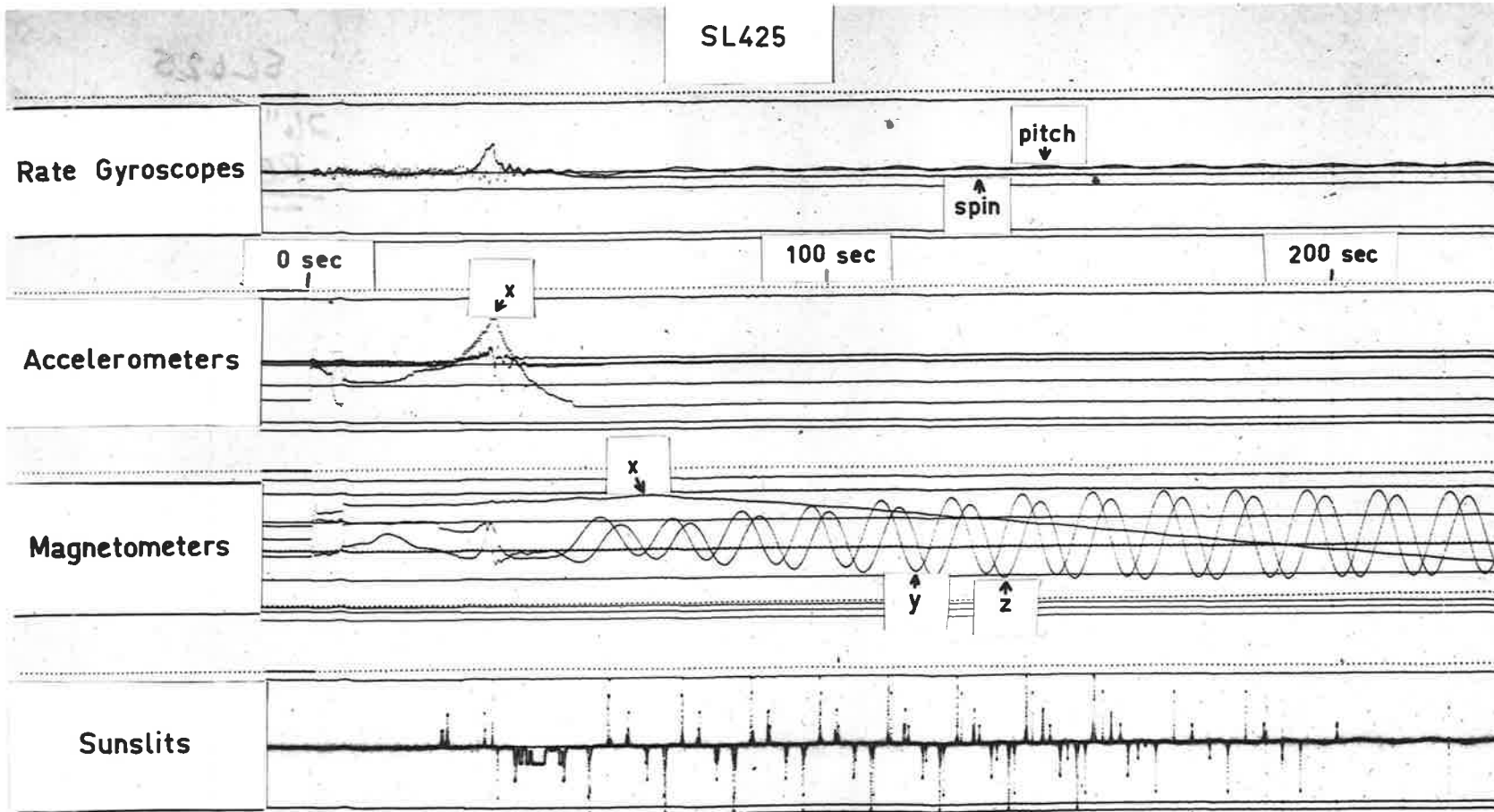
Figure 10. An example of the staircase data received
during Flight I. Each channel was sampled 80
times per second and the individual dots can be
seen. The countrate increased when the
proportional counters responded to the sun,
Cen XR-2 and Sco XR-1. During this time no
significant sources were observed on the second
detection system.

SL426

S1

288s   289s   290s   291s   292s

S2

SUN   CEN XR-2   SCO XR-1

S3

S4
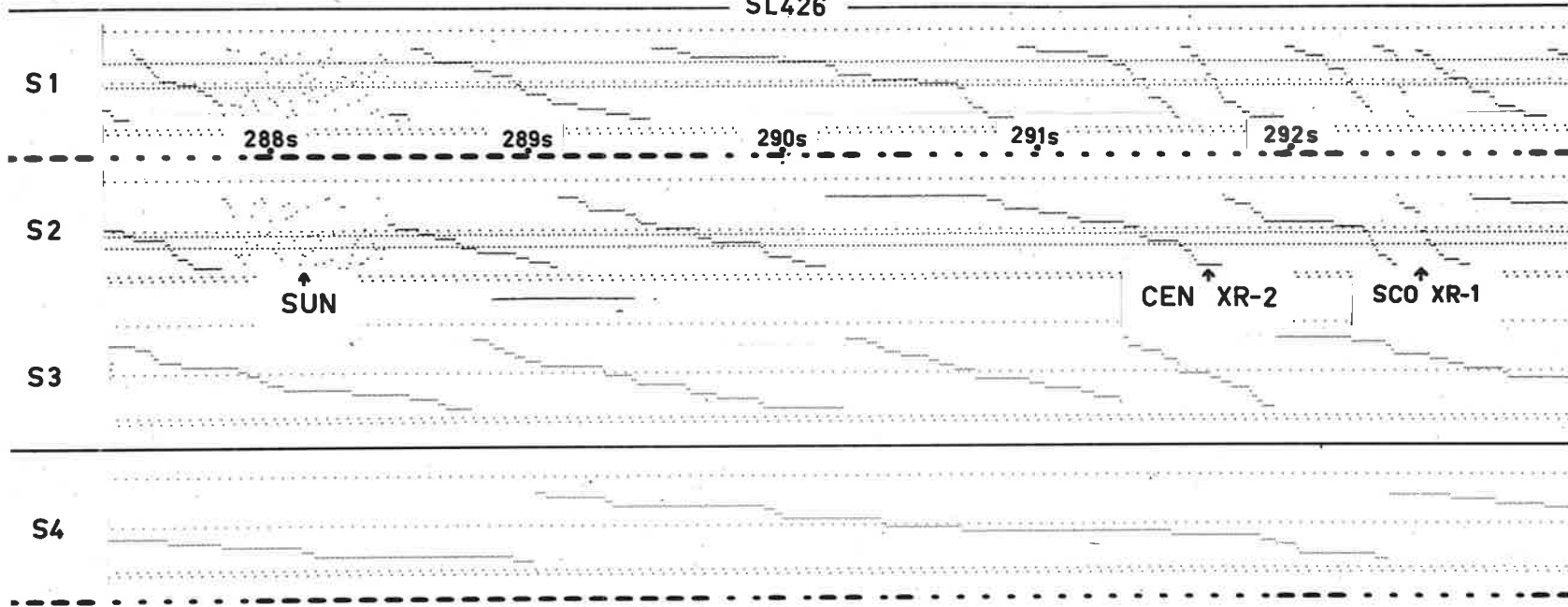
CHAPTER 4

ROCKET ATTITUDE

The motion of the rocket in the force free environment above the atmosphere is a well known problem in the dynamics of rigid bodies. The longitudinal OX axis of the rocket is an axis of symmetry. The moments of inertia about the two lateral axes are equal and much longer than the moment of inertia about the longitudinal axis. It can be shown, e.g. Symon. (1960), that the motion of such a body consists of a spin about the longitudinal axis and the precession of this axis about a cone; with both the spin and the precession in the same sense.

4.1 Description of Attitude Sensors

The Skylark carries four types of instrument to enable the attitude and motion of the rocket to be determined throughout the flight. The output of this standard instrumentation is shown on Figure 9 for Flight II. The first tube (top record) displayed the output from the two rate gyroscopes. The first measured the spin of the rocket; a positive rising trace corresponding to a spin which rotates the +OY axis of the rocket towards the +OZ axis, i.e. clockwise when looking forwards, full scale deflection being ± 200 degrees per second.

Initially as the rocket passed through the atmosphere the spin rate varied, but after 70 seconds the gyroscope indicated a stable positive spin of about 30 degrees per second. The pitch gyroscope measured the rotation about the OY axis, positive pitch rotated the +OZ axis towards the +OX axis (the forward direction), and the instrument was calibrated for a full scale deflection of ± 20 degrees per second. The output of this gyroscope after 70 seconds consisted of a sinusoidal oscillation about a zero value. These oscillations were due to the instantaneous spin axis being displaced from the +OX axis by the precession motion of the rocket. The spin axis however precessed about the OX axis and so its projection on the +OY axis produced the sinusoidal pitch response.

Three orthogonal accelerometer outputs were displayed on the second tube, Figure 9. Positive accelerations produced rising telemetry displays and full scale deflections corresponded to the range -3 g to +15 g for the OX accelerometer and -1.8 g to +1.8 g for the OY and OZ axes. The OX accelerometer showed the resultant acceleration due to first the Cuckoo boost motor which was jettisoned at +5 seconds, when the Raven motor ignited producing a peak acceleration of 10 g and finally dying out at +51 seconds. From 51 seconds to 428 seconds, when the head and motor were separated prior to reentry, the accelerometers indicated that the rocket underwent no acceleration and was in a force free environment. A calibration trace verified that the voltage supplied to the accelerometers did not change.

Three flux gate magnetometers measured the components of the geomagnetic field along the three rocket axes and their output was displayed on tube 3, Figure 9. These were calibrated over the range +0.7 to -0.7 oersteds (compared to the geomagnetic field strength of about 0.6 oersteds). However, the ground calibration of the magnetometers was of limited value because significant changes in the magnetisation of the round occurred when the rocket left the launcher, and again when the Cuckoo boost motor was jettisoned.

The MY and MZ outputs were identified by noting the order of 'dots' on the high speed record and verified by using the direction of spin obtained from the rate gyroscopes to determine whether MY or MZ would reach a maximum first. The MY and MZ magnetometer results showed the spin of the rocket while the slow change in MX was due to the motion around the precession cone. A rising trace on the telemetry record indicated that the geomagnetic field had a positive component along the positive direction of the rocket axis.

There were four sets of crossed sunslits located at the +OY, +OZ, -OY, -OZ axes of the rocket, each consisting of a vertical and a diagonal slit backed by a photo-sensitive element. The diagonal slit was inclined at 45 degrees to the vertical slit, so that the time difference between the output from the two slits was a function of the angle that the sun was above or below the equatorial plane of the rocket. This time displacement was measured from the high speed

records (2 inches per second) providing accurate information on the
angle between the sun and the OX axis. There were periods during both
flights when the sun was more than 40 degrees away from the OYZ plane
and it could not be observed by the diagonal slit. The output pulse
from each slit had a different amplitude, four positive and four
negative, and were all combined on one output line and transmitted on
four telemetry channels giving a sampling rate of 320 times per second.

4.2 Attitude Solution Method

Already, from the discussion of the magnetometers, sunslits and
rate gyroscopes a general idea of the motion has been presented. The
rate gyroscopes showed that on Flight I the rocket had a positive
spin while on Flight II it had a negative spin. The Y and Z
magnetometers confirmed the spin motion, while the X magnetometer
indicated a slow precession cone which was not completed by the end of
the flight, and from the peak to peak amplitude, must have had a large
opening angle. The diagonal sunslit observed the sun for the two
periods during both flights, and showed that the sun was perpendicular
to the OX axis at some stage during these periods. By using the
additional fact that the OX axis was approxinately ten degrees west
of the zenith as the rocket came out of the atmosphere, a preliminary
attitude solution can be obtained. This section will present the methods
used to obtain more accurate information on the attitude of the rocket

and hence the direction of look of the counters throughout the flight.

The rocket motion can be considered to be made up of two components, the motion of the OX axis around the precession cone, and the spin of the OY, OZ axes about the OX axis. Most of the following discussion will be concerned w   locating the OX axis; the phase of the OY and OZ axis can be easily found from the times of sun sighting by the vertical sunslits.

Initially, the behaviour of the angle between the OX axis and a fixed direction in space during the flight will be investigated. In the sketch OA is a fixed direction in space, OP is the axis of the precession cone about which OX moves.

The angle $\underline{/POX}$ is the half opening angle of the precession cone and is a constant ρ. Since OP and OA remain fixed in space, the angle POA is also a constant. Angle $\underline{/XPA}$ monotonically increases during the flight and can be expressed as $\Omega t + \phi$, where Ω is the precession rate. Hence by spherical trigonometry,
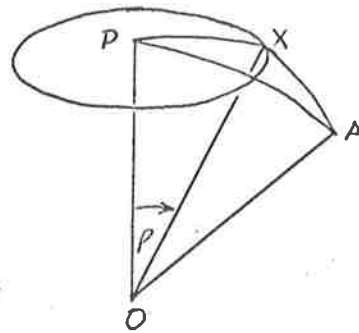
$$\cos \underline{/XOA} = \cos\rho\cos\underline{/POA} + \sin\rho\sin\underline{/POA}\cos(\Omega t + \phi)$$

$$= A + B\cos(\Omega t + \phi) \qquad (4.1)$$

where A and B are constants during the flight. If A and B can be

determined then

$$\rho + \underline{/POA} = \arccos(A - B)$$

$$|\rho - POA| = \arccos(A + B) \qquad (4.2)$$

and values can be determined for ρ and $\underline{/POA}$ although it is not possible
to say which is which.

4.2.1 Magnetometer Data

Equation 4.1 is immediately applicable to the X-magnetometer whose
output is of the form $M\cos\underline{/XOM}$ where M is the geomagnetic field strength.
Hence Mx should be sinusoidal with its maxima and minima determined by
ρ and angle $\underline{/POM}$. It would be possible for Mx never to pass through
zero but in the present flights Mx showed a large variation and passed
through zero.

When the records early in the flight were examined, the magnetometer
outputs were observed to have undergone sharp changes as the rocket left
the launcher and again when the Cuckoo boost motor was jettisoned. It
was also possible that there could be a gradual change as the rocket
heated up in passing through the atmosphere. This meant that any ground
calibration of the magnetometers was of limited value in interpreting
the results. The two principle effects on the magnetometer readings
were first the permanent magnetism of the rocket which was equivalent
to a zero shift in the readings, and second the induced magnetism which

had the effect of amplifying the geomagnetic field and was equivalent
to a change in sensitivity. It was assumed that these effects were
constant throughout the part of the flight above 70 km.

Corrections for both effects were made by using the My and Mz
magnetometers to determine the angle $\underline{/XOM}$.

$$Mx^2 + My^2 + Mz^2 = M^2$$

$$My^2 + Mz^2 = M^2 \sin \underline{/XOM} \qquad (4.3)$$

The spin of the rocket caused the My and Mz magnetometers to alternately
have a positive and then a negative component. At the maxima and
minima of My, Mz must be zero, hence

$$My_{max} = \pm M \sin \underline{/XOM} \qquad (4.4)$$

By using the peak to peak values any zero shift was eliminated. The
correction for the change in sensitivity was made by effectively
calibrating the magnetometers in flight. From equation 4.4, if angle
$\underline{/XOM}$ is 90 degrees, $My_{max} = M = M^*$ and this occurred at least once
in both flights. Hence $\sin \underline{/XOM}$ was obtained by the ratio of the peak
to peak amplitude of the magnetometer output to its maximum for both
My and Mz.

There was however, one complicating factor, the geomagnetic field
changes appreciably with altitude. If the simple dipole approximation
is used the field strength can be expressed as

$$M = M_o \left[(R + h)/R \right]^{-3}$$

$$\simeq M_o (1 - 4.71 \times 10^{-4} h) \qquad (4.5)$$

where M_o is the sea level intensity and h is the altitude in kilometers.
More accurate calculations for Woomera (Herbert 1967) give

$$M = M_o (1 - 4.97 \times 10^{-4} h) \qquad (4.6)$$

Hence from equation 4.4

$$\sin \underline{/XOM} = M_{y\ max} / M_o (1 - 4.97 \times 10^{-4} h) \qquad (4.7)$$

This equation was used to determine the angle $\underline{/XOM}$ at each maximum of
the MY and MZ magnetometers. The general shape of the result was given
by equation (4.1 enabling the angle to be determined at all times
during the flight. Although this defined the position of the OX axis
relative to the geomagnetic field it has not defined the position of
the OX axis in space.

4.2.2 The Solar Sensors

The four sets of sunslits were located at +OY, +OZ, -OY, -OZ and
each set consisted of a vertical and a diagonal slit. Each slit had a
longitudinal field of view of about 120 degrees, and the diagonal slit
was inclined at 45 degrees to the vertical. For positive spin (rotating
OY towards OZ) and for the angle $\underline{/XOS}$ (where S is the sun) less than

90° the diagonal slit observed the sun before the vertical slit. This time difference enabled the angle between the rocket OX axis and the sun to be determined.

On the accompanying sketch of the OY sunslits, the XY-X plane represents the vertical slit and the DY-D the diagonal slit. The rocket was spinning about the OX axis with a slow precession motion, and so the sun followed a helical path on the sphere about the OX axis. Suppose the diagonal slit saw the sun at S, a perpendicular SA is constructed to the YZ plane. Consider the spherical triangle YAS, angle $\angle$SYA is 45°, angle $\angle$YAS is 90°, hence
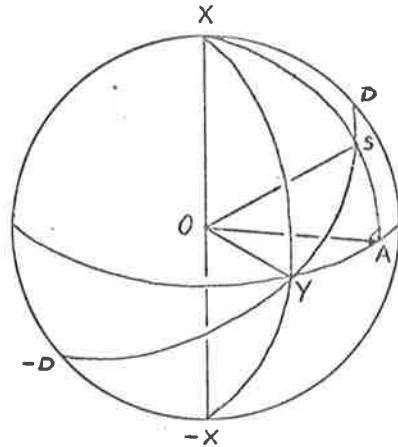
$$\cos \angle\text{YOA } \cos 90^{\circ} = \sin \angle\text{YOA } \cot \angle\text{SOA} - \sin 90^{\circ} \cot 45^{\circ}$$

$$\tan \angle\text{SOA} = \sin \angle\text{YOA}$$

$$\cot \angle\text{SOX} = \sin \angle\text{YOA} \qquad\qquad (4.8)$$

The angle $\angle$SOX defined the position of the sun with respect to the OX axis. The angle $\angle$YOA was found from the time displacement between sighting the sun in the diagonal and the vertical slits $\triangle$T and the total time before the vertical slit is again sighted, T.

Since the sun followed
a helical path up or down the
sphere, the angle $\angle SNR$ was
obtained by

$$\frac{\angle SNR}{360^\circ} = \frac{\Delta T}{T}$$

but $\angle SNR = \angle YOA$

$$\therefore \quad \angle SOX = \text{arcot}\left[\sin\left(\frac{360\,\Delta T}{T}\right)\right] \qquad (4.9)$$
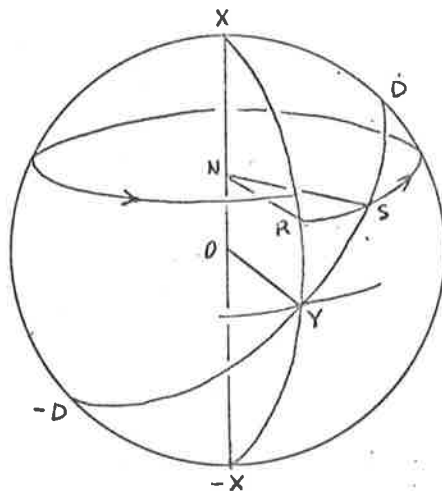
This was valid provided $\angle SOX$ changed monotonically during one
revolution. This was a good approximation because of the small
distance that the OX axis moved per spin period.

The angle $\angle SOX$ was calculated for all diagonal sunslit data, i.e.
whenever the sun was within 40° of the OYZ plane. This provided two
periods of data, one early and one late in the flight.

4.2.3 Obtaining the Position of the OX Axis

The angle that the OX axis makes with the geomagnetic field has
been determined throughout the flight while the angle that the OX
axis makes with the sun line has been determined for parts of the flight.
The position of the OX axis was obtained by triangulating at times
when both types of data existed. The position of the sun in celestial

coordinates (right ascension and declination) was obtained from the 1967 Ephemeris. The geomagnetic field at Woomera was more uncertain, the best experimental value located was 5° $47'$ E declination and 63° $06'$ dip (Bureau Mineral Resources, Bulletin Number 98). Subsequent calculations using the harmonic expansion of the geomagnetic field (Hurwitz et al. 1966) gave the field as 6.2° E declination, 62.8° dip at launch and 5.4° E declination, 62.4° dip at the end of the flight (this subroutine was kindly lent by Mr. A. Beresford). This computed field direction changed by 0.6° during the flight and was in reasonable agreement with the experimental values which were used for the attitude analysis.

The zenith and the geomagnetic field direction were converted to celestial coordinates (Roy 1965) using the geographic coordinates of the Woomera range -30° $56'$ S and 136° $31'$ E. During the seven minutes of flight the rotation of the earth caused the right ascension of the zenith and the geomagnetic field to increase by 2°.

The positions of the sun and magnetic field, Table 4, were marked on a 12 inch celestial globe, and the position of the OX axis obtained by swinging arcs corresponding to the angles SOX and MOX obtained from the sunslit and the magnetometer data. The ambiguity, as to which side of the sun-geomagnetic field line the OX axis was located, was resolved by knowing the direction of spin from the rate gyroscopes and the order of sighting of the sun and the magnetic field. In addition,

the fact that the rocket should come out of the atmosphere somewhat west of the zenith was used as a check on the position.

TABLE 4

CELESTIAL COORDINATES AT THE TIME OF LAUNCH

	Flight I		Flight II	
	R A	declination	R A	declination
Sun	0 h 50 m	5° 21'	1 h 52 m	11° 32'
Zenith	22 h 25 m	-30° 57'	21 h 38 m	30° 57'
Magnetic Field	22 h 35 m	-4° 10'	21 h 46 m	-4° 10'

This triangulation procedure produced two sections of the precession cone which were completed assuming it was circular and that the angular velocity of the OX axis around the cone was constant. For Flight II the two sections were obviously part of a circle and so the resultant precession cone was well defined. On Flight I the sun and the magnetic field were only separated by 33 degrees and the OX axis moved almost directly in line with them early in the flight, hence small errors in the sun or magnetic field angle produced large errors in the position of the OX axis. In this case the two parts of the cone were not part of a circle, although a circle of best fit was drawn.

4.2.4 Orientation of OY, OZ axes

The orientation of the spin axis of the rocket has now been determined throughout the flight. The phasing of the OY and OZ axes was obtained from the times when the vertical sunslits observed the sun. If the direction of look of the counters at -OZ at time T was required, and the preceding sun sighting by the -OZ vertical sunslit was at T1 and the next sun sighting at T2, then the angle after the sun was

$$\theta = 360 \times \left(\frac{T - T1}{T2 - T1}\right) \qquad (4.10)$$

For the preliminary attitude solution a frame was constructed that fitted over the celestial globe at the zenith and indicated the plane of the horizon, measuring it off in 360° of azimuth. Equally, when placed on the position of the OX axis it indicated the OYZ plane around which the angle from the sun sighting could be measured.

For greater accuracy on Flight II a program was written by Mr. Francey to determine the OYZ plane and also the direction of look of the counters in this plane. The attitude and size of the precession cone was fed in as initial data. The times of sun sighting could not be used as input data because the OX axis passed very close to the sun, and so times of sighting the centre of the precession cone had to be used. The times between these sightings should have been constant but

gradually decreased during the flight from 13 seconds soon after launch to 12.5 seconds at the end of the flight (4%). The program then gave the positions of the proportional counters throughout the flight.

4.3 Attitude Solutions - Results

The attitude solutions obtained for each flight by the methods of the last section will be referred to as the UAT solutions. In addition to these solutions the British Aircraft Corporation (BAC), Bristol, U.K., used a least squares fit to the sun slits and magnetometer outputs to determine the attitude through the flight (Herbert 1967). Their method was supposedly considerably more rigorous than that used for the UAT solution, but their results were not very satisfactory.

The different solutions were tested by their ability to predict the time when the counters should observe Sco XR-1, and when the counters or the sunslits observed the sun. For Flight I, Cen XR-2 was observed both at the beginning and near the end of the flight, so it was necessary for the solution to give consistent positions for both sightings.

The UAT solution for Flight I has already been mentioned as somewhat suspect because of the lack of a circular precession cone. The best fit circular cone failed to give consistent positions for the

two sightings of Cen XR-2 although it gave a good position for Sco XR-1.
BAC supplied three solutions for Flight I, each an improvement on the
one before. The final solution gave consistent positions for Cen XR-2
and a good position for the sun, but needed to be rotated 5 degrees
about the sun before it gave a position for Sco XR-1 accurate to
better than 1 degree. Such a rotation would imply an error of 2.5
degrees in the position of the magnetic field. Since the UAT solution
on this flight contained bigger uncertainties this rotated solution
was taken to represent the motion.

For Flight II, the UAT solution gave very satisfactory results
for Sco XR-1 and was selfconsistent. The BAC solution on the other
hand was not able to give accurate positions for the sun or for
Sco XR-1. Hence the UAT solution was used for this flight. The
parameters of the accepted solutions for both flights are listed
Table 5.

TABLE 5

PARAMETERS OF THE MOTION

	Flight I	Flight II
Spin Rate	33.6°/sec	28.2°/sec
Precession Rate	0.87°/sec	0.65°/sec
Half Opening Angle of Cone	66°	66.3°
Coordinates of Axis of Precession Cone	23.0 hr RA -79°dec	17.6 hr RA 22.8°dec

CHAPTER 5

CELESTIAL X-RAY OBJECTS - SKYLARK RESULTS

The data received from the rocket consisted of a set of four staircase voltages each sampled 80 times per second. A section of the telemetry record is shown in Figure 10. The telemetry records S1 and S2 are outputs from the 2 to 5 keV and 5 to 8 keV pulse height analyser channels of one detection system and S3 and S4 are similar outputs of the second detection system. Each step in the telemetry record corresponds to one pulse in the pulse height analyser channel. The detection systems look in opposite directions so that the observation of a source in one system was delayed by a time equal to half of the spin period from the observation in the other detection system. For analysis the number of counts per 0.1 seconds was obtained from the raw data and the resulting countrates for some representative scans are shown in Figure 11.

During the initial part of the flight, there was an abnormally high countrate, but by the time an altitude of 50 km had been attained, all of the system was responding normally. Between 50 and 70 km the countrate was due to high energy charged particles, gamma rays and secondary particles produced by nuclear interactions in the rocket.
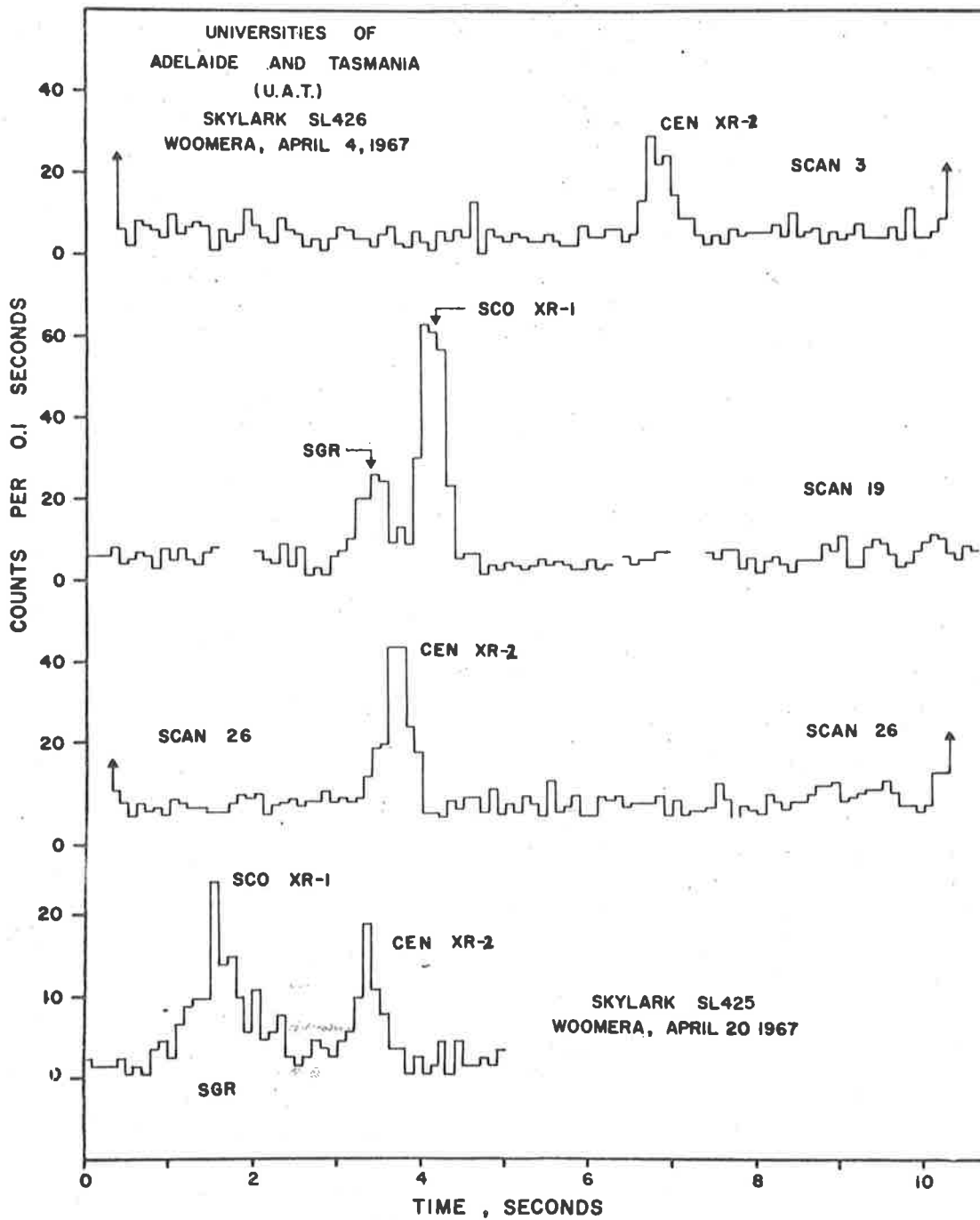
Figure 11. The countrate observed during several representative scans.
The increased countrate at the ends of some of the scans is due
to the detection of solar X-rays.

This countrate will be referred to as the 'high energy background' and was present throughout the flight.

Between 70 and 100 km the countrate underwent a gradual increase due to the detection of celestial X-rays which did not penetrate any further into the atmosphere (see Section 5.2). The magnitude of the increases depended on the direction of look of the counter, whether up or down, and are listed in Table 6. The increase observed when the counters looked at the atmosphere was caused by reflected solar X-rays. This albedo flux and the scattering processes which produce it are discussed in Chapter 6.

TABLE 6

THE INCREASE IN COUNTRATE WITH ALTITUDE

		50 - 70 km counts sec^{-1}	Above 110 km	
			UP counts sec^{-1}	DOWN counts sec^{-1}
FLIGHT I	S1	5.2 ± 0.5	17.4 ± 0.8	16.4 ± 0.7
	S2	5.1 ± 0.5	7.6 ± 0.4	5.2 ± 0.5
FLIGHT II	S1	6.2 ± 0.5	18.1 ± 0.9	10.6 ± 0.7
	S2	5.8 ± 0.5	9.4 ± 0.7	5.1 ± 0.5

Low energy charged particles, and in particular electrons, could contribute to the increase observed between 70 and 90 km. However, the detection systems were comparatively insensitive to low energy charged particles as they only accepted particles which deposited between 2 and 8 keV in the proportional counter. This means that a charged particle must have enough energy to penetrate the beryllium window of the counter and yet emerge with less than 8 keV residual energy. This is equivalent to specifying an energy interval of less than 1 keV at about 90 keV for the incident electrons. Electron fluxes large enough to produce the observed countrate have sometimes been observed (O'Brien 1964). However, such an electron flux would give more counts in the high energy channel due to the variation of the rate of energy loss with total energy in the beryllium window, whereas the observed countrate increase was much larger in the low energy channel.

Above 100 km there was very little attenuation of the incoming celestial X-rays by the atmosphere (Section 5.2) and the discrete X-ray sources were observed superimposed on a background countrate due to the diffuse X-ray flux and the high energy particles, Figure 11. Both flights observed X-rays from the sun but these saturated the telemetry system even at the most glancing sighting and so only enabled a lower limit of 2000 counts cm^{-2} sec^{-1} to be determined. A solar X-ray flux of 9×10^{4} photons cm^{-2} sec^{-1} was required to produce the observed

albedo X-ray flux (Chapter 6).

The most important result of the Skylark flights was the discovery of a strong source of X-rays in the constellation Centaurus, denoted Centaurus XR-2 or Cen XR-2. When first observed, its intensity was 75% of that of Sco XR-1 but by the time of the second flight it had decreased in intensity and its spectrum had become softer. This variability has been confirmed by other experimenters (Chodil et al. 1967b; Cooke et al. 1967) and will be discussed in more detail in Section 5.5.

X-rays were also observed from Sco XR-1 and the group of sources near the galactic centre. The Sco XR-1 results, discussed further in Section 5.4, provided a reference for the comparison of the Cen XR-2 results of the two flights and also with other experimenters. The individual sources at the galactic centre could not be resolved, nevertheless, the total flux from the region was consistent with the intensities observed by Friedman et al. (1967a).

The spin axis precessed by about 10 degrees during each revolution and so the counters covered the sky with scans which were, at most, 10 degrees apart. The slat collimators in front of the counters were $10.5^{\circ} \times 35^{\circ}$ full angles at half transmission with the long axis parallel to the spin axis. Any discrete source of X-rays would therefore be observed on at least six consecutive scans.

Along any given scan a discrete source would give a triangular response with the base equal to T x 21/360 seconds where T is the spin period, i.e. 0.61 seconds for Flight I and 0.73 seconds for Flight II. The staircase outputs were divided into 0.1 second segments for analysis and the counts per 0.1 second were obtained for each channel throughout the flight. Hence, for any source, there were about six countrate data points which were fitted to the triangular response function by the least squares method (Appendix A).

Each source was observed on at least six consecutive scans. In order to determine the position of the source with respect to these scans and also the flux corresponding to normal incidence, it was necessary first to obtain the response function from scan to scan. The attitude solution was used to determine the angular separation between the points on adjacent scans where the source was observed. The collimator had triangular response with a 35° full angle at half transmission in the direction normal to the scan paths. The countrate data for the individual scans were fitted to the theoretical response, derived from the collimator acceptance angle and the angular separation between scans, by the least squares method. This determined the position of the source normal to the scan direction and also its flux for normal incidence on the counter. The least squares procedure is discussed in more detail in Appendix A.

5.1 Positions of Cen XR-2 and Sco XR-1

The position of Sco XR-1 has been accurately measured by a modulation collimator to an accuracy of 1 min of arc (Gursky et al. 1966). The position measured by the present experiment is, therefore, a valuable check on the accuracy of the attitude solution and the collimators. The resulting positions for Sco XR-1, Table 7, are in error by an angle approximately equal to the least squares errors. Unfortunately the errors in the attitude solution are not constant through the flight so that the accuracy of the position for Cen XR-2 could be worse than that for Sco XR-1.

TABLE 7

POSITIONS OF SCO XR-1

	Position		Least Squares	Error
	R A	declination	Error Circle	(note 1)
Flight I	16 h 20 m	-15.3°	1.0°	1°
Flight II	16 h 25 m	-16.2°	1.5°	2°

note 1 : error is the displacement from the position obtained by

Gursky et al. (1966) 16 h 17 m, -15.5°.

TABLE 8

POSITIONS OF CEN XR-2

Date	Group	Position		
		R A	Declination	
April 4	UAT	$208° \pm 6°$	$-63° \pm 3°$	
April 10	LEIC	$200° \pm 4°$	$-60° \pm 2°$	Cooke et al. 1967
April 20	UAT	$210° \pm 6°$	$-64.5° \pm 3°$	
May 18	LRL	$196° \pm 5°$	$-62° \pm 2.5°$	Chodil et al. 1967b
Oct. 15	MIT	$196.5° \pm 3°$	$-64° \pm 2°$	Lewin et al. 1968c
Oct. 24	MIT	$197° \pm 6°$	$-64.5° \pm 3°$	Lewin et al. 1968c

Note : the MIT positions were obtained by a balloon experiment. It

must be assumed that the source they observed at energies $> 20\,keV$

is the same as that observed at rocket energies $\sim 3\,keV$.

The positions of Cen XR-2 are listed in Table 8 together with the

results of other experimenters. There is a disturbing lack of agreement

between the different experiments which precludes making any good

optical identification. Nevertheless, optical searches of the region

have been made by Blanco et al. (1968b) and Eggen et al. (1968) who

have suggested tentative optical identifications. Not surprisingly,

they have suggested different objects as being the optical counterpart of Cen XR-2. Eggen and Lynga (1968) in another search have shown that the region of the sky is very rich in unusual objects, further emphasising that no conclusive optical identification will be possible unless further X-ray results of greater angular precision can be obtained.

5.2 The Absorption of X-rays in the Atmosphere

It is necessary to know the effect of the residual atmosphere above the rocket on the incoming celestial X-rays. The absorption of X-rays depends on their energy and on the zenith angle of their arrival.

The intensity of X-rays reaching the rocket from a source of strength I_o is given by

$$I = I_o \exp(-u\int\rho\,dx) \qquad (5.1)$$

where u is the mass absorption coefficient in gm^{-1} cm^2, and $\int\rho\,dx$ is the amount of matter traversed in gm cm^{-2}. The mass of atmosphere along the line of sight from various rocket attitudes and at various zenith angles was calculated from the US Standard Atmosphere (1962) and is shown in Figure 12. The mass absorption coefficient of air

THICKNESS OF ATMOSPHERE BETWEEN
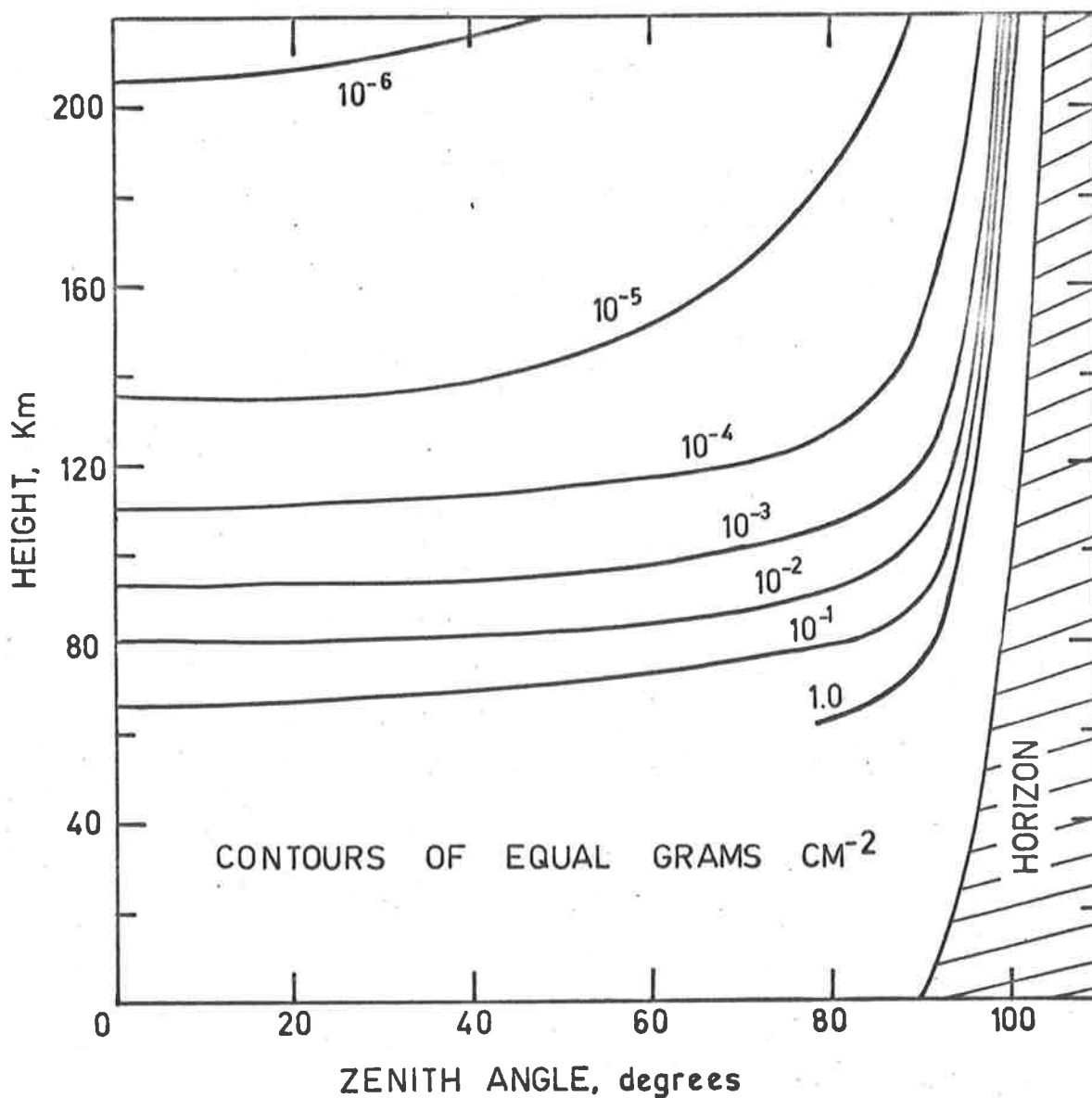ROCKET AND CELESTIAL OBJECT
(BASED ON U.S. STANDARD ATMOS 1962)

Figure 12.   Mass of atmosphere between the rocket and a celestial object.

(Victoreen 1949) is shown in Figure 13. The joint use of these two figures and Equation 5.1 allowed the attenuation of any given energy X-rays to be determined for any altitude and zenith angle. Some representative values are shown in Table 9.

Provided $\int \rho dx$ is less than 10^{-4} there was negligible absorption over the energy range 2 to 8 keV, and this was satisfied at altitudes of greater than 120 km and zenith angles less than $80°$. All of the Cen XR-2 and the Sco XR-1 count rate data used in the analysis satisfied this criterion.

TABLE 9

ATTENUATION OF X-RAYS

Mass of Air gm cm^{-2}	Altitude (1) km	Transmission Coefficient	
		2 keV	6 keV
10^{-2}	80	.09	.79
10^{-3}	93	.64	.98
10^{-4}	108	.96	1.00

Note 1 : zenith angle = 0 degrees

MASS ABSORPTION COEFFICIENT
FOR AIR

$I = I_0 \exp(-\mu \rho x)$

argon K-edge
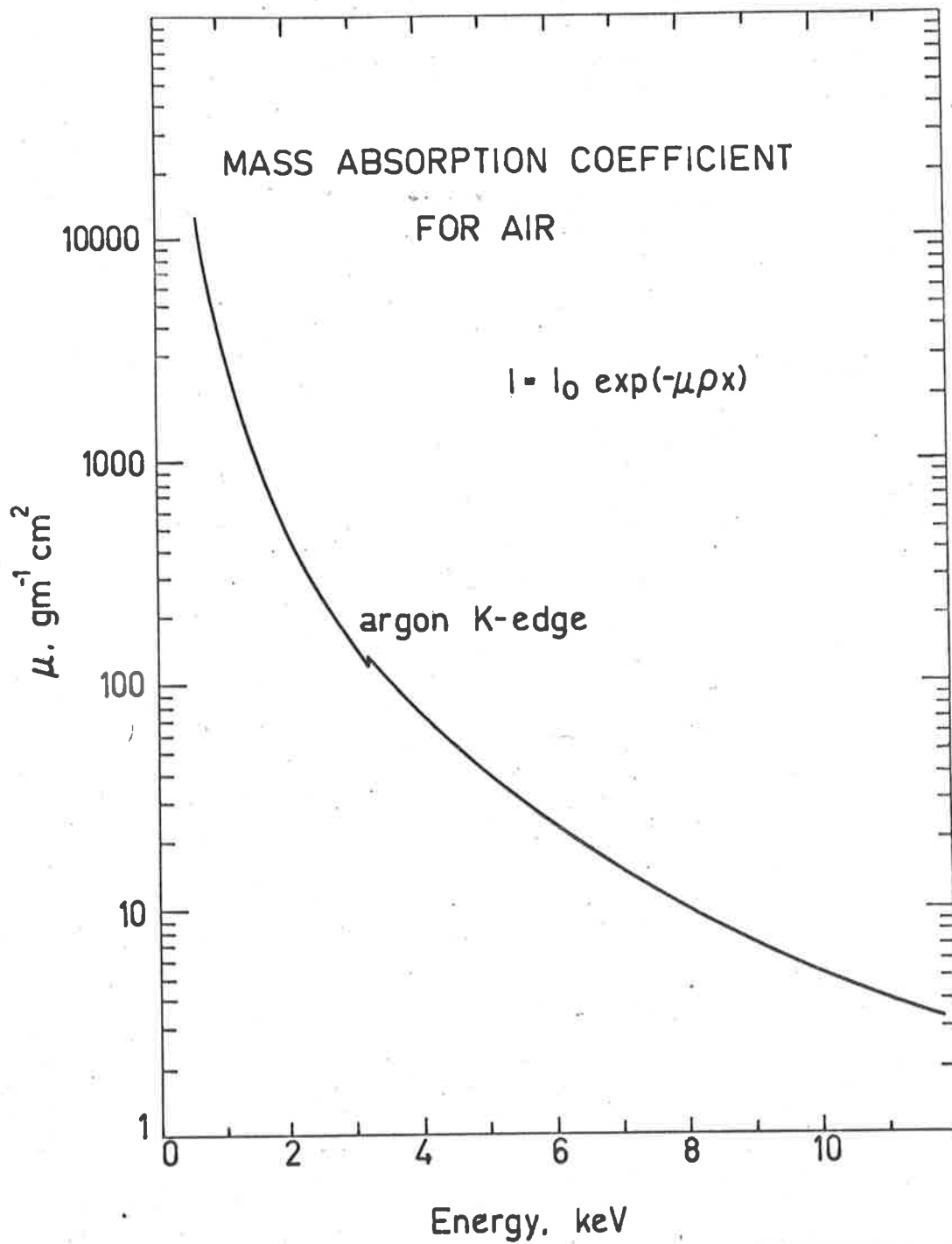
Figure 13.   Mass absorption coefficient for air (Victoreen 1949).

5.3 Spectral Analysis - Method

The pulses from the proportional counters were analysed by a
two channel pulse height analyser with the channels set to accept
photons with energies in the ranges 2 to 5 keV and 5 to 8 keV. This
section will discuss the methods used to reconstruct the incident
X-ray spectrum from the count rate data.

The problem was initially turned around, the incident X-rays were
assumed to have various two parameter spectra and the resulting
countrates in the pulse height analyser channels were calculated. The
three most likely mechanisms that could produce celestial X-rays are
bremsstrahlung from a thin hot plasma, synchrotron emission and
blackbody radiation (Section 1.3). Each of these processes gives a
continuous spectrum of X-rays under conditions which might exist in
stellar objects. Electron bremsstrahlung from a thin hot plasma
(free-free transitions) produces an exponential spectrum of the form

$$\frac{dN}{dE}(E) \;=\; A_e \exp(-E/T_e)/E \quad \text{photons keV}^{-1} \text{ sec}^{-1} \text{ cm}^{-2} \qquad (5.2)$$

where T_e is the effective plasma temperature in keV. A blackbody
emits radiation with a Planck distribution,

$$\frac{dN}{dE}(E) \;=\; \frac{A_b E^2}{\exp(E/T_b) - 1} \quad \text{photons keV}^{-1} \text{ sec}^{-1} \text{ cm}^{-2} \qquad (5.3)$$

The spectrum of X-rays resulting from synchrotron radiation depends on the energy spectrum of the electrons, but if the electrons are assumed to have a power law spectrum then the X-ray spectrum is also power law (see Section 1.3), i.e.

$$\frac{dN}{dE}(E) = A_s E^{-\alpha} \text{ photons keV}^{-1} \text{ sec}^{-1} \text{ cm}^{-2} \qquad (5.4)$$

Although each of these formulae apply to idealised situations, they were assumed to represent the range of spectral types that could be expected from a celestial X-ray source. Although the two channel pulse height analyser results did not contain enough information to differentiate between these three types of spectra, the value of A and the spectral index (T_e, T_b or α) could be determined when the type of spectrum was specified.

Initially, the incident spectrum was assumed to be exponential, Equation 5.2, as Sco XR-1 had been reported to have this type of spectrum over the range 2 to 8 keV. This spectrum of X-rays was traced through the detection system to determine the resultant countrates in the pulse height analyser channels. The transmission of the photons through the beryllium window was calculated using the analytical expression for the mass absorption coefficient given by Victoreen (1949). The absorption in the xenon-methane mixture was greater than 99% for energies less than 6 keV and at most was 96% at 8 keV. Hence, it was assumed that all the photons transmitted by the

beryllium window were absorbed in the gas. The spectrum of photons in the counter gas was

$$\frac{dN}{dE}(E) = \exp\left[-\mu(E)\rho x\right] A_e \exp(-E/T_e) \tag{5.5}$$

where $\mu(E)$ is the mass absorption coefficient of beryllium, ρ is the density and x is the window thickness.

Most of the proportional counters had poor resolutions, the best exhibiting values of 20% full width at half maximum (FWHM) but others were as great as 70 to 100%, Table 2. The theoretical resolution of a proportional counter can be calculated from the statistical processes which take place and is approximately

$$FWHM = 44E^{-\frac{1}{2}} \% \tag{5.6}$$

The worsened resolution of the present counters was probably due to slackness in the anode wire producing variations in the multiplication factor for different pulses. In this case the resolution can be expressed as a combination of the theoretical resolution, which is energy dependent, and an energy independent factor to bring the resolution up to that observed at 5.9 keV with an iron 55 source, i.e.

$$FWHM = 44E^{-\frac{1}{2}} + \left[FWHM(5.9 \text{ keV}) - 18\right] \% \tag{5.7}$$

The spectrum of output pulses was then given by the convolution integral

$$\frac{dN}{dE}(E_o) = \int_o^\infty \frac{1}{\sqrt{2\pi}\,\sigma} \exp\left[\frac{-(E - E_o)^2}{2\sigma^2}\right] \exp(-\mu\rho x)A_e \exp(-E/T_e)E^{-1}dE \quad (5.8)$$

where σ = FWHM / 2.355 E. The effect of the counter resolution on the pulse height spectrum from the proportional counter is shown on Figure 14.

The counters flown on Flight II had significant end-effects and the spectrum was modified to simulate this. Observations with 5.9 keV X-rays showed that the pulse distribution could be considered to consist of two parts: a gaussian component containing two thirds of the counts, and a rectangle from zero energy to the incident energy containing one third of the counts. Equation 5.8 was modified for Flight II as follows

$$\frac{dN}{dE}(E_o) = \frac{2}{3}\int_o^\infty \frac{1}{\sqrt{2\pi}\,\sigma} \exp\left[\frac{-(E - E_o)^2}{2\sigma^2}\right] \exp(\mu\rho x)A_e \exp(-E/T_e)E^{-1}dE$$

$$+ \frac{1}{3}\int_{E_o}^\infty E^{-1}\exp(-\mu\rho x)A_e \exp(-E/T_e)E^{-1}dE \quad (5.9)$$

End-effects were avoided with the counters on Flight I by the use of field forming electrodes.

The countrate in each channel was obtained by integrating the pulse height spectrum over the ranges 2 to 5 keV and 5 to 8 keV. The two counters of the second detection system on Flight I underwent a
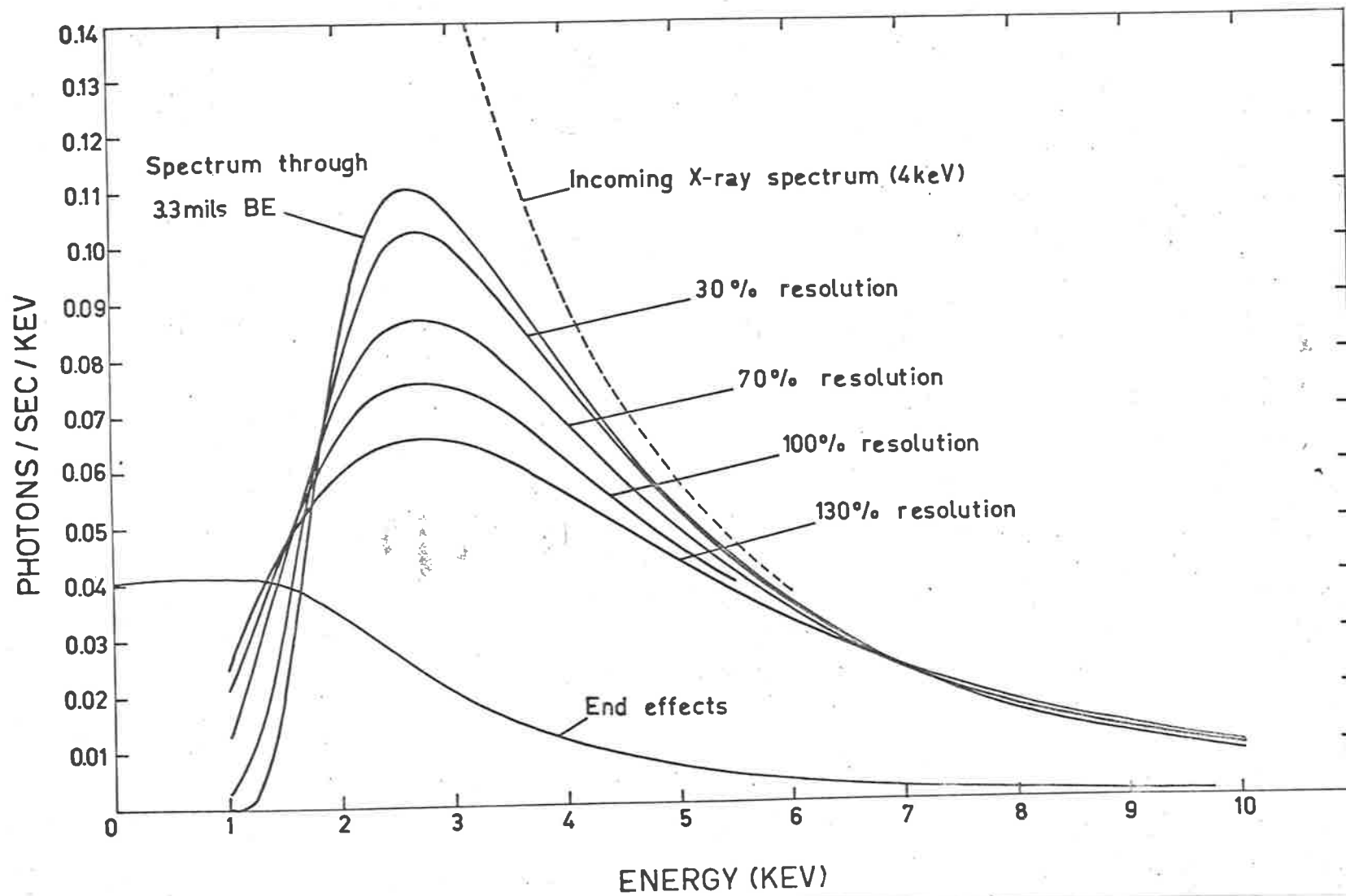
Figure 14. The effect of the counter resolution on an incoming exponential spectrum.

gain decrease before launch so that the 5.9 keV X-rays produced pulses of approximately 2.2 V.

The calculations were performed for spectral temperatures (T_e) over the range 2 to 6 keV. The ratio of the counts in the two pulse height analyser channels was a function of the temperature, enabling the temperature corresponding to the observed countrate ratio to be determined. Then, knowing the temperature, the sum of the observed countrate in both channels determined the value of the constant A. The earlier calculations were performed with A = 1, so that the real value of A was simply the ratio of the total predicted countrate to the observed countrate.

5.4   Sco XR-1 Spectra

The Sco XR-1 spectrum obtained by the method of the last section from the results of Flight II agreed well with the spectrum observed by other groups during April and May 1967 (Chodil et al. 1967b; Cooke et al. 1967). But on Flight I, although the total countrate was in agreement with the Flight II data, the ratio was very different and could not be explained by any reasonable spectral temperature. Data for Cen XR-2 obtained during Flight I also indicated an unreasonably hard spectrum. Measurements on the recovered round indicated that the second bias level of Flight I had changed since the preflight

calibration and that the channels were in fact covering the energy
ranges 2 to 4.5 keV and 4.5 to 8 keV. When this correction was
applied to the spectrum for Sco XR-1 the results for the two flights
were in excellent agreement. Of course, when the gain change of the
second detection system was allowed for, its bias levels now became
2.75 to 6.2 keV and 6.2 to 11.0 keV.

The resulting Sco XR-1 spectra agreed with the measurements of
Chodil et al. (1967b) on May 18, 1967, and Cooke et al. (1967) on
April 10, 1967, Figure 15. This Sco XR-1 spectrum is, however, about
half as intense as the spectrum obtained from earlier flights by the
Lawrence Radiation Laboratory group (LRL) (Chodil et al. 1965; Grader
et al. 1966). It is not certain whether this is an instrumental or a
real effect (see Section 1.1). However, the agreement between the
Sco XR-1 spectra measured by the various experiments in April-May 1967
establishes a reference for the comparison of the Cen XR-2 spectrum.

5.5 The Variability of Cen XR-2

The most significant result of the Skylark rocket experiments
was the observation of the variability of Cen XR-2. The UAT countrate
data were analysed on the assumptions of the three types of incident
spectra; exponential, power law and blackbody, and the results are
shown on Table 10. The source became less intense and the spectrum
became softer in the time between the two flights. A further flight

TABLE 10

UAT CEN XR-2 FLUXES

	Flight I Photons cm^{-2} sec^{-1}	Flight II Photons cm^{-2} sec^{-1}
Exponential	$(18.0 \pm .8)\exp -\dfrac{(E-4)}{(3.6 \pm .5)}$	$(12.5 \pm .7)\exp -\dfrac{(E-4)}{(2.4 \pm .4)}$
Power Law	$(4.0 \pm .3)\left(\dfrac{E}{4}\right)^{-(2.15 \pm .15)}$	$(2.5 \pm .2)\left(\dfrac{E}{4}\right)^{-(2.75 \pm .25)}$
Blackbody	$(0.33 \pm .02)E^2\left[\dfrac{\exp(4/T)-1}{\exp(E/T)-1}\right]$ $T = 1.04 \pm .06$	$(0.21 \pm .02)E^2\left[\dfrac{\exp(4/T)-1}{\exp(E/T)-1}\right]$ $T = 0.95 \pm .06$

by the LRL group showed that this weakening and softening of the spectrum continued at least to May 18, 1967 (Chodil et al. 1967b). Over the 40 days covered by these three flights the 2 to 8 keV flux decreased by a factor of 5.4 and the spectral temperature decreased by a factor of two. The results, from these three flights, are shown on Figure 15. This figure also shows the excellent agreement obtained for the Sco XR-1 spectrum for the three flights, enabling it to be used as a reference for comparison of the Cen XR-2 flux.
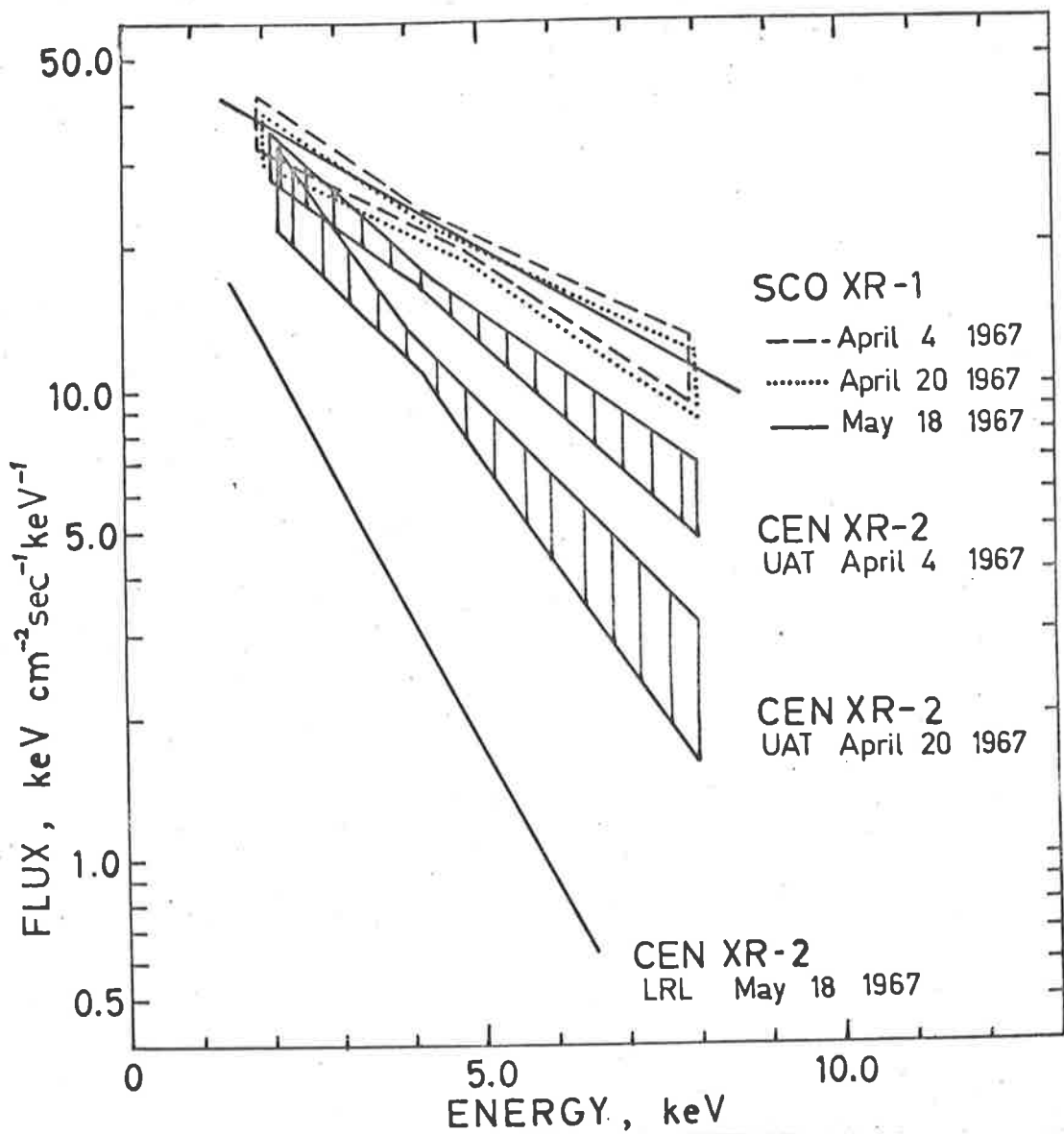
Figure 15. The variation in the spectrum of Cen XR-2 during April and May 1967. The good agreement between the Sco XR-1 spectrum observed on each flight serves as a reference between the experiments.

There have been several experiments that have obtained data on Cen XR-2 and these are all listed in Table 11. The early upper limit was obtained by the LRL group (Chodil et al. 1967a, 1968c) when their detector scanned the region without observing the source. The December 1966 experiment by Bowyer et al. (1968) had attitude problems, but they reported a 'strong' source at a position within 10 degrees of Cen XR-2. Then there was the UAT flight on April 4 followed by an experiment by the University of Leicester (LEIC) (Cooke et al. 1967) which noted that the Cen XR-2 spectrum was softer than that of Sco XR-1 but only reported the integrated 2 to 5 keV flux. The comparison of their flux with the UAT results would suggest that the Cen XR-2 passed through a maximum after April 4. However, it is doubtful if one can compare the results of different experimental groups this closely. After the second UAT flight and the LRL flight on May 18, LRL had another flight on September 28, 1967 (Chodil et al. 1968c) when they found that the source was too weak to observe.

All of the results to the end of September indicated that Cen XR-2 was a transitory phenomena, however Lewin et al. (1968a,c) have reported observing a source in the vicinity of Cen XR-2 using balloon-borne instrumentation on October 15 and 24, 1967. They report having observed a change in the flux of $35 \pm 17\%$ between their two flights. This measurement is at a higher energy than those employed by UAT and LRL, and if the spectrum is extrapolated to lower energies,

TABLE 11

THE VARIABILITY OF CEN XR-2

Date	Group	Exponential Temp. (keV)	Blackbody Temp. (keV)	Power Law Index	Flux erg cm^{-2} sec^{-1}	
Oct. 28 1965	LRL (1)				$< 2 \times 10^{-9}$	(2 - 8 keV)
Dec. 13 1966	Bowyer (2)				'strong'	
April 4 1967	UAT	$3.6 \pm .5$	$1.21 \pm .07$	$2.15 \pm .15$	$(1.5 \pm .1) \times 10^{-7}$	(2 - 8 keV)
April 10 1967	LEIC (3)				1.6×10^{-7}	(2 - 5 keV)
April 20 1967	UAT	$2.4 \pm .4$	$1.10 \pm .07$	$2.75 \pm .25$	$(1.0 \pm .1) \times 10^{-7}$	(2 - 8 keV)
May 18 1967	LRL (1)	1.5	.73	3.8	2.8×10^{-8}	(2 - 8 keV)
Sept. 28 1967	LRL (1)				$< 3 \times 10^{-9}$	(2 - 5 keV)
Oct. 15 1967	MIT (4)			1.2	4×10^{-9}	(20 - 52 keV)
Oct. 24 1967	MIT (4)				2.5×10^{-9}	(20 - 52 keV)
Feb. 29 1968	Buselli (5)				$(7.0 \pm 3) \times 10^{-10}$	(30 - 40 keV)

(1) Chodil et al. 1967b, 1968c; (2) Bowyer et al. 1968; (3) Cooke et al. 1967;

(4) Lewin et al. 1968a, c; (5) Buselli 1968.

the energy intensity in the interval 2 to 5 keV is almost equal to the upper limit obtained by LRL on September 28. However, the rate of cooling observed in the UAT and LRL flights would have suggested that Cen XR-2 would be well below the limit of detectability by October. Buselli (1968) had a tentative observation (at low statistical precision) of high energy X-rays from Cen XR-2 during a balloon flight on February 29, 1968. His fluxes are in agreement with the results of the second balloon flight of Lewin et al. (1968c). This opens the possibility that the source observed by the balloon experiments could be a time invariant object which is in approximately the same direction as the variable source observed by the rocket experiments. This matter clearly requires resolution through the performance of further surveys of this region of the sky, particular care being taken to obtain directional determinations of high statistical precision.

Friedman et al. (1967a) surveyed the Centaurus region for X-ray sources during an experiment on 25 April 1967. They did not observe a source at the position of Cen XR-2, but this could have been obscured by the horizon. It is possible, however, that the source Cen XR-1 at 217° R A and -63° declination with a flux of 0.17 counts $cm^{-2} sec^{-1}$ (2×10^{-9} erg $cm^{-2} sec^{-1}$) might be the same source as Cen XR-2. This would add further weight to the hypothesis of variability of the X-ray object.

The important results can be summarised as follows: the 2 to 8 keV
flux of Cen XR-2 increased by at least two orders of magnitude between
October 1965 and April 1967. During April and May 1967 the intensity
was observed to decrease and the spectrum become softer. In the five
month period from April to September its 2 to 8 keV flux had decreased
by at least a factor of 50. In October, 1967, high energy X-rays were
observed which appeared to come from Cen XR-2. This high energy flux
showed a small decrease of 35% over 9 days but then was constant over
the next four months.

Cen XR-2 is a unique source in X-ray astronomy in that it has
shown large scale variability and which has been observed by several
groups. The cooling rate of the source is very similar to the decay
rate of the light curves of supernovae and novae. Only further
experiments will be able to determine if Cen XR-2 was an unusual
phenomenon, or if it represents a transient stage in the life of most
X-ray stars. Some theoretical modes of Cen XR-2 are discussed in
Chapter 7.

5.6 Diffuse X-ray Background

The countrate due to the diffuse background was measured at a
time when the counter was not looking at, or near, any known sources.
The usual up-down difference could not be used because of the large

albedo X-ray flux from the earth (Chapter 6). The high energy charged particle component was assumed to be constant throughout the flight and so the countrate observed below 70 km was subtracted. Many higher energy measurements have shown that the diffuse background was best fitted by a power law spectrum (Seward et al. 1967; Gould, 1967). Hence, an incident power law spectrum was assumed and fitted to the data. The resulting spectral index $\alpha = 1.75 \, {}^{+\,1.7}_{-\,0.9}$ was in agreement with other experimenters who have obtained values between 1.6 and 2.0 over much larger energy ranges. The results are plotted, Figure 16, together with other measurements. The present results are slightly high, but not significantly so.
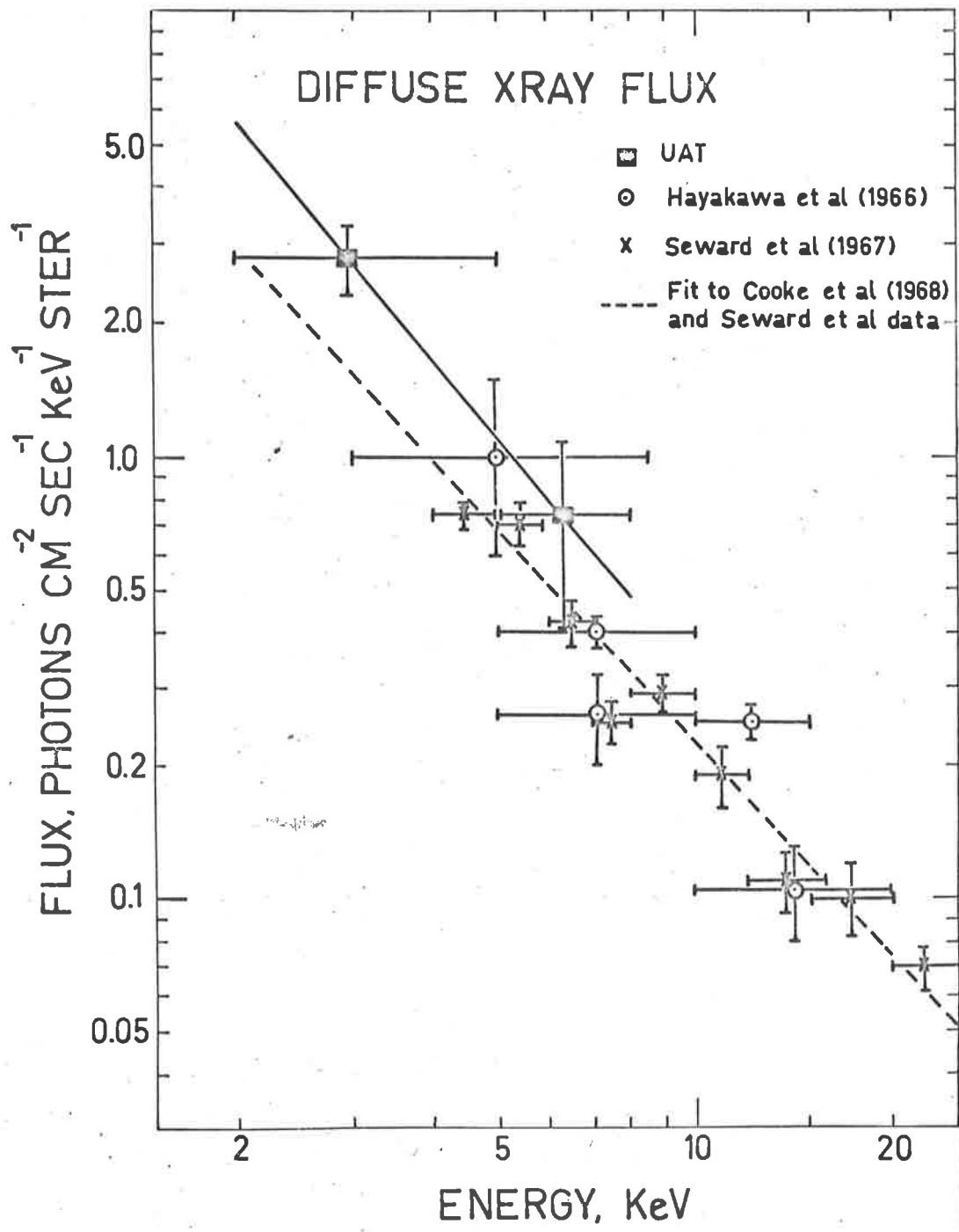
Figure 16. The diffuse flux observed on the UAT experiment compared with the results of other experimenters.

CHAPTER 6

THE X-RAY ALBEDO FROM THE EARTH

A flux of X-rays was observed from the direction of the earth during both flights. This albedo flux was comparable to the celestial diffuse X-ray flux in the 2 to 5 keV energy channel but was not observed in the 5 to 8 keV channel, showing that it had a soft spectrum.

The averaged countrates from four scans which passed close to the zenith are shown on Figure 17. If there were no albedo flux present the countrate should have decreased to the charged particle background when the counters looked at the earth. On Flight I, the scans through the zenith also passed through the sun and Cen XR-2, and the albedo flux showed a distinct peak on the horizon closest to the sun, Figure 17. The Flight II scans were normal to the sun-zenith line and did not show a peak in the albedo flux.

The direct solar flux saturated the detection system and only a lower limit of 2000 photons cm^{-2} sec^{-1} could be determined. However, the solar X-ray flux was expected to be considerably higher than this (Mandelstam 1965).

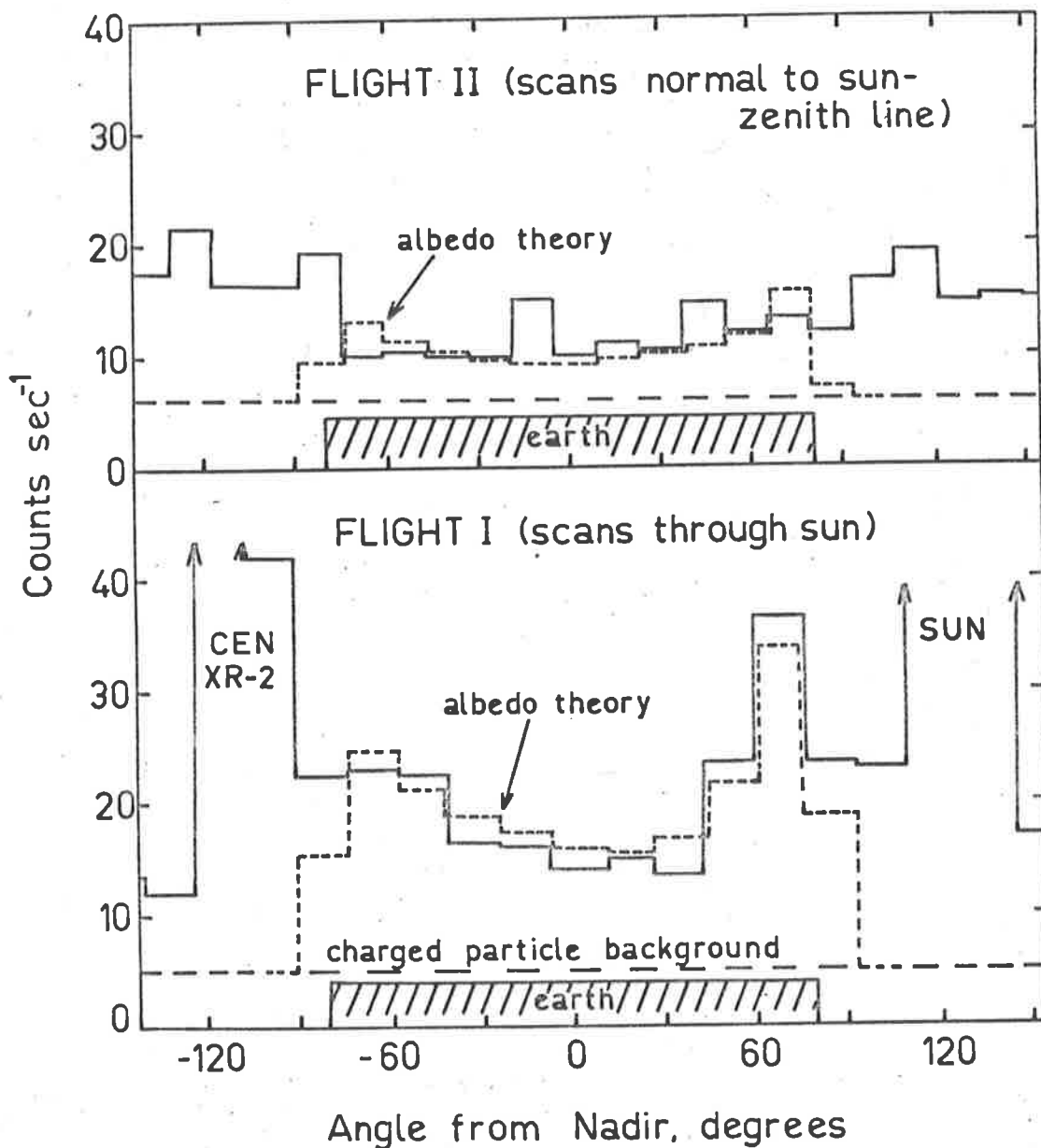Two processes contributed to the observed albedo: the scattering

95

Figure 17. Averages of five (Flight II) and four (Flight I) scans through the nadir showing the X-rays observed from the earth. The Flight I scans show the peak albedo at the horizon closest to the sun.

of the solar X-rays by molecular electrons, and the generation of
fluorescent K X-rays by the solar X-rays absorbed in the atmospheric
argon. Most of the X-rays incident on the atmosphere were absorbed
by the photoelectric effect in oxygen and nitrogen. Although the
recombination of the ion pairs produced low energy X-rays, these were
at 0.53 keV for oxygen and 0.39 keV for nitrogen, both of which were
considerably less than the lower energy channel.

6.1 Scattered X-rays

X-rays are scattered by individual free electrons according to
the Thomson cross section:

$$\frac{d\sigma_e}{d\Omega} = 3.976 \times 10^{-26}(1 + \cos^2\phi) \quad cm^2 \ ster^{-1} \qquad (6.1)$$

where ϕ is the scattering angle. A 3 keV photon has a wavelength
of 4 A, which is comparable with the diameter of the nitrogen atom,
and so the phases of the photons scattered from the different electrons
in the same atom would be closely related. In the limit of long
wavelength the amplitudes of the scattering function must be added
coherently, i.e. for an atom with atomic number Z, the cross section
would be proportional to Z^2. At short wavelengths there is no phase
relation and the cross section would be proportional to Z.

A theoretical treatment of the scattering process is given by Compton and Allison (1935). They show that for a monotonic gas the scattering cross section is

$$\frac{d\sigma_s}{d\Omega} = \frac{d\sigma_e}{d\Omega} \left[F^2 + (1 + \frac{2h\lambda}{mc} \frac{\sin^2\phi/2}{\lambda^2})^{-3}(Z - \Sigma f_n^2) \right] cm^2 \ ster^{-1}$$

$$(6.2)$$

where $d\sigma_e/d\Omega$ is given by equation 6.1, F is the atomic scattering factor and Σf_n^2 is the incoherent scattering function. Compton and Allison give tables of F and Σf_n^2 which are calculated from the electron wave functions of the atom. Both F and Σf_n^2 are functions of $\sin(\phi/2)/\lambda$.

For diatomic gases interference occurs between the scattering from the two atoms and the cross section for a molecule is given by

$$\frac{d\sigma_s}{d\Omega} = 2\frac{d\sigma_e}{d\Omega} \left[F^2(1 + \frac{\sin x}{x}) + (1 + \frac{2h\lambda}{mc} \frac{\sin^2\phi/2}{\lambda^2})^{-3}(Z - \Sigma f_n^2) \right]$$

$$cm^2 \ ster^{-1} \qquad\qquad (6.3)$$

where $x = 4\pi s_{mn} \sin(\phi/2)/\lambda$, and s_{mn} is the interatomic distance (1.09 A for nitrogen and 1.22 A for oxygen). The cross sections for nitrogen, oxygen and argon are shown on Figure 18, and are considerably above the sum of the cross sections for the individual electrons scattering incoherently (1 barn = 10^{-24} cm^2).
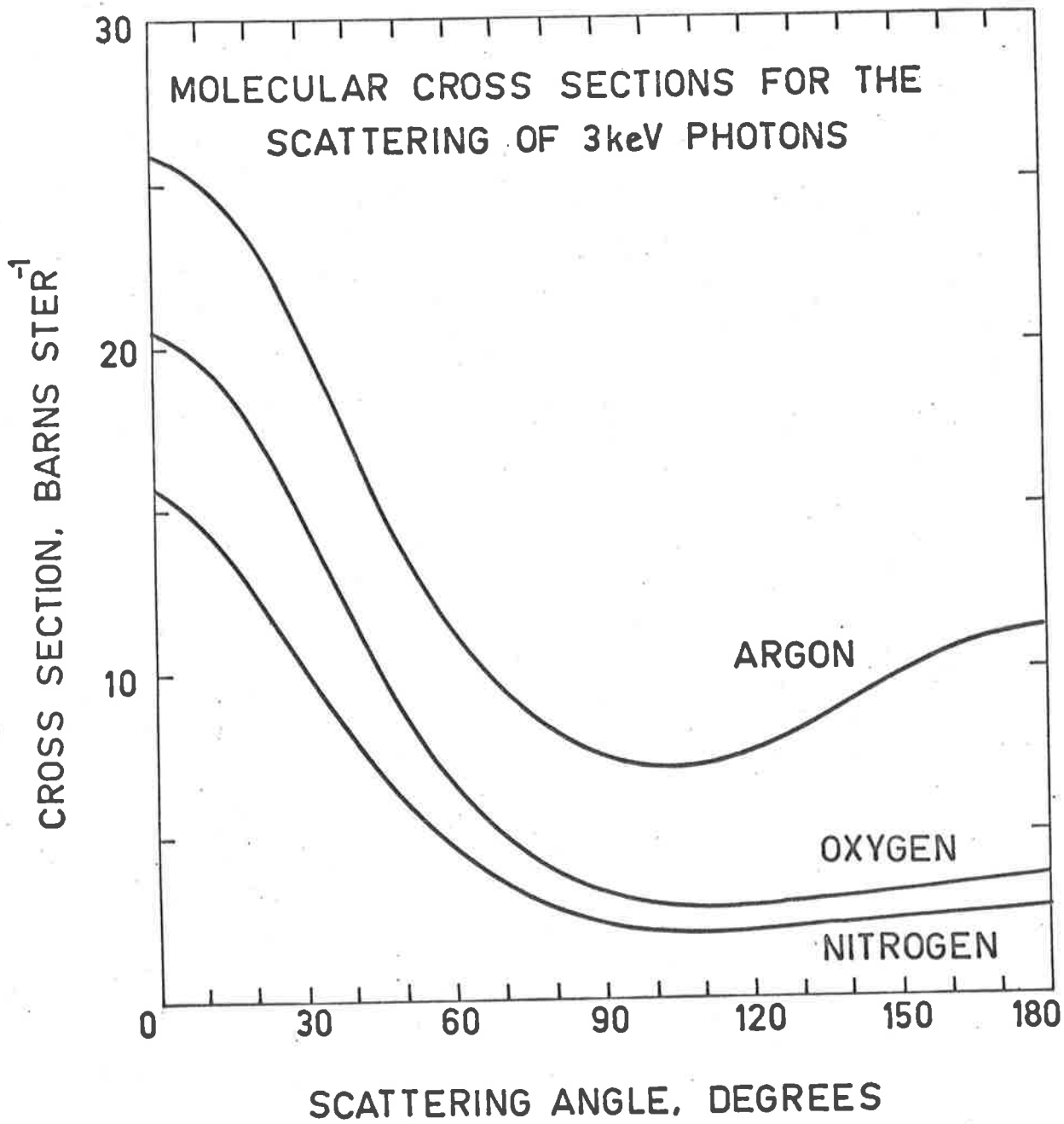
Figure 18. The X-ray scattering crossections for the atmospheric gases
(1 barn = 10^{-24} cm^2).

The photons can be absorbed by the photoelectric effect either before or after the collision. Consider an element of volume dV, area da and thickness dh in the atmosphere at an altitude h. The intensity of solar X-rays at this element is

$$I(h) = I_0 \exp\left[- \frac{\mu}{\cos\theta} \int_h^\infty \rho(x)dx\right] \qquad (6.4)$$

where I_0 is the intensity above the atmosphere, θ is the zenith angle of the sun, μ is the mass absorption coefficient of air, and $\rho(x)$ is the density at altitude x. The number of molecules n(h) in this volume element is

$$n(h) = \rho(h)(N/A)\, dhda \qquad (6.5)$$

where N is Avogadro's number and A the molecular weight. The number of scattered photons from these molecules is

$$\frac{dI_s}{d\Omega}(h) = I(h)\, n(h)\frac{d\sigma}{d\Omega} \qquad (6.6)$$

These photons can also be absorbed in the atmosphere so the intensity of X-rays finally reaching the rocket is

$$\frac{dI}{d\Omega} = \frac{dI_s}{d\Omega}(h) \exp\left[- \frac{\mu}{\cos\mathfrak{Z}} \int_h^\infty \rho(x)dx\right] \qquad (6.7)$$

where $\mathfrak{Z}$ is the zenith angle of the line from the scattering region

to the rocket. Combining the equations 6.4, 6.5, 6.6 and 6.7 and integrating over all values of h to get the scattered intensity gives

$$\frac{dI}{d\Omega} = I_0 \frac{N}{A} \frac{\cos\theta \cos\zeta}{u(\cos\theta + \cos\zeta)} \frac{d\sigma}{d\Omega}(\phi)da \qquad (6.8)$$

Since θ and ζ are measured at the point of scatter, their values can be calculated for a curved atmosphere. Most of the scattering and absorption in the atmosphere occurs in a layer about 20 km thick at about 80 km altitude. The collimator defines the total area of this layer that contributes to the albedo observed at the rocket. This area is

$$a = l^2\omega/\cos \qquad (6.9)$$

where l is the slant distance to the region of scatter and ω is the solid angle of the collimator. The scattering must also be integrated over the solid angle determined by the counter window area α ,

$$\Delta\Omega = \alpha/l^2 \qquad (6.10)$$

The resulting scattered X-ray flux observed by the counter is

$$I(E) = 2.08 \times 10^{22} I_0(E)\frac{\alpha\omega}{u(E)} \frac{d\sigma}{d\Omega}(\phi)\left[1 + \frac{\cos\zeta}{\cos\theta}\right]^{-1}$$

$$\text{photons sec}^{-1} \qquad (6.11)$$

6.2 Fluorescent X-rays

The production of fluorescent K X-rays from atmospheric argon also contributes to the albedo flux in the 2 to 5 keV range. The K-absorption edge for argon is at 3.2 keV, and above this energy 91% of the X-rays absorbed in argon will produce a K-shell vacancy. The argon fluorescent yield is 0.12 (Fink et al. 1966), hence, in 12% of the cases a K X-ray of 2.95 keV will be emitted as these vacancies are filled. The fraction (p) of the incident solar X-rays absorbed by argon (1.3% by weight in the atmosphere) is

$$p = 0.013\, \mu_{argon}/\mu_{air} \qquad (6.12)$$

When the absorption of the fluorescent flux in the atmosphere and the solid angle of the collimator are taken into account, as was done for the scattered flux, the total fluorescent flux reaching the proportional counters is

$$I_F(2.94) = 0.0012\alpha\omega \int_{3.2}^{\infty} I(E)\left[\frac{\mu(2.94)}{\mu(E)} + \frac{\cos\zeta}{\cos\theta}\right]dE$$

$$\text{photon sec}^{-1} \qquad (6.13)$$

6.3 Total Albedo

The total albedo flux was calculated from equations 6.11 and
6.13 for an exponential solar X-ray spectrum of the form

$$I(E) = A \exp(E/T)/E \quad \text{photons cm}^{-2} \text{ sec}^{-1} \text{ keV}^{-1} \quad (6.14)$$

where T is the effective plasma temperature in keV. The predicted
countrate was obtained by correcting for the counter efficiency and
resolution, and by integrating the flux over the 2 to 5 keV and the
5 to 8 keV channel.

The predicted variation in the albedo flux with zenith angle
agreed very well with the observed flux, Figure 17. The theoretical
variation was almost independent of the value of T over the range
0.2 to 0.5 keV (2.3×10^6 to 5.8×10^6 °K), with a value of 0.4 keV
giving a minimum least squares error. At 0.4 keV the flux in the
5 to 8 keV channel was about two orders of magnitude less than that in
the 2 to 5 keV channel, while the albedo due to fluorescence was 20%
of that due to scattering. Both of these ratios depended on the
spectral temperature.

The solar X-ray flux required to produce the observed albedo was
9.5×10^4 photons sec^{-1} cm^{-2} above 2 keV for Flight I and 8×10^4
photons sec^{-1} cm^{-2} for Flight II. The difference in the magnitude of

the albedo flux on the two flights is larger than the difference in the solar flux, and is due to the solar zenith angle which was 49 degrees on Flight I and 74 degrees on Flight II.

These predicted solar X-ray fluxes agreed with that observed by the NRL Solar Radiation Monitoring satellite and the McMath-Hulbert X-ray experiment on OSO-3 (Solar Geophysical Data, October and November 1967). The fluxes are shown on Figure 19, where they are plotted against the threshold of the energy channel. Although upper limits were quoted for some of the satellite energy channels, the flux was decreasing so rapidly with energy that they could be considered to be integral channels. The UAT flux value is plotted for a 2.2 keV threshold since in this case the flux derived from the observed albedo was almost independent of the assumed effective plasma temperature. The extremely good power law fit between the flux predicted here, and that observed by other experimenters, must be somewhat fortuitous, since at these energies most of the X-ray flux is concentrated in emission lines. Even so, it does show that the flux predicted by the albedo theory is of the correct order of magnitude. The differential solar X-ray spectrum satisfied the power law

$$\frac{dN}{dE} = 1.08 \times 10^{-2} E^{-4.5} \ \text{erg cm}^{-2} \ \text{sec}^{-1} \ \text{keV}^{-1} \qquad (6.15)$$

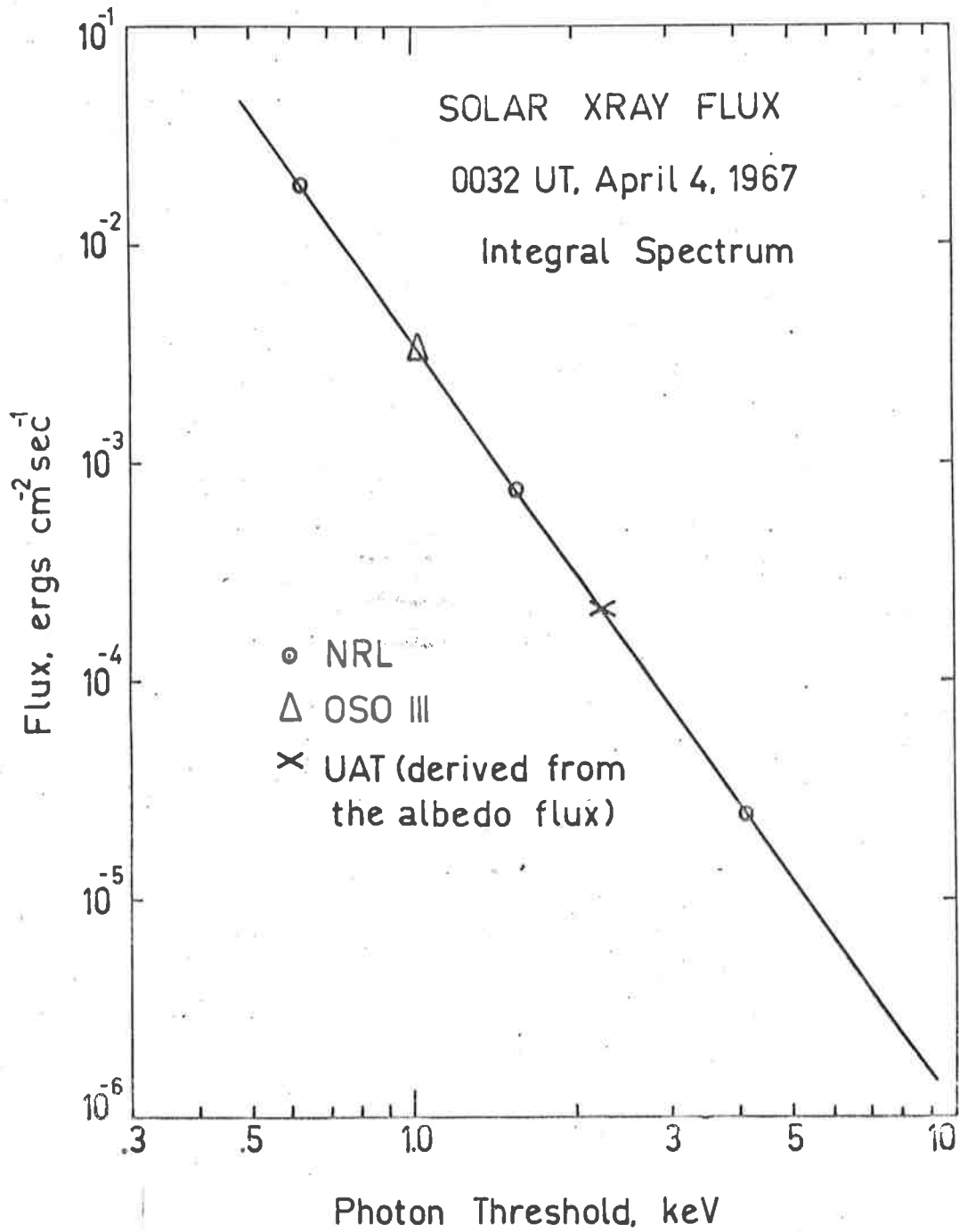and the effective plasma temperature at 2.2 keV was 0.5 keV.

Figure 19. The solar X-ray flux derived from the albedo flux compared
with the flux observed by other experiments at the same time.

Unfortunately satellite data were not available during Flight II so a similar check was not possible.

The albedo X-ray flux from the earth has been shown to be principally produced by solar X-rays which are scattered in the atmosphere. Grader et al. (1968) have recently reported the observation of a low energy X-ray albedo flux at about 0.6 keV. They attribute this flux to atmospheric nitrogen and oxygen Kα lines resulting from fluorescent excitation by solar X-rays.

The presence of such an albedo flux has important consequences for the measurement of the celestial diffuse background. This has usually been determined by observing the 'up-down' difference in counting rate under the assumptions that (1) there was a negligible X-ray flux from the earth, and (2) the charged particle background would be the same whether the counter was looking up or down. The present observations show that assumption (1) is not valid below 5 keV during the daytime, and it is probably questionable at higher energies at times of higher solar activity. Fortunately, to date, most of the experiments that have measured the diffuse flux have flown at night (Byram et al. 1966; Hayakawa et al. 1966b; Cooke et al. 1967; and Seward et al. 1967) so that their results are not affected by the possibility of any scattered solar X-rays.

CHAPTER 7

THEORETICAL MODELS FOR CEN XR-2

This chapter will consider some of the possible theoretical models
of celestial objects which would give a variable X-ray flux similar
to that observed from Cen XR-2 by the rocket experiments.

7.1 An Expanding Thin Hot Plasma

The first model is an extremely idealised situation; an optically
thin hot plasma is created and allowed to expand (Manley, 1967; Chodil
et al. 1968c; Edwards, 1968). The plasma will be considered to consist
of only protons and electrons and no heavier ions. Then the X-rays
are emitted by bremsstrahlung, and the flux at the earth will be

$$\frac{dN}{dEdSdt} = 8.22 \times 10^{-13} \frac{n_e^2 V}{d^2} T^{-\frac{1}{2}} E^{-1} \exp(E/kT) \text{ photons sec}^{-1} \text{ cm}^{-2} \text{ keV}^{-1}$$

$$(7.1)$$

where V is the volume of the plasma and d its distance from the earth
(see equation 1.1). Equation 7.1 is a good approximation to the flux
from a plasma with the cosmic abundances of elements provided $T > 10^7$ $^\circ$K
(Tucker 1967). Table 12 shows the values of T and $n_e^2 V/d$ corresponding
to the observed data.

TABLE 12

CEN XR-2 AS A HOT PLASMA

Date	T		$\frac{n_e^2 V}{d^2}$
	$10^7\ ^\circ K$	keV	
4 April 1967 UAT	4.2 ± .6	3.6 ± .5	$(4.3 \pm .5) \times 10^{17}$
20 April 1967 UAT	2.8 ± .5	2.4 ± .4	$(4.3 \pm .6) \times 10^{17}$
18 May 1967 LRL	1.7	1.5	2.3×10^{17}

If the mass of plasma is conserved, $n_e V$ is a constant and $n_e^2 V/d^2$ is proportional to V^{-1}. Hence between 4 April and 20 April, the plasma cooled apparently with a constant volume, and then started to expand. Alternate explanations for its behaviour could be that the plasma was not optically thin on April 4, but had thinned out by May 18, or it could indicate that matter was still being injected into the plasma when the first observation occurred. (April 4). However, the errors are rather large and it is possible that V was monotonically increasing over the whole period of the observation. Without trying to decide between these alternatives, the implications of a constant mass plasma cooling from $3.4 \times 10^7\ ^\circ K$ to $1.7 \times 10^7\ ^\circ K$ in 35 days while the $n_e^2 V/d^2$ decreases from 4.3×10^7 to 2.3×10^7 will now be

investigated.

The total power radiated by the bremsstrahlung process for equation (1.1) is

$$\frac{dE}{dt} = 1.43 \times 10^{-27} n_e^2 T^{\frac{1}{2}} V \quad \text{ergs sec}^{-1} \qquad (7.2)$$

while the energy content of the plasma is

$$E = 3n_e kTV$$

$$= 4.14 \times 10^{-16} n_e TV \quad \text{ergs} \qquad (7.3)$$

An upper limit to n_e can be obtained by assuming that the cooling of the plasma over the 35 days was due only to the radiation. Then,

$$\Delta E/E = 3.44 \times 10^{-12} n_e T^{-\frac{1}{2}} \Delta t \qquad (7.4)$$

which implies

$$n_e < 3 \times 10^8 \ cm^{-3} \qquad (7.5)$$

The plasma can be considered to behave like an ideal gas, with the one constraint, that the electron density distribution must be almost identical to the proton density distribution from charge considerations. The adiabatic expansion of a plasma is given by

$$TV^{\gamma - 1} = \text{constant} \qquad (7.6)$$

where γ is the ratio of the specific heat at constant pressure to

that at constant volume and for spherically symmetric particles γ = 1.67. If cooling from each of the UAT values in Table 12 to the LRL value are considered, the experimental results give

$$\gamma = 2.1 \pm .4 \tag{7.7}$$

This indicates that $39 \begin{smallmatrix} + & 16 \\ - & 35 \end{smallmatrix}\%$ of the cooling is due to radiated photons. When this result is combined with equation (7.4) the electron density becomes

$$n_e = (9.0 \begin{smallmatrix} + & 5.0 \\ - & 8.1 \end{smallmatrix}) \times 10^7 \text{ cm}^{-3} \tag{7.8}$$

Now the velocity of expansion of our ideal plasma will be less than the speed of sound in the plasma. Only the proton component need be considered as this will be the limiting velocity.

$$v = (1.67 \, P/\rho)^{\frac{1}{2}}$$

$$= (1.67 n_e kT / n_e m_p)^{\frac{1}{2}}$$

$$= 1.2 \times 10^4 T^{\frac{1}{2}} \tag{7.9}$$

and for $T = 3 \times 10^7 \, ^\circ K$

$$v = 6.4 \times 10^7 \text{ cm sec}^{-1} \tag{7.10}$$

This can be compared with the mean thermal velocities of the protons and electrons at this temperature which are

$$v_e = 2.4 \times 10^9 \text{ cm sec}^{-1}$$

$$v_p = 7.1 \times 10^7 \text{ cm sec}^{-1} \qquad (7.11)$$

Now if the plasma expands with the velocity of sound, the volume V will be

$$V \sim 9.1 \times 10^{23} t^3 \text{ cm}^3 \qquad (7.12)$$

where t is the time in seconds since the plasma was ejected. The plasma doubled its volume in 35 days, hence its age in mid-April was

$$t \sim 1.1 \times 10^7 \text{ sec} \sim 4.4 \text{ months} \qquad (7.13)$$

with a volume

$$V \sim 1.4 \times 10^{44} \text{ cm}^3 \qquad (7.14)$$

The distance from the earth can be estimated from $n_e^2 V/d^2$ to be

$$d \sim 1.6 \times 10^{21} \text{ cm}$$

$$\sim .5 \text{ kpc} \qquad (7.15)$$

These calculations indicate the order of magnitude of the properties of a thin plasma which could have produced the Cen XR-2 X-rays. Chodil et al. (1968c) derived a distance of between 5 and 14 kpc by extrapolating the X-ray spectrum to optical wavelengths and arguing on the basis of behaviour of the average novae. This method, however, is very rough, although the assumption of an "average" novae

is, perhaps, no more extreme than the assumption of an isothermal, hydrogenic plasma.

The electron density, volume of emission and temperature of the source are consistent with those obtained from optical observation of recurrent novae (Walkrstein 1961) where the hot gas is produced by shock heating of a circumstellar envelope. Edwards (1968) has considered the type of radial dependence of the matter in the envelope which would give the observed Cen XR-2 spectral variation. He found that $(n_e^2 V/T)$ was a constant for an adiabatic strong shock which propagates radially outwards through a nonuniform gas envelope with the density

$$n \quad \propto \quad r^{-2} \tag{7.16}$$

All of the X-ray emission occurs from a shell behind the shock front, with an approximate volume of $2.5R^3$ and the temperature and radius of the shock front. The observed twofold decrease in temperature in 3×10^6 seconds implies that the shock was only two weeks old when first observed, and the observed flux indicates a distance of 300 pc. The lack of optical observation of the nova could be due to obscuration by dust in the disc of the galaxy.

Novae outbursts could be more important as X-ray sources than the recurrent novae because of the larger energy release, if they

are surrounded by a circumstellar envelope. The production of a hot plasma by a supernova explosion has been considered by Tucker (1967a). He finds that a Type II supernova could produce X-rays either by shock wave heating or by the presence of a hot plasma in the ejected supernova envelope.

Prendergast and Burbidge (1968) have suggested a plasma model for Cen XR-2 in which the plasma is produced by the accretion of matter onto a white dwarf from a close binary partner. Rapid variations in the X-ray flux could be produced by variations in the accretion rate, or by the eclipsing of the emitting region. In the latter case the hottest part of the plasma could be obscured, leading to a progressive decrease in the observed temperature and intensity of the source.

7.2 Neutron Star

The theory of a neutron star has been presented in Section 1.3, where it was shown to have a short lifetime as an X-ray emitter and hence is a candidate as a model for Cen XR-2. It will be assumed that no hot plasma was produced by the supernova which resulted in the formation of the neutron star.

The neutron star has an extremely strong gravitational field and

so it is necessary to allow for a gravitational redshift. General relativity shows that the light emitted at a distance R from a sphere of mass M is redshifted by an amount

$$E = E_o(1 - 2GM/Rc^2)^{-\frac{1}{2}} \qquad (7.20)$$

where E_o is the photon energy at radius R, E is the photon energy at infinity, and G is the gravitational constant. For a neutron star with one solar mass and radius 10 km, the change in photon energy is

$$E/E_o = 0.85 \qquad (7.21)$$

Hence the spectrum at the earth would correspond to a blackbody whose temperature is 15% less than the surface of the neutron star (equation 1.3). The cooling rate was found to agree with the blackbody temperature observed on the two UAT flights, Figure 20. However, the strong dependence of the cooling rate on temperature meant that the star would not have cooled enough to fit either the LRL measurement on May 18 or their upper limit on September 28, 1967.

The neutron star, if it exists, would be about 1 kpc from the solar system (equation 1.3), and it should have been observed optically if it was formed in a supernova during March 1967. In view of all of these difficulties, the neutron star model must be rejected.
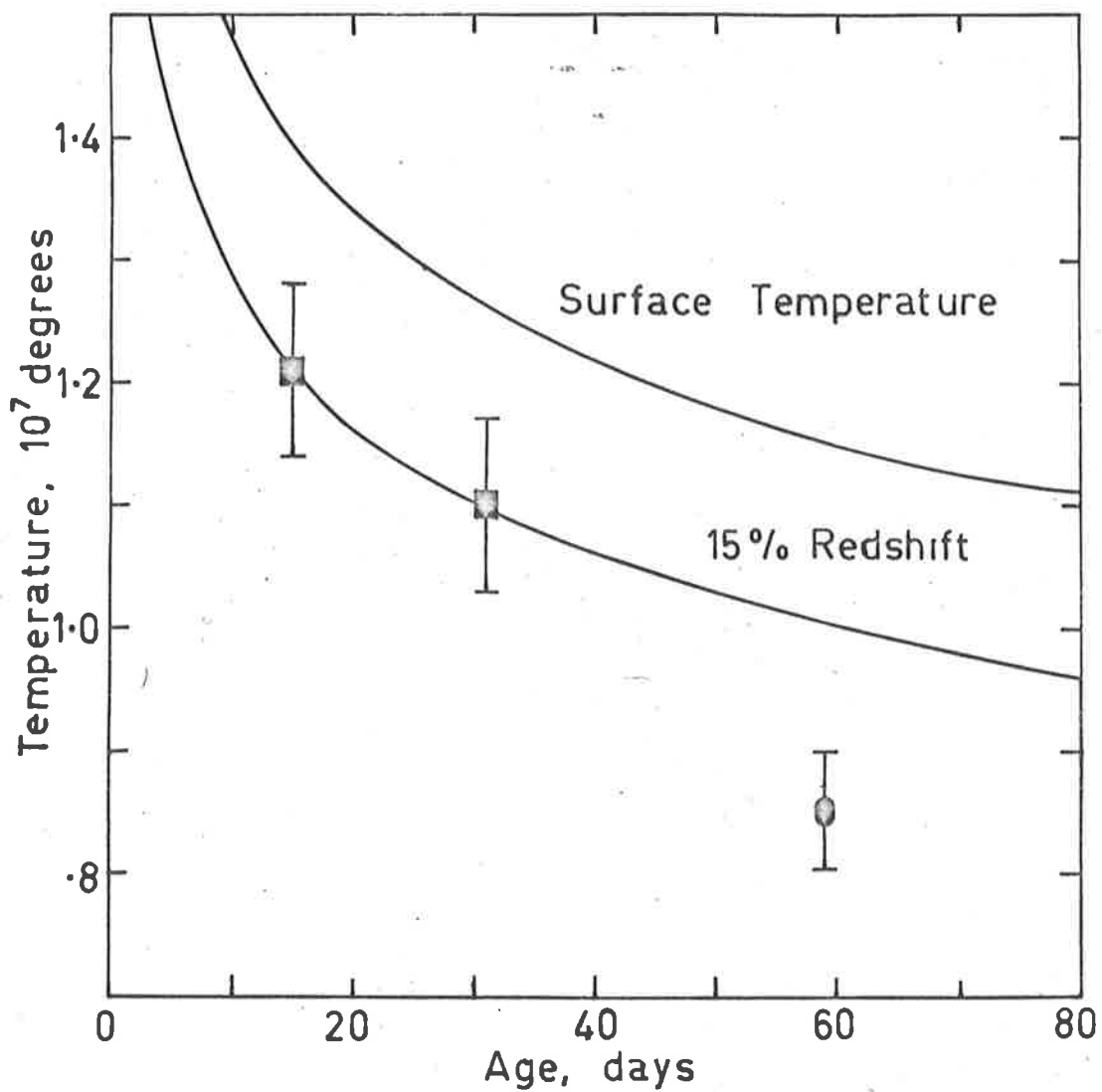
Figure 20. Theoretical neutron star cooling curves compared with the observed blackbody temperatures for Cen XR-2.

7.3 Synchrotron Models

In this section the Cen XR-2 emission will be considered to be produced by synchrotron emission when electrons are injected into a region of magnetic fields.

The electron spectrum is modified by two processes, the energy loss in synchrotron emission, and the adiabatic expansion of the plasma. An electron with an energy of $5 \times 10^5 H^{-\frac{1}{2}}$ MeV produces radiation with a maximum at 4 keV. The radiation lifetime of this electron is $5 \times 10^2 H^{-3/2}$ seconds (equation 1.12). After this time the photon distribution will have moved to lower energies so that the peak in the distribution will be at 1 keV. Evidently, by suitably choosing the magnetic field the spectrum could be made to decrease with a time constant of about one month, the variation observed for Cen XR-2. Adiabatic expansion of the region occupied by the magnetic field and the electrons modifies both the field and the electron spectrum. For a power law electron spectrum (equation 1.9) the radiation flux varies with the dimension of the region according to the law

$$\frac{dN}{dVdEdt} \propto L^{-2\gamma} \propto t^{-2\gamma} \qquad (7.22)$$

where the last relation holds for a constant radial velocity.

Tucker (1967a) has considered these effects for a power law electron spectrum and he found that there was a "break" in the photon spectrum at

$$E_b = 4.5 \times 10^{-9} H^{-3} t_{yr}^{-2} \quad keV \qquad (7.23)$$

The spectral shape and time dependence of the photon spectrum with only synchrotron losses is

$$\frac{dN}{dVdEdt} \propto \begin{cases} E^{-(\gamma + 1)/2} & E \ll E_b & (7.23a) \\ \\ t^{-(\gamma + 5)/3} E^{-(2\gamma + 4)/3} & E \gg E_b & (7.23b) \end{cases}$$

Suppose that in early April the 2 to 8 keV spectrum was given by 7.23a, i.e. $E_b > 8$ keV, but by May 18 the break in the spectrum moved through the 2 to 8 keV energy interval and so the spectrum was given by 7.23b. The spectrum was $78E^{-2.15}$ photons sec^{-1} cm^{-2} keV^{-1} on April 4, which would imply a post break spectrum of $140E^{-3.6}$ photons sec^{-1} cm^{-2} keV^{-1} on May 18. This is extremely close to the observed LRL spectrum of $143E^{-3.8}$ photons sec^{-1} cm^{-2} keV^{-1}.

The age of the source and the magnetic field on April 4, 1967 are given from equation 7.22 to be

$$t = 2 \times 10^6 \; sec$$

$$H = 5 \times 10^{-3} \; gauss \qquad (7.24)$$

The volume of the source, its distance and electron spectrum coefficient are related by equation 1.10 so that

$$Vk/d^2 = 1.5 \times 10^{22} \qquad (7.25)$$

where the electron spectrum is

$$\frac{dN_e}{dVdE} = kE^{-3.3} \text{ electrons } cm^{-3} \text{ keV}^{-1} \qquad (7.26)$$

Hence the data can be fitted extremely well by a synchrotron model in which there is an impulsive injection of electrons into a region of magnetic fields and the electrons then lose energy by synchrotron emission.

The principle problem associated with this model is that equation 7.23 is strictly valid only at energies well away from the break energy. Nevertheless the agreement between the model and the observed results is very satisfactory. Again the model is extremely idealised and it is doubtful if any injection process would give a strictly power law electron spectrum.

7.4 Summary

Several models have been proposed that would give a time variation similar to that from Cen XR-2. It must be emphasised that

each of the models considered represents an idealised situation, but one which has some resemblance to a real astronomical situation. The opacity of the gas to X-rays has been ignored and this can be an important factor early in the life of the X-ray source. Consequently some time after the initial injection, or the beginning of the blast wave, the decrease in opacity will produce a maximum in the X-ray emission before the flux decreases by the methods discussed in this chapter. It is interesting to note that the novae, binary star and synchrotron models suggest conditions that could reoccur, so that Cen XR-2 could be observed again in new outbursts.

The models presented in this chapter have only attempted to explain the three rocket measurements of Cen XR-2 in April and May 1967. They can be readily expanded to include the possible observation of Cen XR-2 in December 1966 by Bowyer et al. (1968). More difficult to explain is the unexpected high energy component observed by Lewin (1968a,c) in balloon borne experiments. If this source is, in fact, the same as that observed at rocket energies one explanation could be a dilute high temperature source co-existing with the low energy source observed at rocket energies (Manley 1968). Further experiments are needed to determine if the source exhibits a recurrent variation and to increase the accuracy of the spectral information.

PART B

SOLAR AND CELESTIAL X-RAY OBSERVATIONS FROM IMP F

CHAPTER 8

THE PROPORTIONAL COUNTER EXPERIMENT

8.1 The Satellite and SCAS Experiment Organization

The IMP F satellite was launched at 1405 UT on 24 May, 1967, it
carried eleven scientific experiments, and was injected into an
eccentric orbit (e = 0.941, apogee = 211,000 km, perigee = 250 km)
perpendicular to the ecliptic. The period of the orbit was 4.3 days
and, of this, 3.4 days were spent at radial distances greater than
110,000 km, which is well beyond the radiation belts. The satellite
had a spin period of 2.6 seconds with the spin axis normal to the
ecliptic plane.

One of the experiments carried investigated the anisotropy of
the cosmic rays and its temporal and energy variation during solar
flares. This experiment was designed and built by the Southwest
Center for Advanced Studies, Dallas, Texas, (SCAS) and consisted of
(1) a scintillator and solid state detector combination to detect

protons of energy 1 to 107 MeV, and electrons of energy 3 to 25 MeV, and (2) a proportional counter to detect electrons greater than 80 keV and X-rays greater than 3 keV. It is this proportional counter, its modes of operation and its results that are the subject of this part of the thesis. The candidate was responsible for the design and calibration of this portion of the SCAS experiment.

The SCAS experiment was mounted on the octagonal platform of the spacecraft and since the spin axis was positioned normal to the ecliptic, the detectors scanned around the ecliptic plane every 2.6 seconds. In the basic mode of operation of the experiment, each spin rotation was divided into eight sectors of 45 degrees, and the counts received in each sector were accumulated in different scalers. The output from the proportional counter was 'Octant Divided ' in this manner once every 81.92 seconds providing a continuous monitor on the solar X-ray flux and a measure of the electron anisotropy during solar flares. In addition, on the average of once every 20.48 seconds, the azimuth of the spacecraft was measured to an accuracy of $\pm$ 0.7^o at the instant of observation of a low energy pulse in the proportional counter. This 'Azimuth Measurement' provided data on the positions and spectra of celestial X-ray sources.

The data from the SCAS experiment were accumulated concurrently into 10 separate scalers provided by the spacecraft. Nine of the

scalers (SCA 1 to SCA 9) were ten bit 'ST' scalers; they accumulated countrate data up to a maximum of 512 and then counted clock pulses (50 Hz) for the rest of the accumulation period. Hence, a number less than 512 was an actual count, while a number greater than 512 determined the period during which the 512 counts were accumulated. This scheme extended the dynamic range and eliminated any overflow problems. The tenth scaler (SCA 10) was six bits long and was used for two units of housekeeping data, in particular, to provide information on the start and stop octants during octant division. The total SCAS data train consisted of 96 bits, divided into eleven units of information.

The spacecraft telemetry was organised into sequences of 2048 bits, and was transmitted at 100 bps. For convenience the sequence was divided into sixteen frames, each of 128 bits, and each frame divided into sixteen channels of 8 bits. The SCAS data was transmitted to earth twice in each sequence, in channels 4 to 15 of frames 3 and 11 (counting 0 to 15). Hence, SCAS data was transmitted once every 10.24 seconds.

The experiment cycled through eight different types of measurements, (e.g. different logic or energy levels) with each measurement lasting 9.28 seconds and the experiment changing to a new measurement during the 0.96 seconds of telemetry readout. These eight measurements were identified by the subscripts $L = 0$ through 7.

Part of measurement L = 7 was further subcommutated, making a complete subcommutation cycle of 64 measurements for the SCAS experiment, however, this did not involve the proportional counter data. The proportional counter data appeared in this cycle as follows: (1) in measurement L = 5 the proportional counter output was 'Octant Divided' into SCA 1 through 8, and (2) in measurement L = 4 through 7 the azimuth data was transmitted in SCA 9. That is, a proportional counter octant division measurement was made every 81.92 seconds while an azimuth measurement was made on the average once every 20.48 seconds.

8.2 The Proportional Counter

The IMP F proportional counter was filled with a xenon-methane (90%-10%) mixture at just over one atmosphere pressure and had a 0.002 inch beryllium window. Its window area was 3.1 cm^2 but after allowing for the thicknesses of the collimator slats the effective area was 2.2 cm^2. The counter was constructed of aluminium and was 1.0 inch deep, Figure 21. A second, similar counter but without a window was constructed behind the first counter. It was intended to be used as a guard counter, but space and power limitations precluded its use. The counter was made by LND Inc., Oceanside, Long Island, N.Y., and was rigidly non-magnetic so that it would not interfere with the interplanetary magnetic field measurements also being made from the
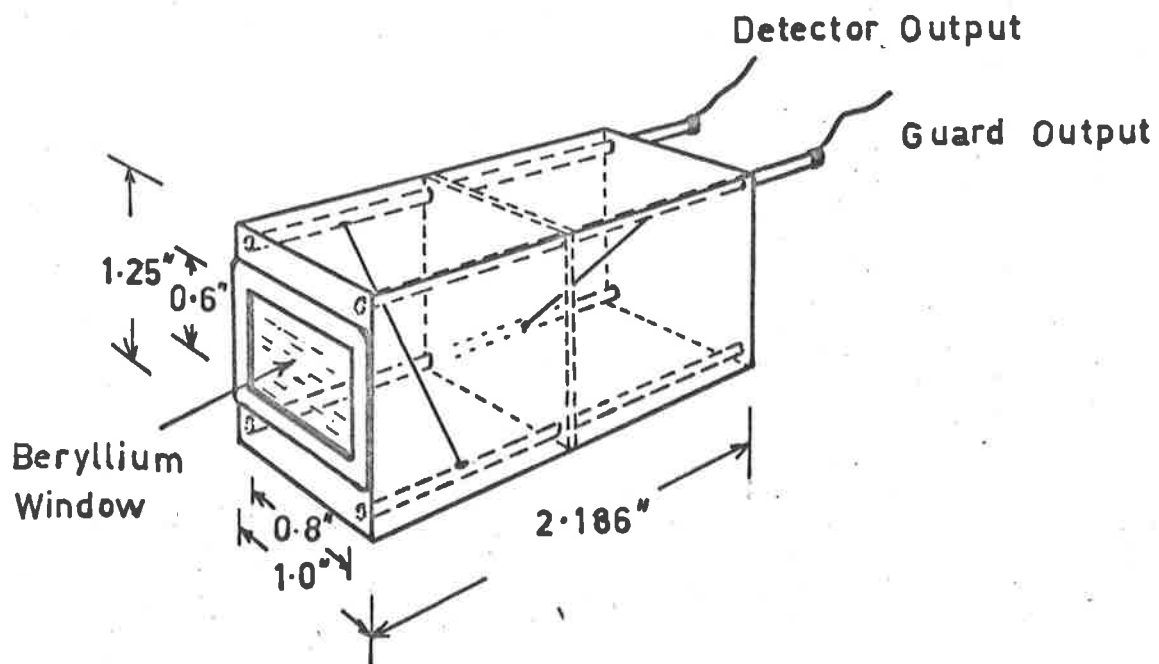
Figure 21. The proportional counter flown on the IMP-F satellite.

satellite.

The anode wire was 0.006 inch diameter stainless steel and was
supported diagonally across the counter 0.5 inch behind the window.
This unusual configuration was found to minimise the end effects for
such a small counter with a relatively large window. Point counters,
which have a point or a small sphere as the anode, were considered as
they can be made equally small, but they had the disadvantage of long
pulse collection times at low countrates. The gain of the counter
flown varied by less than 20% over the whole window and its overall
resolution for 5.9 keV X-rays was about 25%. The anode voltage
employed was 1350 volts which was passed through a 133 Megohm filter
potted on the back of the counter. The filter removed interference
from the high voltage line and protected the power supply in the
event of a counter breakdown. This voltage was also used as the anode
supply of one of the photomultipliers in the cosmic ray experiment.

Much of Section 2.1 on the operation of the Skylark proportional
counters is applicable to the counter flown on IMP F and so will not
be repeated here. The efficiency of the counter for normally incident
X-rays was calculated using equation 2.1, and the result is shown on
Figure 22. The energy ranges of interest in this experiment were
2.7 to 5.9 keV and 6.0 to 8.6 keV for celestial X-rays observed in the
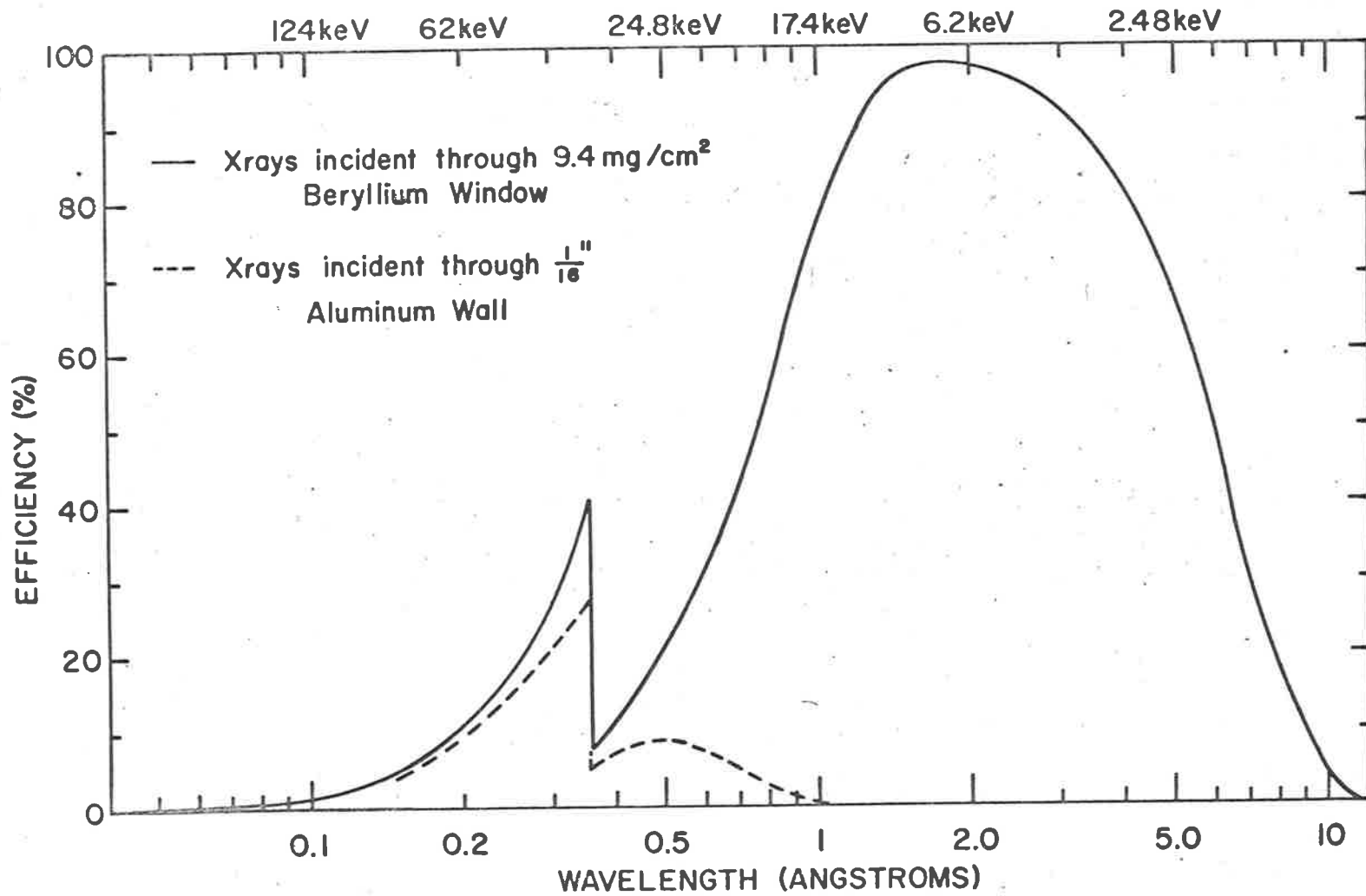azimuth measurement and greater than 2.7 keV for solar X-rays observed

Figure 22. Efficiency of the IMP-F proportional counter to X-rays.

in the octant division measurement. The efficiency for the detection
of X-rays incident through the 0.0625 inch thick aluminium walls was
calculated and was a maximum of 26% at 34.5 keV, Figure 22.

Protons and electrons were also detected by the counter. The
energy deposited in the counter by protons with different incident
energies was calculated from the range-energy relations (Barkas and
Berger 1964) and is shown in Figure 23. Only protons with a very
small range of incident energies will deposit between 2.7 keV and
8.6 keV in the counter. Above 20 MeV, the protons begin to enter
the counter from all directions and some could deposit small amounts
of energy in the counter by passing across an edge.

The octant division measurement accepts all pulses that correspond
to more than 2.7 keV being deposited in the proportional counter (in
contrast to the azimuth measurement when only pulses in a narrow energy
interval are accepted). Hence, all protons with energy above 2.1 MeV
will be octant divided.

The range energy relations of electrons are not as well defined
as for protons because the electron can lose a significant amount
of its energy in each ionising collision. Chang et al. (1953)
measured the electron transmission coefficient for aluminium and
platinum foils and postulated a theoretical model to fit the results.
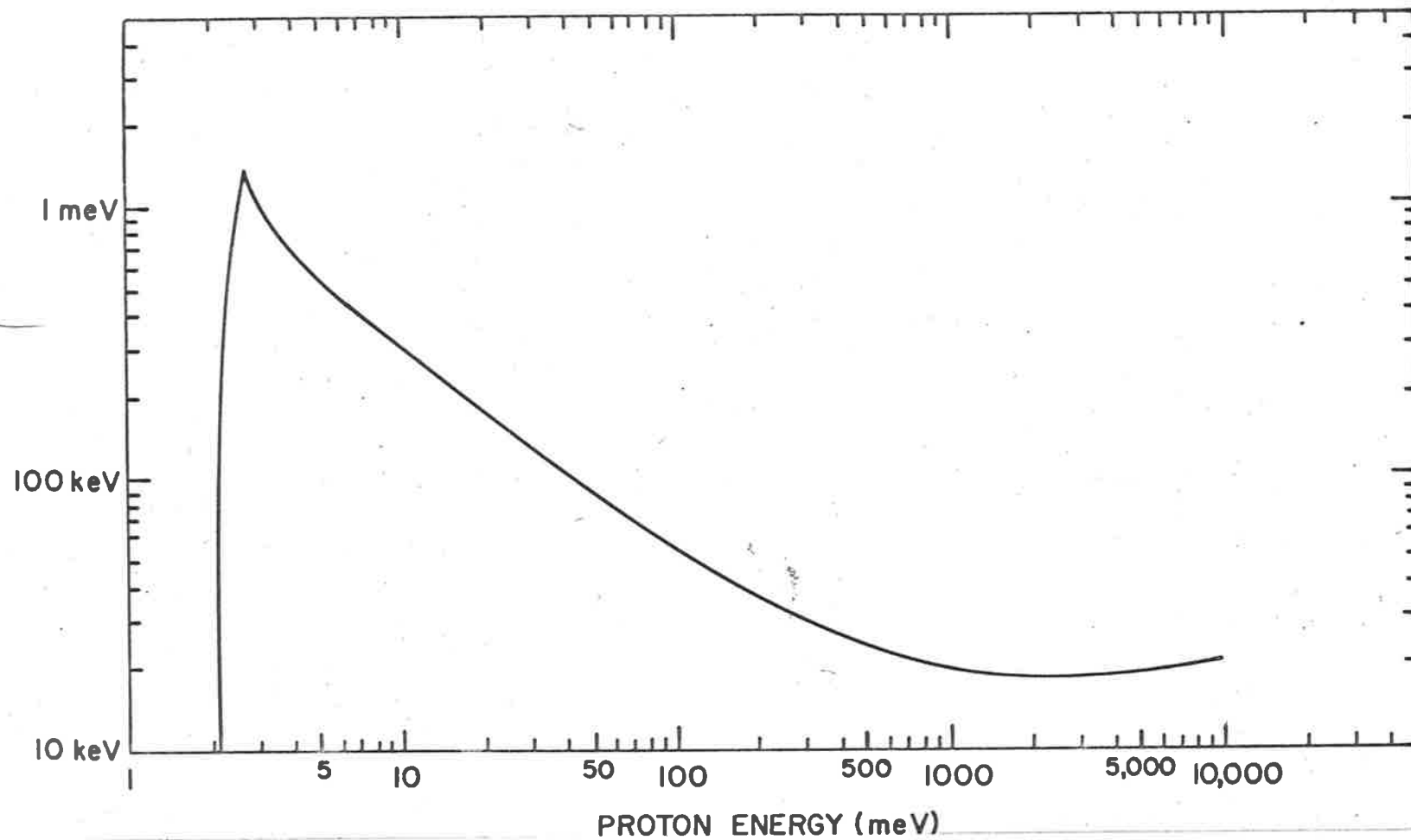Somogyi and Body (1965) refined the theory and found a close agreement

Figure 23. Energy deposited in the IMP-F proportional counter by protons.

with the experimental results. Their method has been used to calculate the electron transmission coefficient for the beryllium window of the counter, Figure 24. Due to the high degree of straggling it is not possible to determine the residual energy of the electrons as they emerge from the window. Nevertheless, most of the transmitted electrons have more than 3 keV residual energy and so the transmission coefficient was used as the efficiency for detection of electrons in the octant division measurement.

8.3 Collimator

The field of view of the counter was restricted by a collimator made from 0.010 inch aluminium slats. The slats were semicircular with a spacing of 0.022 inch, giving a full transmission angle of 5 degrees. Aluminium was used for the collimator, because it is nonmagnetic and the 1.5 keV fluorescent X-rays produced by charged particles, or higher energy X-rays, caused pulses in the counter that would be rejected by the lower discriminator. In addition, spectral reflection was less from an aluminium surface than from any other metal, (Compton and Allison 1935; Hendrick 1957; and Rieser 1957).

The satellite spin axis was normal to the ecliptic and so the proportional counter scanned around the ecliptic plane. The
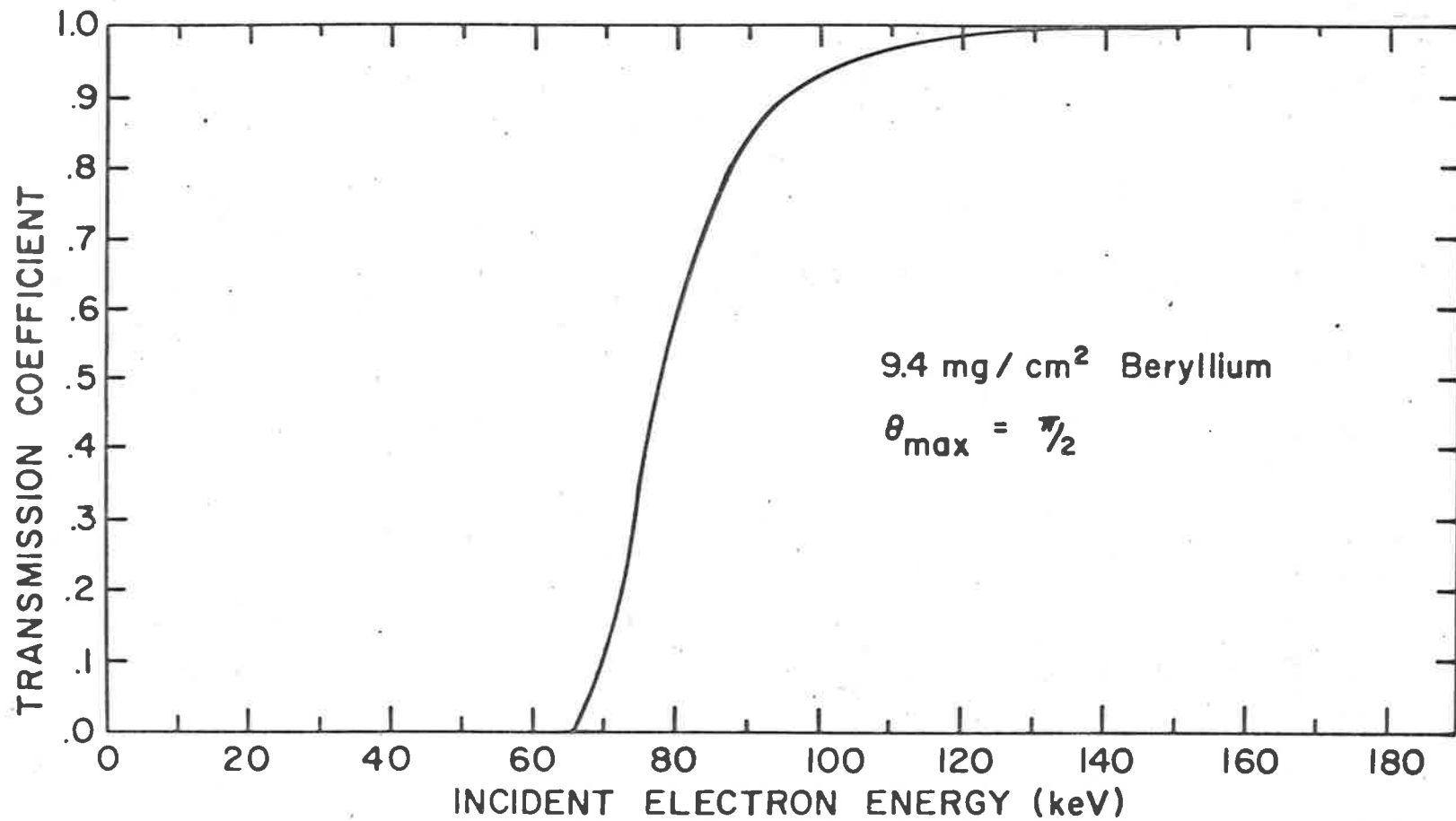
Figure 24. Calculated electron transmission coefficients for
0.002 inch beryllium foil.

semicircular design of the collimator compensated for the change in effective area of the proportional counter for sources above and below the ecliptic. This enabled the flux from the source to be measured without requiring an accurate position. The width of the response will depend on the ecliptic latitude of the source and so provided a means of measuring the position.

Assume initially that the radius, r, of the collimator is large compared with height, h, of the counter window, and that the window extends along the centres of the semicircular slats, see diagram. The full acceptance angle of the collimator, ϕ , is the same for all sources regardless of their latitude because of the semicircular design, and is given by
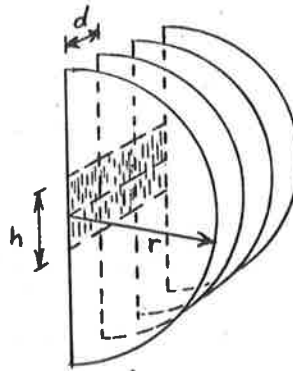

$$\phi = 2 \arcsin (d/r) \qquad (8.1)$$

where d is the slat separation.

As the collimator rotates about the satellite spin axis, the increment in azimuth, ψ , that corresponds to the acceptance angle, ϕ , for a source at latitude θ is

$$\psi = \phi /\cos\theta \qquad (8.2)$$

Hence the full azimuth range for
the detection of a given source
depends on its ecliptic latitude.
The satellite spin rate, ω, is
constant and so the total time
for observation of a source is

$$\Delta t \quad = \quad \frac{\psi}{\omega}$$
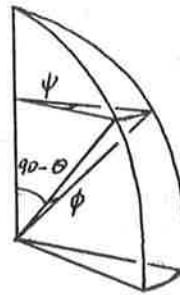
$$= \quad \frac{\phi}{\omega \cos\theta} \tag{8.3}$$

This equation shows that a source at a higher latitude would be looked
at for a longer period than one at a lower latitude (ϕ is independent
of θ). Equation 8.3 could be used to calculate the cosine of the
latitude of a source if a sufficiently accurate response peak was
obtained.

Suppose a source at a latitude θ has an X-ray intensity of J_o
photons cm^{-2} sec^{-1}, then the countrate observed at time t is

$$\frac{dN}{dt} = J_o A \cos\theta(1 - 2|t - t_o|/\Delta t) \quad \text{photons } sec^{-1} \tag{8.4}$$

$$\text{for } 2|t - t_o| < \Delta t$$

where A is the area of the counter and t_o is the time when the counter
looked directly at the azimuth corresponding to the source. The

cosine term projects the area A onto the direction of arrival of the photons and the time term arises from the triangular response of the collimator. The total number of photons observed from the source during one scan is

$$N = \int_{t_o - \Delta t/2}^{t_o + \Delta t/2} \frac{dN}{dt} dt$$

$$= \tfrac{1}{2} J_o A \cos\theta \, \Delta t$$

$$= \frac{J_o A \phi}{2\omega} \quad \text{photons} \qquad (8.5)$$

Hence the total number of counts observed depends directly on the source intensity and is independent of its latitude.

The collimator flown on IMP was not much larger than the window; the height of the window being 0.6 inch while the radius of the slats was 0.5 inch. Nevertheless, the response, Figure 25, was very close to the results calculated for the narrow window. At latitudes higher than $\pm 60°$ the collimator construction began to obscure the counter window. One complicating factor was the increased thickness of the beryllium window and the decreased depth of the counter at higher latitudes. For a latitude of $60°$ the window thickness was effectively
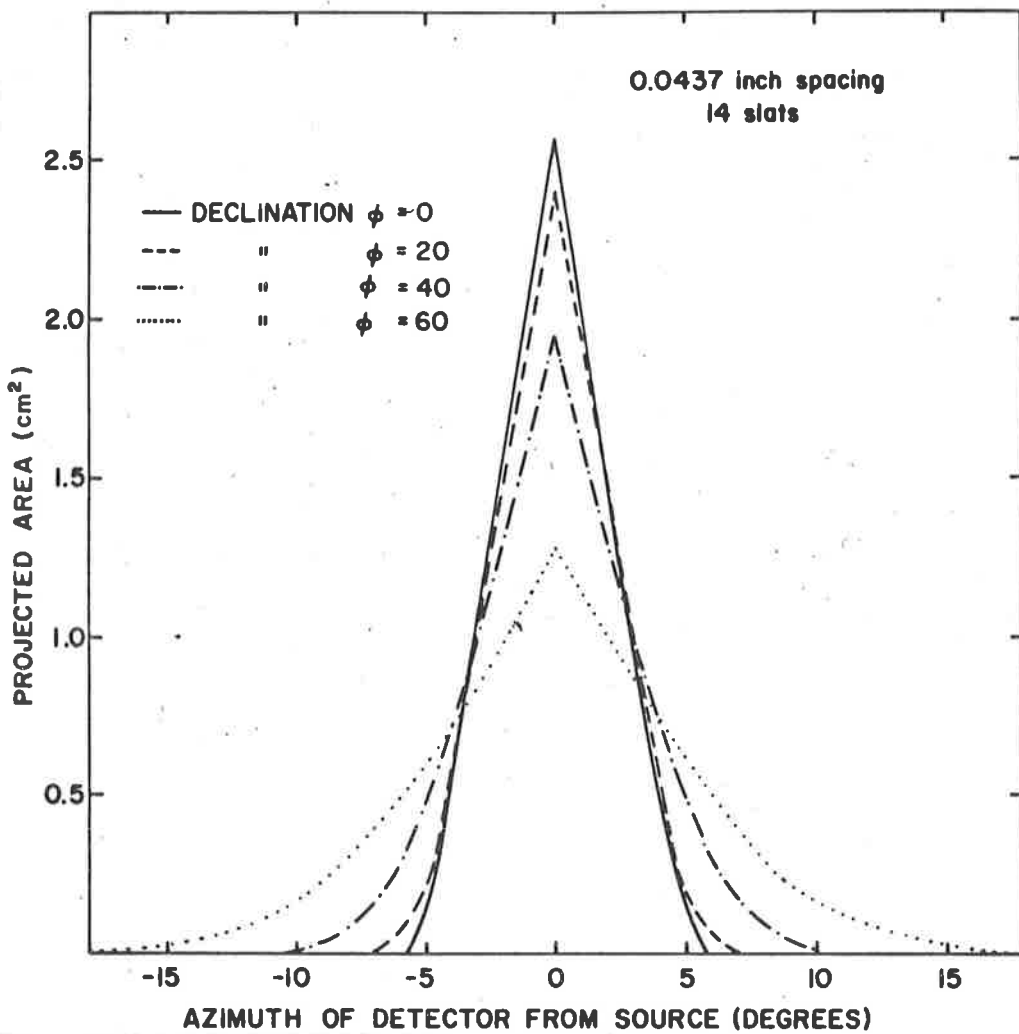
Figure 25. Response of a semicircular collimator to sources at various declinations (ϕ). This diagram refers to a collimator of 5° full width at half transmission. The actual collimator flown was 2.5° full width at half transmission and its maximum area was 2.2 cm^2.

doubled causing a loss of counter efficiency at lower energies.

8.4 Electronics

Much of the electronics involved with the proportional counter was common with the rest of the SCAS experiment. The same power supply supplied the anode voltages for the counter and the photomultipliers; common octant division logic was used with a variety of inputs including the proportional counter; and the output scalers, which were part of the satellite and not the SCAS experiment, had different inputs on each measurement. Consequently there was a complex interrelation between the different parts of the experiment. This section will describe the proportional counter electronics and cover enough details of the associated electronics so that the results can be properly understood.

A block diagram of the proportional counter electronics is shown on Figure 26. The pulses from the proportional counter were amplified by a voltage sensitive amplifier so that 5.9 keV X-rays in the counter gave positive pulses with an amplitude of 3 V. The amplifier was mounted very close to the proportional counter and was completely shielded, except for the feedback resistor which was accessible to enable the gain to be changed.

8.4.1 The Azimuth Measurement

The amplifier output pulses were fed to two discriminators, Figure 26, which set the lower and upper limits of the one window pulse height analyser. Pulses were accepted for the azimuth measurement only if they fired DISC-1 but not DISC-2. A strobe pulse was generated 8 usec after the lower discriminator fired. If, after this delay, DISC-2 still had not fired, the pulse amplitude must have been between the two discrimination levels. Hence the strobe pulse, the Q pulse from DISC-1 and the $\bar{Q}$ pulse from DISC-2 were inputs to AND-1. The strobe pulse was also used in the octant measurement for the input to the octant division logic, which will be discussed in the next section. The discrimination levels were changed between measurements by shorting out the last resistor on the resistance chain. This caused the discriminators to form an energy window of 1.7 to 3.6 V for measurements L = 4 and 5 and 3.7 to 5.2 V for measurements L = 6 and 7.

Only the first suitable pulse after a telemetry readout was analysed for direction of arrival in the azimuth measurement. The Freeze pulse prevented any accumulation into the scalers during the telemetry readout of the SCAS data. It also caused the experiment logic to change ready for the next measurement. The end of the Freeze pulse left the flipflop reset, which made $\bar{Q}$ positive and opened AND-1. However, as soon as a pulse was transmitted by AND-1,
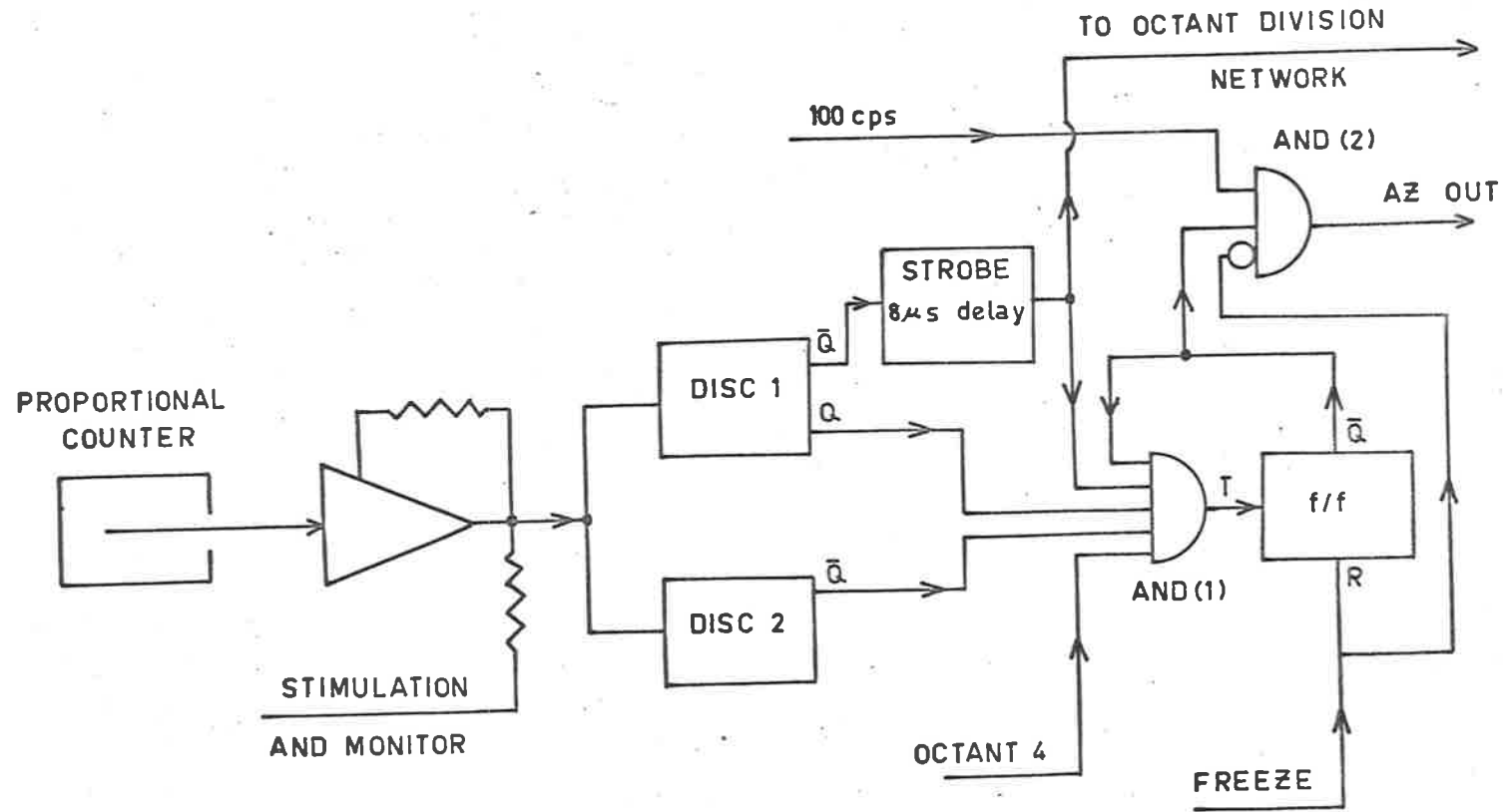
Figure 26. Block diagram of the logic employed by the proportional counter on IMP-F.

the $\bar{Q}$ of the flipflop went to zero to shut AND-1 and prevent any more pulses being transmitted. The sun was known to be a copious emitter of X-rays which could have occupied much of the azimuth measurement. To avoid this situation the AND-1 gate was held closed during the octant centred on the sun, hence the octant 4 input to AND-1. A 100 Hz squarewave was transmitted by AND-2 from the end of the Freeze pulse until the first pulse which satisfied the conditions on the gate AND-1. The output from AND-2 was fed to the output scaler 9 during measurements L = 4 through 7.

The number in scaler 9 gave the duration in units of 0.01 seconds between the end of the Freeze pulse and the instant when a suitable pulse was received. This data was converted to the azimuth with respect to the sun by using the time from the beginning of a telemetry sequence to the next sun pulse which was measured by the spacecraft optical aspect system and was provided on the SCAS data tapes. By integrating many days of this azimuth data the countrate could be obtained as a function of azimuth (see Chapter 10).

8.4.2 Octant Division

During measurement L = 5, the strobe pulses were fed to the octant division circuits where they were routed to one of the eight scalers (SCA 1 through 8) depending on the spacecraft azimuth at that

time. The azimuth was divided into eight equal sectors, and all
pulses received while the counter azimuth was in the Nth octant were
fed into the Nth scaler.

The octants were defined relative to an aspect signal from the
spacecraft consisting of 65 pulses per spin period and a dead time
pulse. The first pulse of this pulse train was in coincidence with
a 'sun pulse' from the solar sensor, and the pulses thereafter
defined 64 accurately equal intervals. The time between the last
pulse and the next sun pulse was variable, but was within the range
0.625 to 5.547 msec. During this time a 'dead time' pulse inhibited
accumulation of the data. The system could adjust to any changes in
the spin period and also would insert a pseudo sun pulse after
5.625 msec if a sun pulse did not occur. The octant division circuits
took the 64 equal intervals and produced eight equal time intervals
which controlled the accumulation of data into the eight scalers.
This aspect determining system is identical to one described by
Bartley et al. (1967).

The sun sensor was located on a different facet of the spacecraft
platform 135° in azimuth before the SCAS detectors. Hence, the dead
time pulse occurred $3T/8$ seconds (where T is the spin period) before
the SCAS detectors would see the sun. The octants were displaced $22\frac{1}{2}^{\circ}$
with respect to the sun pulse so that the proportional counter would

see the sun in the centre of an octant. The dead time pulse inhibited accumulation for a period in the middle of octant 1. The directions of view of the octants are shown in Figure 27. Since the spin period was 2.6 seconds and each measurement took 9.28 seconds, data were accumulated into each scaler from 3 or 4 octant sightings.

To avoid having a nonintegral number of octant sightings, data were not accumulated at the beginning of a measurement until the beginning of a new octant and accumulation ended with an end of octant before the initiation of the data readout. The octant number at which accumulation began and ended were transmitted in SCA 10. From this start-stop information and the spin period, the total number of octants of data accumulated into each scaler could be determined.

8.5 Data Organization

Telemetry from the satellite was received by the GSFC STADAN stations around the world and sent to the NASA-Goddard Space Flight Center where the data from the different experiments were separated, merged with orbit and spacecraft information, and some preliminary data reduction carried out. One copy of the output magnetic tape containing the SCAS data for each orbit was sent to the Southwest Center for Advanced Studies, Dallas, Texas, and one to the University
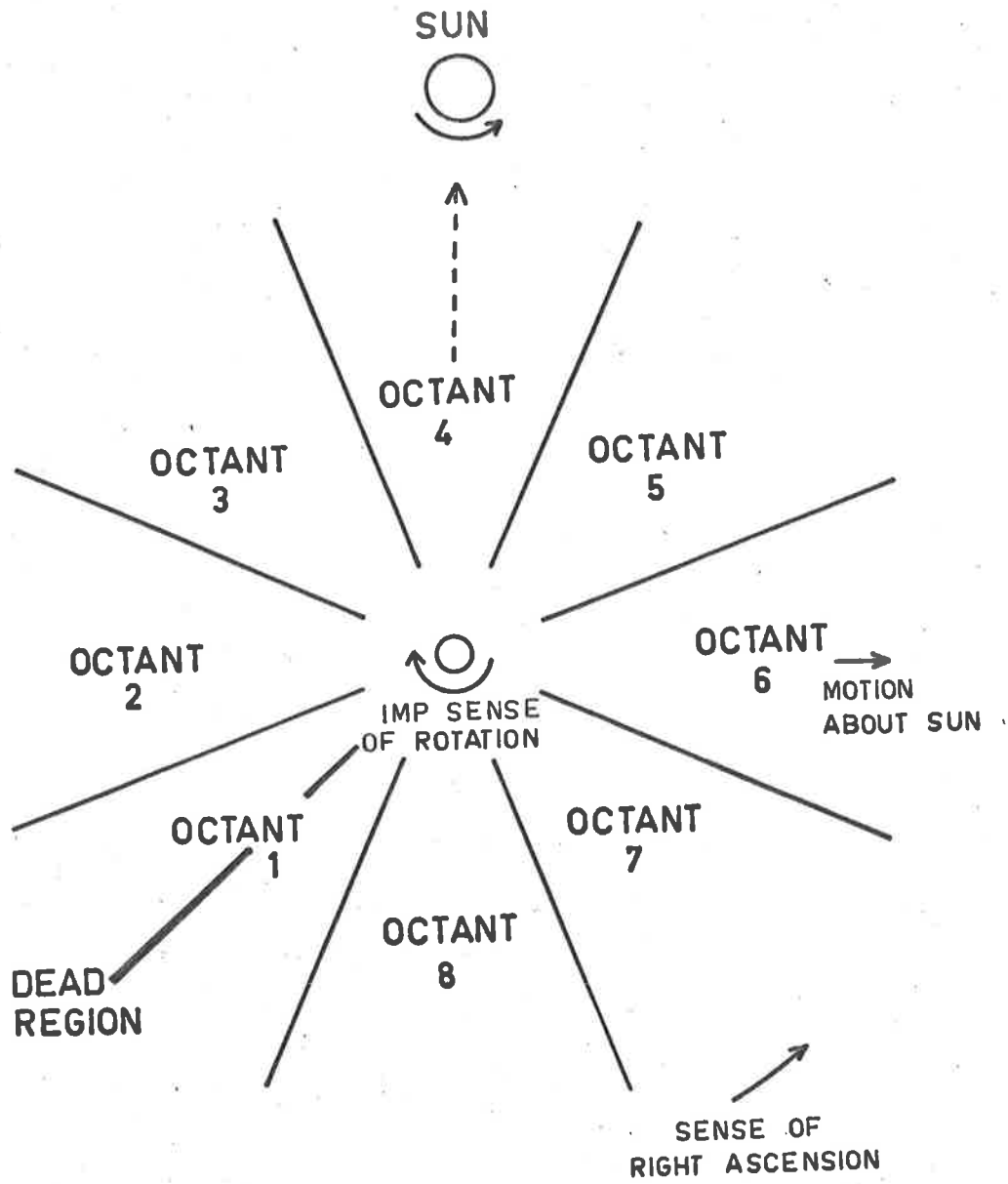
Figure 27. The orientation of the octants used in the octant division logic. The solar X-rays are all observed in Octant 4.

of Adelaide.

The tape was organized around the 64 measurement experiment subcommutation cycle which took eleven minutes to complete. The data from each measurement consisted of eleven units of information transmitted from the spacecraft, one each from Scalers 1 through 9, and two in Scaler 10, and will be referred to as DATA(M) where M = 1 to 11. Fifteen additional units of information DATA(12) to DATA(26) were also supplied as follows:

DATA(12) total number of complete spin periods,

DATA(13) experiment synchronization,

DATA(14) to DATA(21) number of acquisitions for octants 1 through 8,

DATA(22) relative phase between sun and telemetry,

DATA(23) sequence counter,

DATA(24) data condition indicator,

DATA(25) corrected value of DATA(10),

DATA(26) corrected value of DATA(11).

DATA(12) to DATA(21) were calculated from the raw data, while DATA(22) to DATA(24) were obtained from other spacecraft systems. The sequence counter assigned a unique number to every telemetry sequence from launch and served to identify the data. The data condition indicator was a measure of the quality of the received telemetry signal. DATA(22) contained the time in milliseconds between the beginning of the telemetry sequence and the first observed sun pulse.

Each cycle on the tape was preceded by a block of summary data
and was followed by the orbital and performance parameters.

CHAPTER 9

SOLAR X-RAYS

Solar X-rays were observed when the proportional counter output was octant divided, and appeared as an increased countrate in the octant centred on the sun compared with the adjacent octants. A review of the theory and previous experimental results on solar X-rays has been given in Section 1.2.

The octant division measurement has been discussed in Section 8.4. If the scaler did not go into time mode, i.e. DATA(M) < 512, then the counts per octant from the octant M is given by

$$\text{RATE}(M) = \text{DATA}(M) / \text{DATA}(M + 13) \qquad (9.1)$$

where the notation DATA(M) has been discussed in Section 8.5. The solar X-ray flux was then calculated from the counts observed in octants 3, 4 and 5 using the relation

$$\frac{dN}{dt}(\text{counts sec}^{-1} \text{ cm}^{-2}) = 65.4 \times \left\{ \text{RATE}(4) - \tfrac{1}{2}\left[\text{RATE}(3) + \text{RATE}(5)\right] \right\}/T$$
$$(9.2)$$

where T is the spin period. The normalising factor allowed for the very short time during which solar X-rays were transmitted into the

133

counter by the 2.5 degree full width at half transmission collimator.

If the scaler was in time mode the calculation of the countrate was more complex. The total number of octants including the fraction of an octant during which the 512 counts were accumulated was calculated from DATA(M) by using the optical aspect information DATA(22), the start and stop information DATA(25) and DATA(26), and the spin period of the spacecraft. As the sun was only observed for 0.034 seconds in the centre of octant 4 the 50 counts per second did not accurately determine the time within a given sun acquisition when the scaler went into the time mode. Nevertheless, the time mode could determine the number of sun sightings that were required to accumulate the 512 counts. The maximum accumulation time of 9.28 seconds allowed three or four sunsightings and, hence, three or four saturation levels in the time mode, each corresponding to the range of flux values shown in Table 13.

Most of the time the countrate in the other seven octants was isotropic, the only exceptions to this were during charged particle flare effects and while the spacecraft was in the radiation belts. If these periods were excluded and if the countrates in the adjacent octants were constant, then the excess countrate in octant 4 could only be due to solar X-rays. Charged particles would be scattered by the interplanetary magnetic field, and so any increase due to charged

TABLE 13

SOLAR X-RAY SATURATION LEVELS

No. of Sunsightings	Counts cm^{-2} sec^{-1}	
	Lower Limit	Upper Limit
1	12,900	-
2	6,450	12,900
3	4,290	6,450
4	3,220	4,290

particles in octant 4 would be accompanied by an increase in the adjacent octants. Also, the impulsive X-ray bursts usually occurred at the same time as optical flares and radio bursts, whereas charged particles would take longer to travel from the sun.

The solar X-ray flux could be divided into two components, a slowly varying component which changed over several days, Figure 32, and impulsive X-ray bursts with durations between 5 minutes and several hours, Figures 28 and 29. On very active days up to 30 bursts were observed but the average rate was about 10 bursts per day. The
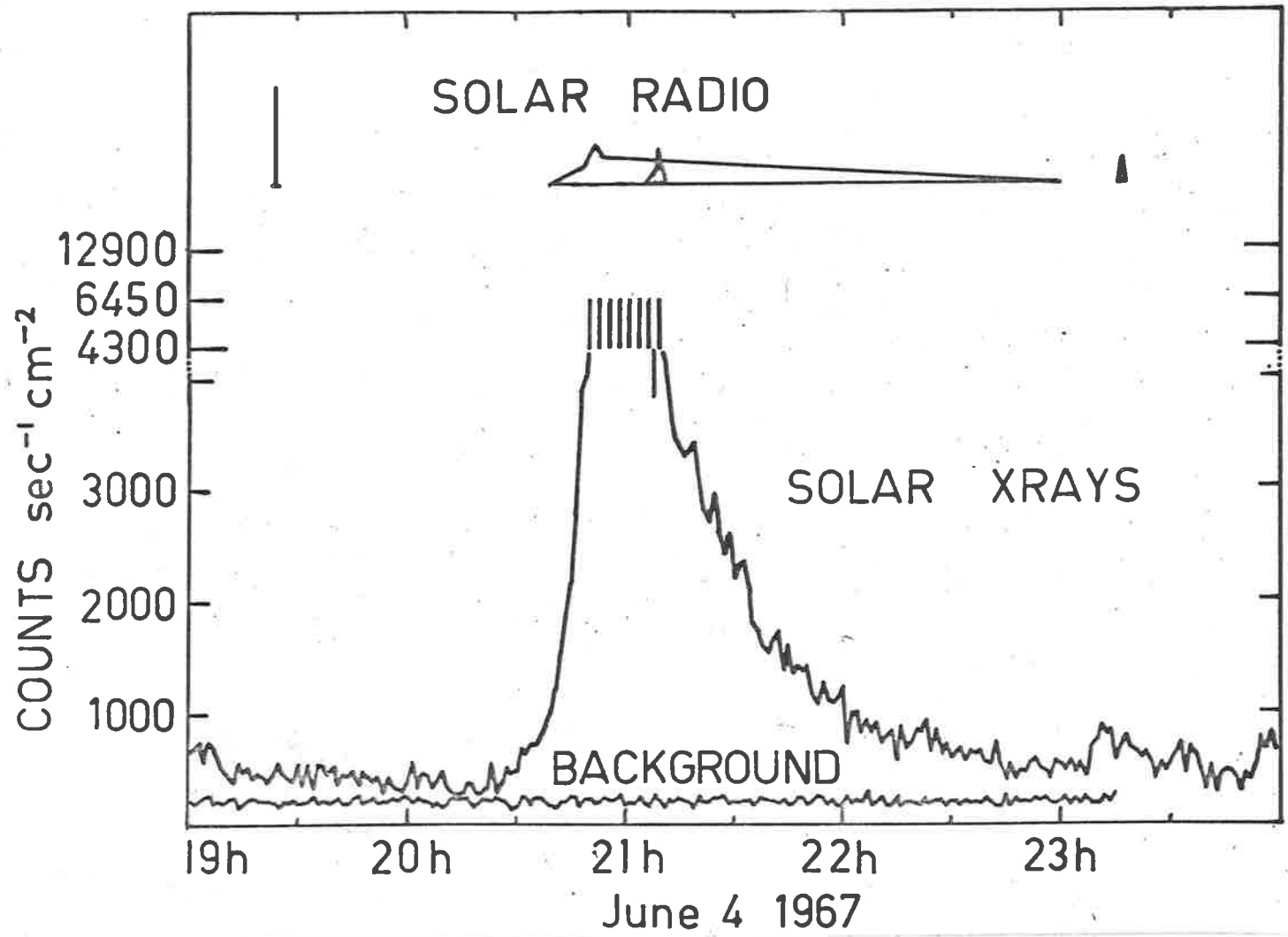
Figure 28. An example of one of the impulsive solar X-ray bursts showing the correlation with radio emission bursts.
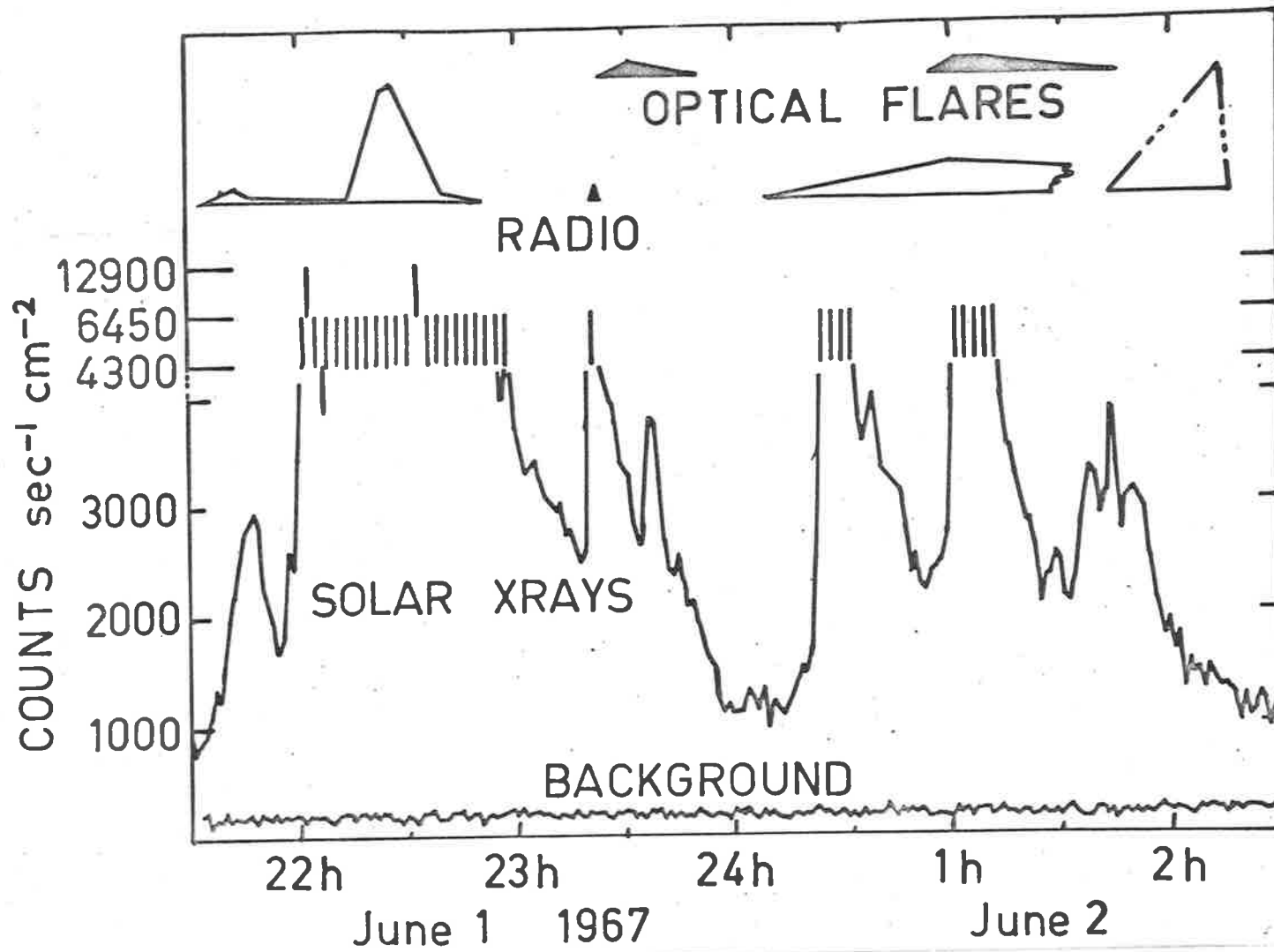
Figure 29. X-ray bursts observed during a period of high solar activity.

TABLE 14

INTENSITY LEVELS

Intensity Level	Counts cm^{-2} sec^{-1}	
	Lower Limit	Upper Limit
0	0	376
1	376	660
2	660	1,150
3	1,150	2,000
4	2,000	3,500
5	3,500	6,200
6	6,200	10,800
7	10,800	

duration, rise time and decay times varied from burst to burst, but an 'average' low intensity burst had a rise time (10%-90%) of 3 minutes, and a decay time of 6 minutes, while an 'average' intense burst had a rise time of 6 minutes and a decay time of 30 minutes.

For analysis it was convenient to divide the maximum amplitude of the X-ray bursts into the seven exponential intensity levels shown in Table 14. The divisions were chosen to fit in with the saturation levels shown in Table 13. Provided the charged particle background was less than about 60 counts sec^{-1}, which was true most of the time, the highest saturation level would be intensity 7 and so on down. Note that intensity 0 includes all countrates up to 376 counts cm^{-2} sec^{-1}, and so could possibly contain small X-ray bursts. The X-ray flux below this level was often very variable, and it could not be separated into well defined bursts.

9.1 Correlation with Optical Flares

Solar flares are observed at optical wavelengths as sudden brightenings in almost all of the Fraunhofer lines, particularly the Hα line at 6563 A. The hydrogen in the chromosphere is optically thick at this wavelength and normally produces an absorption line on the optical photospheric emission. During a flare, the temperature of a region in the chromosphere rises to about 10^4 °K producing increased emission at Hα . The mean altitude of the optical flare is about 10^4 km above the photosphere. Although this emission mechanism is very different from that for X-rays, both occur at the same time as

TABLE 15

Hα FLARE IMPORTANCE SCHEME

Area of Flare	Optical Intensity		
'corrected' sq. deg.	Faint	Normal	Bright
2.0	-f	-n	-b
2.1 - 5.1	1f	1n	1b
5.2 - 12.4	2f	2n	2b
12.5 - 24.7	3f	3n	3b
24.7	4f	4n	4b

a result of the sudden release of energy in a solar flare, and it is worthwhile to investigate the relationship between the two effects.

The solar emission of Hα is continuously monitored by various observatories around the world and the flares are listed in the ESSA Solar Geophysical Data Bulletins (1967). The flare classification used is shown in Table 15. The intensity is a qualitative figure that each observatory assigns using its experience. The correlation between the intensity of the Hα flare and its area is rather poor (de Jager 1959).

The IMP-F X-ray bursts for 52 days in June and July 1967 were compared with the reported Hα flares. Data were used at all times for which the following conditions held, (1) the satellite was beyond the radiation belts, (2) the received data was of good quality, as determined by the tracking station, (3) no charged particle flare effects were present, (4) the solar activity was not too high so it was possible to associate a particular X-ray burst with a unique listed Hα flare, and (5) there was cinematographic flare patrol coverage. For 80% of the time all of these conditions were satisfied, and yielded 472 X-ray bursts to be compared with 687 Hα flares.

Not many of the weaker Hα flares were associated with observable X-ray bursts, but the association improved for the more intense flares, Table 16. Unfortunately very few Hα flares with area importance 2 or greater were observed during the analysis period.

Figure 30 shows the distribution of the intensity of the X-ray bursts associated with a given importance Hα flare. The distribution for 1b flares showed a peak at intensity 6 X-ray bursts, while the distributions for the weaker and smaller flares did not show any such peak. These distributions show that Hα flares of larger area and greater intensity tended to produce the more intense X-ray bursts. However, there was not a simple relationship, some small area faint flares produced more intense X-ray bursts than larger area bright
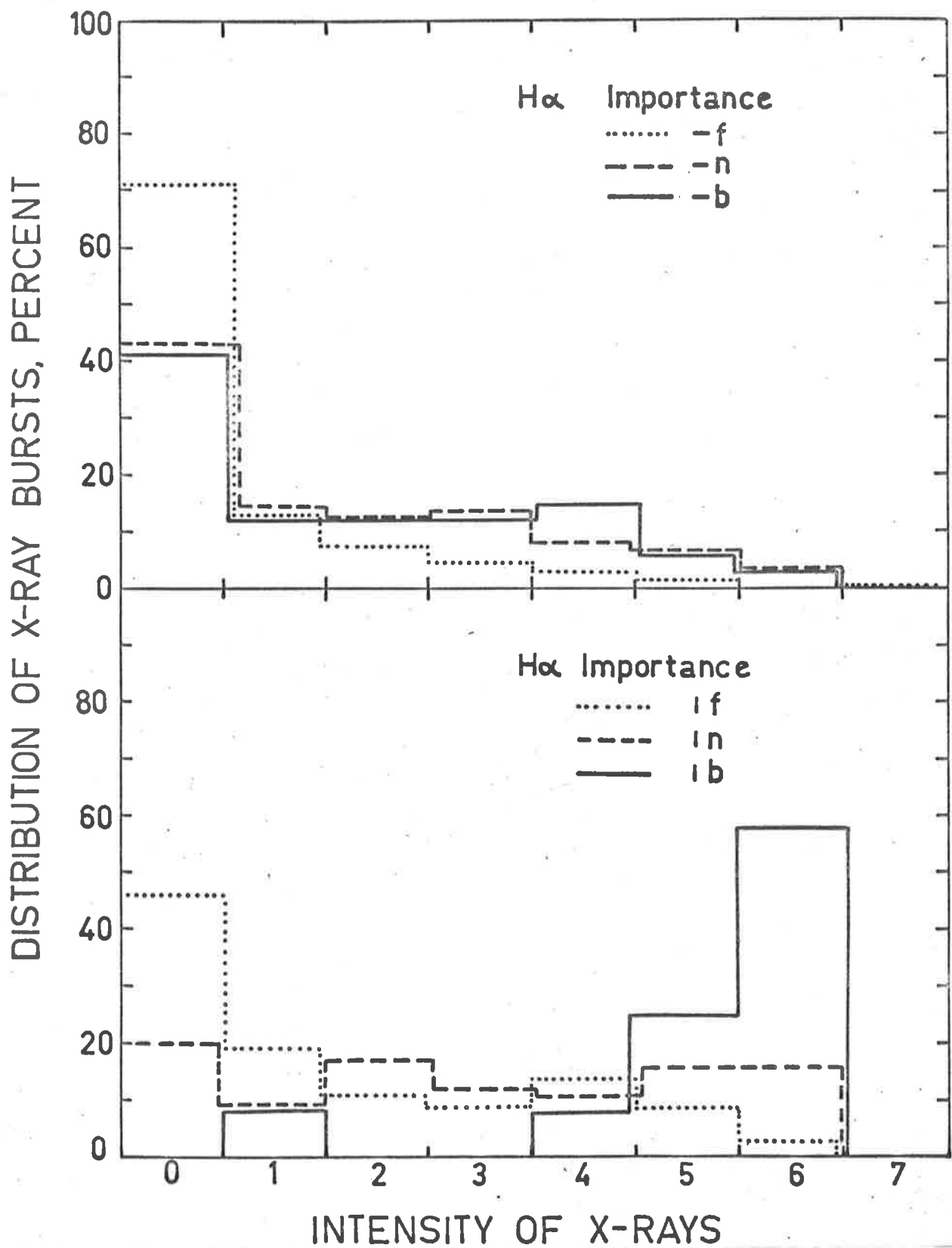
Figure 30. The distribution of the X-ray burst intensities that are associated with a given importance Hα flare.

TABLE 16

FRACTION OF Hα FLARES THAT WERE ASSOCIATED WITH X-RAY BURSTS

Area	Intensity		
Importance	Faint (f)	Normal (n)	Bright (b)
-	.29 ± .03	.57 ± .03	.59 ± .08
1	.54 ± .08	.80 ± .05	1.0 ± .08

flares. It would probably be necessary to compare the visual appearance
of the flare with the X-ray intensity to determine an accurate
relationship.

A surprisingly large fraction of the X-ray bursts were not
accompanied by listed Hα flares. This fraction varied from 0.29 for
the lowest intensity X-ray bursts to 0.18 at highest intensities.
Although some of these could be caused by poor coverage in the Hα
flare patrol they all occurred at times when there was both visual and
cinematographic patrol coverage. There were two possible explanations,
either (1) X-ray bursts occurred without any significant associated
Hα emission or (2) the flare occurred close to or around the solar
limb. The probability of a flare occurring within $20°$ longitude of

either limb on a given day was assumed to be proportional to the total

sum of the number of flares that occurred on the east limb on the day

and the two following days, and the number that occurred on the west

limb on the day and the two preceeding days. For this calculation,

limb flares were defined to be those that occurred at radial distances

greater than 0.95 (i.e. at longitudes greater than 72° relative to the

centre of the solar disk) and only normal intensity and bright flares

were counted. The number of X-ray bursts observed on a given day was

normalised to 24 hours of observation. The results of the comparison

are shown on Figure 31. The majority of the X-ray bursts for which

there was no associated Hα flare occurred when there was maximum limb

activity. The effect was more marked when only X-ray bursts of

intensity 3 and greater were considered. Some of the smaller bursts

could have been associated with weak Hα activity on the disk that was

not reported.

The alternative explanation of X-ray bursts without Hα emission

from the whole of the solar disk can be shown to be very unlikely by

comparing the temporal distribution of these bursts with the total

number of Hα flares observed each day, Figure 31. There is virtually

no similarity between the two distributions.

The number of reported Hα flares per degree of solar longitude

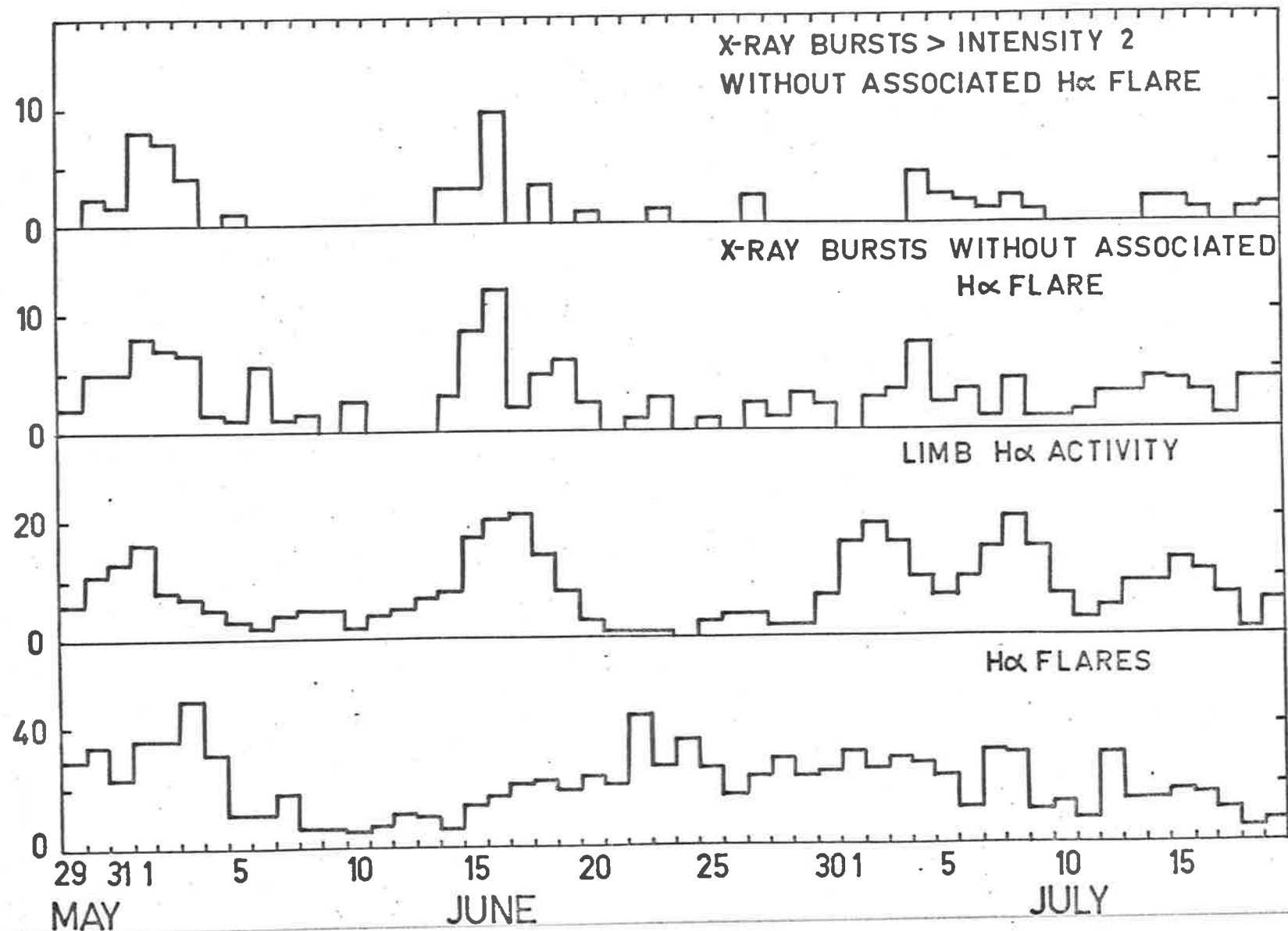did not change significantly out to the limb, showing that the

Figure 31. Daily variation of X-ray bursts that occurred without an associated Hα flare.

probability of the flare patrol not observing a flare because of foreshortening was small. This fact, and the similarity of the distributions in Figure 31 leads to the conclusion that the unassociated bursts must have been caused by flares which occurred around the limb and that the optical Hα emission, which occurs low in the solar atmosphere, was obscured by the limb.

The fraction of bursts without associated Hα flares varied from $(29 \pm 4)\%$ at low intensities to $(18 \pm 5)\%$ at high intensities. Eighteen percent of the bursts would correspond to $20°$ of longitude around each limb if bursts were emitted uniformly at all solar longitudes. There are two possible mechanisms whereby a flare this far around the limb could produce X-rays observable from the earth. Either the X-ray emission occurred high in the solar atmosphere or else streams of electrons from the flare travelled to the near side of the limb where they produced bremsstrahlung X-rays when they were stopped in the chromosphere.

X-rays emitted high in the atmosphere around the limb will be principally attenuated by photoelectric absorption. Using the density of the chromosphere given by de Jager (1959, p. 141), significant absorption would occur for X-rays that passed within about 400 km of the photosphere. For $(18 \pm 5)\%$ of the bursts to occur around the limb and still be observed at the earth, it is necessary that the emission

region must be $(4 \pm 2) \times 10^4$ km above this absorption level. The errors are large compared with the height of the absorption level above the photosphere, so this altitude can be equally considered to be measured from the photosphere. This altitude is in agreement with that inferred by Broadfoot (1967) and Acton (1968) for isolated bursts.

If a large flare occurred more than the 20° around the limb, then the upper part of the X-ray emitting region might still be observed from the earth. This effect would make the biggest contribution to the lower intensity X-ray bursts and could explain the larger fraction of low intensity bursts that were not associated with Hα flares. This would imply an e-folding height of about 5×10^4 km for the X-ray region. Alternatively, the extra X-ray bursts at low intensity could have been associated with low level Hα activity on the disk that was not reported.

The possibility of a high energy electron stream travelling some distance before producing X-rays when it is stopped in the corona does probably happen on occasions, however, because of the small number of inverted Type III radio bursts associated with X-ray emission (Kundu 1965) it is unlikely to occur often enough to explain the present results.

9.2 Correlation with Radio Emission

The solar radio emission can be divided up into three components originating from the quiet sun, from bright regions, and from transient disturbances (Kundu 1965). Previous experimenters have shown that the generation of solar radio waves at centimeter wave lengths was associated with the production of X-rays and this is confirmed by the present results.

The slowly varying component of the X-ray flux was determined by taking sample periods of 10 minutes every four hours away from any burst activity. The comparison between the slowly varying X-ray and radio fluxes is shown in Figure 32 for various frequencies. The X-ray background was found to be more variable than the radio emission, but had the same general features as the emission at 4995 or 2800 MHz. This similarity in behaviour arises because both the radio and X-ray slowly varying components are produced from coronal condensations above active regions (see Section 1.2).

The solar X-ray bursts were compared with the radio bursts recorded from several stations in the western hemisphere covering frequencies from 486 to 10700 MHz, which were tabulated in the ESSA Solar Geophysical Data Bulletins (1967), Table 17. Unfortunately no information was provided on coverage so that the lack of observation
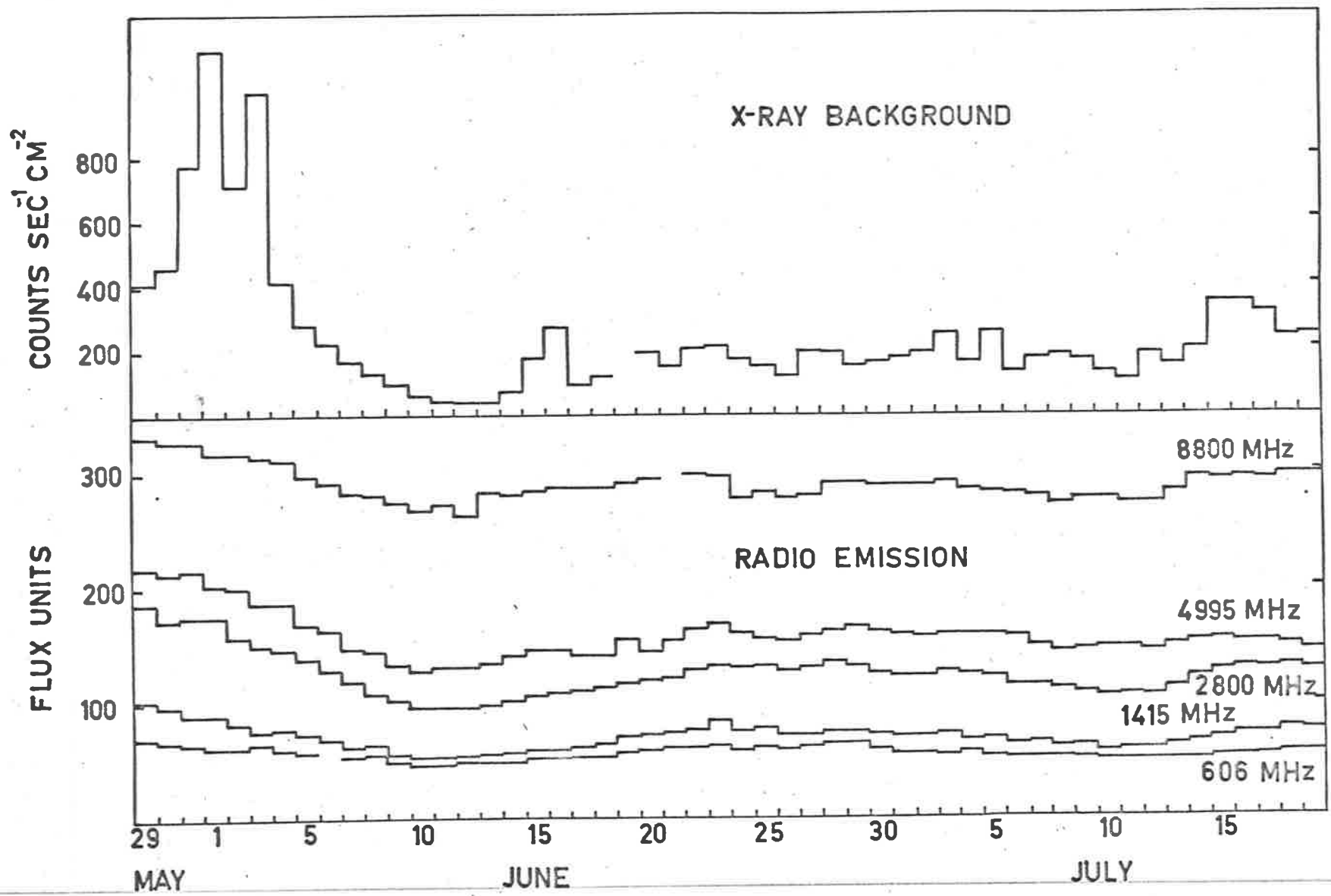
Figure 32. The slowly varying component of the solar X-ray flux. The very large fluxes at the beginning of June were at times of high solar activity and are probably due to the X-ray burst activity.

TABLE 17

STATIONS REPORTING OUTSTANDING RADIO OCCURRENCES

Frequency	Station
486	Washington State University
606	Air Force Cambridge Research Laboratory - Sagamore Hill
1415	Air Force Cambridge Research Laboratory - Sagamore Hill
2695	Air Force Cambridge Research Laboratory - Sagamore Hill
2700	Dominion Radio Astrophysical Observatory - Penticton, B. C.
2700	Pennsylvania State University
2800	Algonquin Radio Observatory - Ottawa
4995	Air Force Cambridge Research Laboratory - Sagamore Hill
8800	Air Force Cambridge Research Laboratory - Sagamore Hill
10700	Pennsylvania State University

by one station did not necessarily mean that a radio burst did not occur; the station might not have been operating. In view of this problem the radio and X-ray bursts were only compared when there was radio data available.

The correlation coefficient between the logarithm of the maximum intensity of the X-ray burst and the logarithm of the maximum intensity of the radio burst was calculated. The correlation coefficient between the two sets of values x_i, y_i is defined as

$$r = \frac{\sum(x_i - \bar{x})(y_i - \bar{y})}{\left[\sum(x_i - \bar{x})^2 \sum(y_i - \bar{y})^2\right]^{\frac{1}{2}}}$$

$$= \frac{\text{covariance}}{\text{product of variances}} \qquad (9.3)$$

It lies between -1 and $+1$; if all points lie on the regression line then $r = \pm 1$, but if the two variables are totally unrelated, then $r = 0$. Logarithms were used to decrease the dependence of r on a few high intensity radio bursts and was equivalent to assuming a power law relation between the two phenomena. Each station was considered separately to avoid problems of the calibration between the different receivers.

The correlation coefficient had a maximum in the range 3000 to 5000 MHz, i.e. 10 to 6 centimeters wavelength, Figure 33. The correlation coefficient between the X-ray and the radio bursts observed at 2700 MHz by Pennsylvania State University is shown by the dotted line since the result is probably invalid. This station observed many bursts which were not associated with any X-ray bursts and, furthermore,
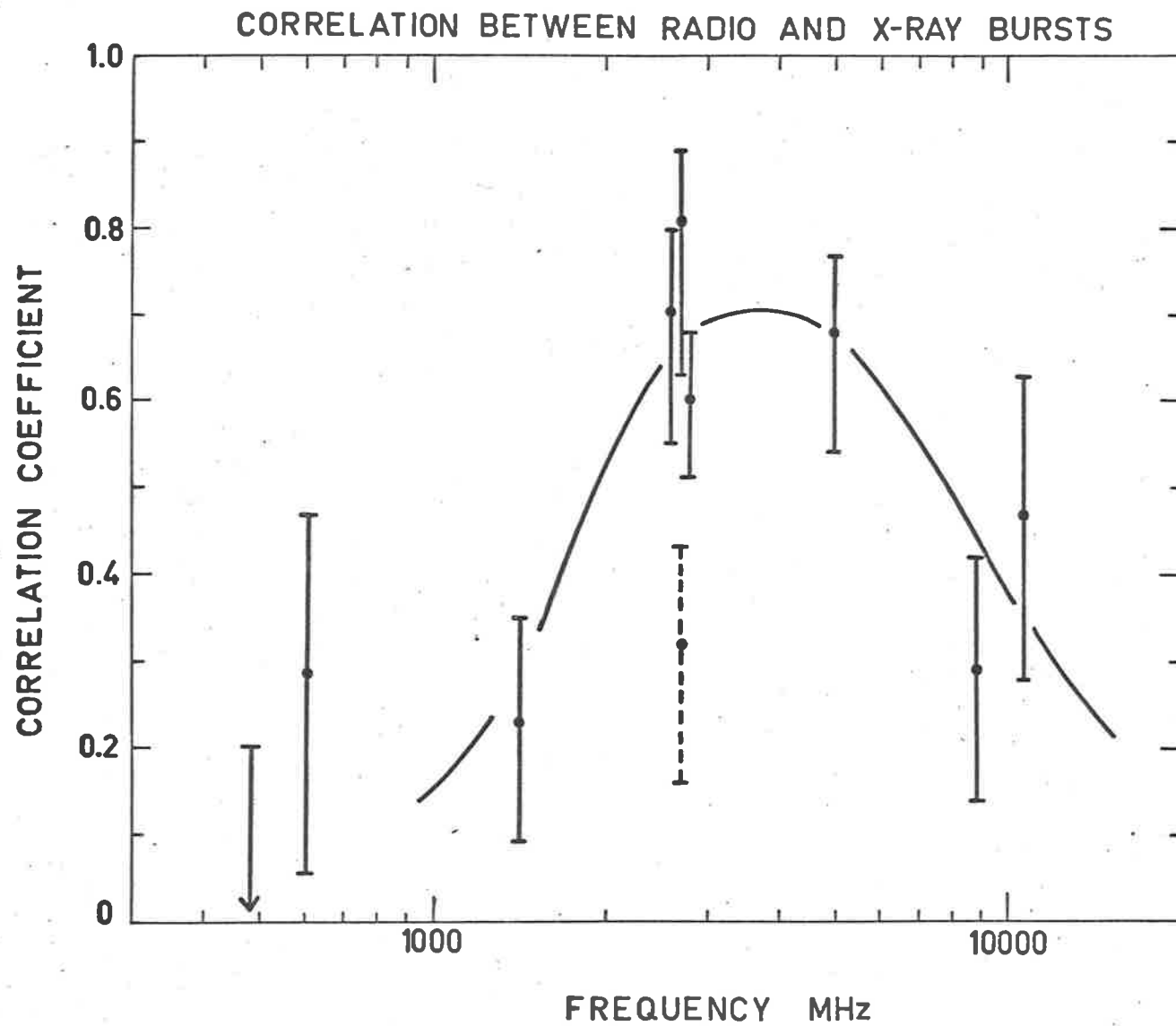
Figure 33. The correlation between the peak intensities of the X-ray and the radio bursts.

which were not observed by any of the other three stations at
2695, 2700 and 2800 MHz.

9.3 Conclusions

The observed properties of the solar X-ray bursts can be
summarised as follows

(1) The X-ray bursts are associated with both Hα flares and
microwave radio bursts.

(2) The more intense X-ray bursts tend to be associated with the
brighter, larger area Hα flares, and although there is no
simple relationship between the two phenomena, there is no
evidence that X-ray bursts occur without any associated Hα
activity.

(3) The rise time and decay time vary from burst to burst, but the
average rise time (10% to 90%) was about 3 minutes for low
intensity bursts and 6 minutes for intense bursts. The decay
time ranged from about 6 minutes for lower intensity bursts
to 30 minutes for higher intensity bursts. A few very large
bursts were observed that continued for up to 5 hours.

(4) The X-rays are emitted from a region $(4 \pm 2) \times 10^{4}$ km above
the photosphere.

(5) The emission region probably extends upwards with a scale

height of about 5×10^4 km.

(6) The intensity of the X-ray burst is correlated with the peak
intensity of microwave bursts in the range 3000 to 5000 MHz.
The correlation decreases away from this frequency range.

The intensity of the X-ray bursts observed ranged from 400 to
10^4 counts cm^{-2} sec^{-1}. A solar emission region with a total strength
of 1.4×10^{31} photons sec^{-1} would produce a flux of 5000 photons $cm^{-2}sec^{-1}$
at the earth. An upper limit to the emission measure $\int n_e^2 dV$ can be
determined by assuming that all of these photons are produced by thermal
bremsstrahlung and that the temperature of the emission region is
0.3 keV (3.5×10^6 $^{\circ}$K). This is the temperature observed for an active
region (Neupert 1967; Evans and Pounds 1968) and should be a lower
limit to the temperature in a flare region. Equation 7.1 then gives

$$\int n_e^2 dV \sim 1.8 \times 10^{50} \quad cm^{-3} \qquad (9.4)$$

The electron density at 4×10^4 km in the quiet corona is only
about 2×10^8 cm^{-3}, but above an active region it is increased by at
least an order of magnitude (Neupert 1967). Hence, an upper limit to
the volume of the emitting volume can be obtained by assuming that the
electron density in the flare region will be greater than the preflare
electron density (i.e. 2×10^9 cm^{-3}) then

$$V < 5 \times 10^{31} cm^3 \cdot = 5 \times 10^{16} km^3 \qquad (9.5)$$

This volume is at least an order of magnitude greater than the volume of a coronal active region (Neupert 1967) although the burst X-rays would be expected to be emitted within the active region. This shows that either the temperature or density of the flare region must be greater than assumed, or that thermal bremsstrahlung plays a very small part in the process.

Several processes have been suggested to account for the enhanced X-ray emission during flares. Neupert et al. (1968) observed that most of the radiation above 4 keV was from the emission lines of iron. Neupert (1968) suggested that this X-ray emission originates in a hot plasma produced by the thermalisation of the fast electrons probably responsible for the impulsive radio burst. It was necessary for the plasma to have a temperature of $\sim 3 \times 10^7$ $^{\circ}$K and an emission measure of $\sim 2 \times 10^{48}$ cm^{-3} to account for the emission during one 3bHα flare. This very high temperature could be avoided if the ionisation was produced by a flux of nonthermal electrons. However, the difficulty would then be to prevent nonthermal bremsstrahlung becoming the dominant process, as this would not produce the observed emission lines.

Acton (1968) and Arnoldy et al. (1968) have suggested that the intensity variations with time of the X-ray and the microwave bursts reflect the time variations of the electron acceleration process. They assume that the X-ray emission is by nonthermal bremsstrahlung and, as

such, would appear to give an X-ray emission region considerably below 4×10^4 km and would not produce the emission lines observed by Neupert et al. (1968). Therefore, it is unlikely that this process is dominant at about 3 keV although it could be important at higher energies.

The actual processes involved in the solar X-ray burst emission are still very poorly known even though solar X-rays have been observed for many years. This reflects both the lack of definitive data and the complexity of the solar atmosphere. The processes will only be understood when more accurate experiments, at both X-ray and radio wavelengths, can give concurrent information on the energy spectra and the spatial distribution of the emission regions.

CHAPTER 10

THE TEMPORAL STABILITY OF CELESTIAL X-RAY OBJECTS

- IMP RESULTS

The azimuth measurement of the proportional counter was designed
to determine the positions and strengths of galactic X-ray sources.
A single channel pulse height analyser selected a suitable pulse
from the proportional counter and the azimuth of the satellite was
determined at the instant when this pulse was detected. The single
channel of the pulse height analyser was varied between measurements
so that two different portions of the X-ray spectrum were measured.
The method of measurement has been discussed in Section 8.4. One
azimuth measurement was performed each 20 seconds and consequently
data had to be accumulated over several days to obtain significant
results.

For measurement L = 4 and 5 the pulse height analyser channel
limits were set to 1.6 and 3.5 V and the data were treated separately
from those for L = 6 and 7 when the channel was 3.55 to 5.1 V. These
voltages corresponded to the energy channels 2.7 to 5.9 keV and 6.0
to 8.6 keV. The effect of the single channel was to make the azimuth

measurement more sensitive to X-rays than charged particles, which tended to deposit too much energy in the counter.

The optical aspect information transmitted with each telemetry sequence enabled the azimuth of the spacecraft to be determined with respect to the sun. An even coverage of all azimuths was obtained by activating the azimuth logic after the telemetry readout. This effectively randomised the start times of the scans over all azimuths. It was necessary to define the zero of the spacecraft azimuth scale with respect to the celestial sphere. For the first month after launch the spin axis was less than 2° from the pole of the ecliptic and to the end of 1967 it was never more than 6.5^o away. Hence, the zero of the azimuth scale could be set to the equinox by subtracting the ecliptic longitude of the sun (the spacecraft was spinning in the opposite sense to the ecliptic longitude).

DATA(9) was the length of time in units of 0.01 seconds for which the system was activated ready to receive a pulse. That is, DATA(9) determined both the azimuth when the pulse was received, and also the range of azimuths that the counter scanned before observing the pulse. Hence, it was possible to normalise the number of pulses detected by the time of observation. For purposes of analysis, the azimuth scale was divided into one degree intervals. The ratio of the number of times a pulse was received while the satellite azimuth

was in one of these intervals to the number of times that the
activated counter system looked in this direction was calculated.
At high countrates this ratio had to be corrected because the azimuth
measurement logic only accepts one pulse in a given measurement. More
than one pulse could have occurred in any 0.01 second interval, but
this would appear exactly the same as if only one pulse had been
observed. The countrate corresponding to an observed ratio, R counts
degree^{-1}, is from Poisson statistics

$$N = \dot{-} 100 \ln \left[1.0 - (3.6/T)R \right] \quad \text{counts sec}^{-1} \quad (10.1)$$

where T is the spin period. Provided R is small, this reduces to

$$N = R(360/T) \quad \text{counts sec}^{-1} \quad (10.2)$$

The difference between equations 10.1 and 10.2 was less than 10% for
all the values of R observed from the experiment. The maximum ratio
was R = 0.12 which was obtained for the Sco XR-1 sighting.

The resultant distribution of the data from the orbits 2 through
13 (May 28 to July 19, 1967) for the range of azimuths including
Sco XR-1 and the galactic centre is shown in Figure 34. Data were
excluded whenever the countrates in the octant division mode were
high, because this indicated an increased charged particle flux
which would swamp the azimuth measurement. The longitude scale in
the figure has been adjusted by about one degree to put the Sco XR-1
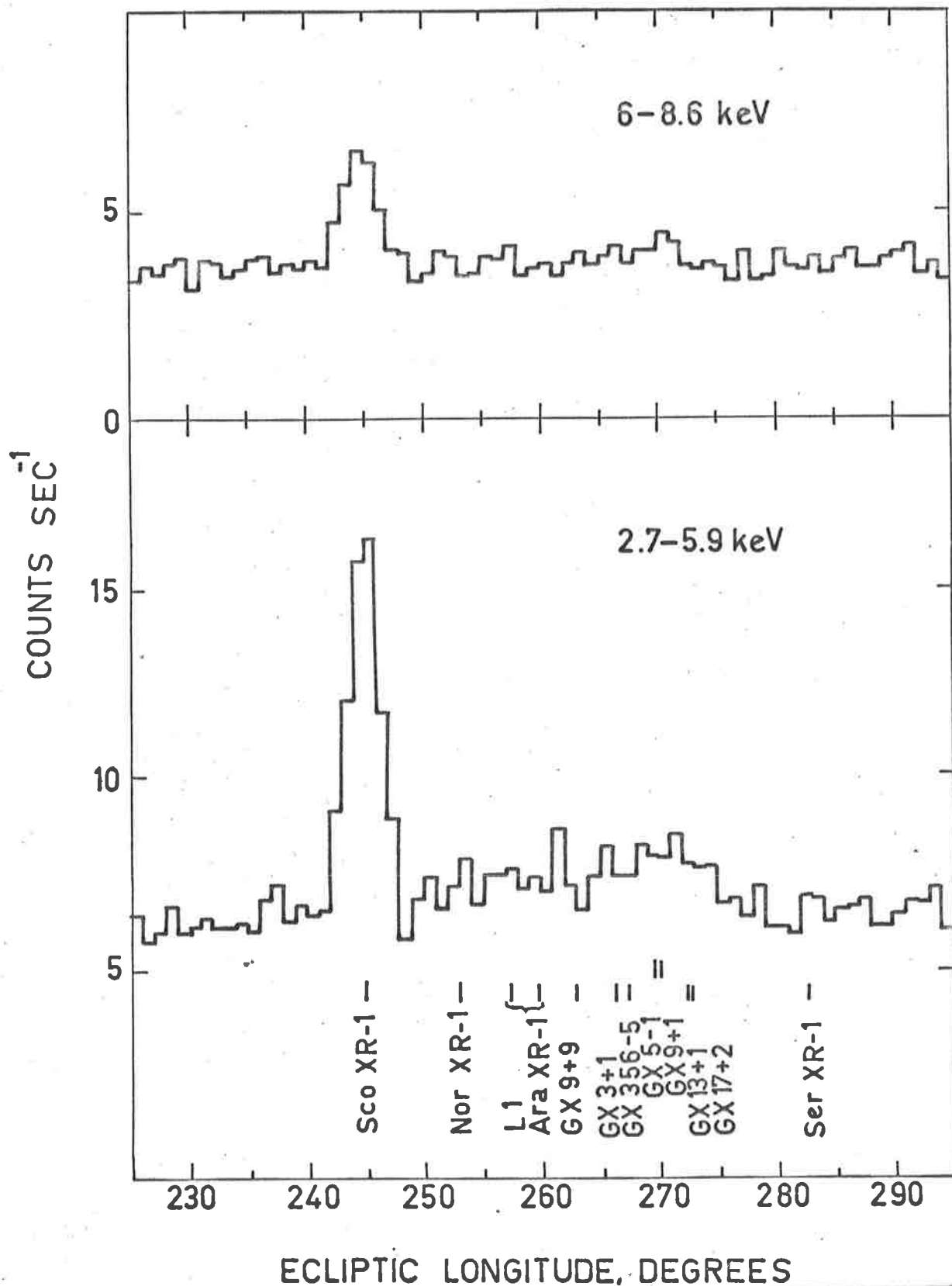at the correct ecliptic longitude of 245 degrees. An error of this

Figure 34. The celestial X-rays observed on IMP-F.

magnitude could be expected due to the uncertainties in the phasing of the 100 Hz signal used to time the azimuth. The full width of the Sco XR-1 peak is consistent with the 5° full width collimator for a source on the ecliptic after convolutions over the 0.01 second time and the one degree angle intervals have been taken into account.

An increase in the countrate was also observed from the galactic centre region, Figure 34. The region of the increase agrees with the known source locations but none of the individual sources were resolved. The countrate was isotropic over all other azimuths that were scanned. The blanking out of the sun octant obscured Tau XR-1 which might have given a flux above the threshold of detectability. Cen XR-2 was about 50° off the ecliptic plane and hence was scanned by the detector, but was not observed. This means that it must be less than about 0.1 Sco XR-1 which is in agreement with the extrapolation of the rocket results, Table 11.

The countrate observed from Sco XR-1 was less by a factor of 2 or 3 than would be expected on the basis of results of other experimenters (Chodil et al. 1968). This could be due to either a partial obscuration of the counter window or to deterioration of the counter characteristics. A bias level shift or gain change would need to be so large as to make the solar X-ray results unreasonable. The most likely cause is deterioration of the counter between the time it was last tested and when it was launched. This deterioration could

manifest itself in a very poor counter resolution and perhaps a slow
pulse rise time due to the presence of electronegative gases. Both
of these effects would necessitate the use of a different correction
factor to the two pulse height analyser channels.

A fixed normalising factor was applied to all the IMP data so
that the results for orbit 30, September 26 to October 1, 1967, agreed
with the Sco XR-1 spectrum measured by Chodil et al. (1968b) on
September 28, 1967. A separate normalising factor was determined for
each of the two pulse height analyser channels. The resulting fluxes
for Sco XR-1 are shown in Figure 35, together with the Skylark
measurements reported in Section 5.4 of this thesis and the results of
Chodil et al. No data was obtained from orbit 1 due to the presence of
a large charged particle flare. The results from orbits 2 and 3 are
shown but they probably represent the effect of the vacuum on the
epoxy used in the counter construction and the associated partial
restoration of the counter characteristics.

Consider first the low energy channel, 2.7 to 5.9 keV, the flux
observed by Chodil et al. (1968b) on May 18, 1967, agrees with the
IMP results during June. Then, about July 10, the flux increased by
almost 50% to the level that Chodil et al. observed at the end of
September. Although one must be wary of reading too much into the
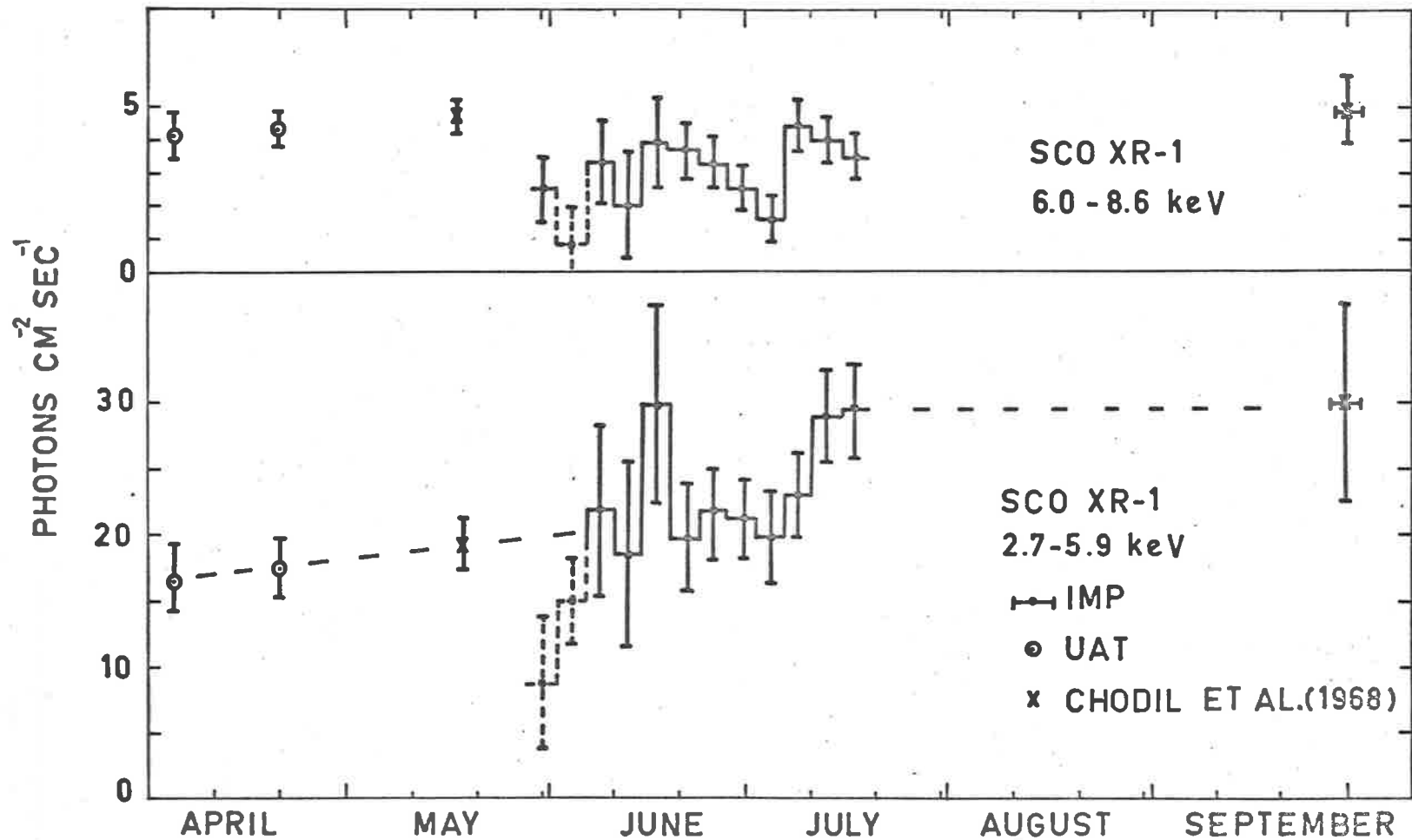data because of the unknown counter condition and the size of the error

Figure 35. The variation in the Sco XR-1 flux. Each IMP data point corresponds to one orbit of 4.3 days.

bars, the results tend to confirm the low energy increase observed by Chodil et al. and to suggest that the change occurred abruptly over less than four days.

The results for the higher energy channel are also shown on Figure 35, again a constant normalising factor has been used, so that the IMP results agree with the results of Chodil et al. (1968b) on September 29. These results indicate a possible softening of the spectrum prior to the increase observed in the lower energy channel.

These results suggest that the Sco XR-1 X-ray spectrum was steady until the beginning of July, when the spectrum initially softened and then the intensity increased with a constant spectral index. One possible explanation of this behaviour could be the obscuration of a high temperature region of the source a short time before the appearance of another larger but cooler region. Obscuration could be due to either occultation by a binary partner or even by rotation of the source. However, it is hard to explain the close time relation between the disappearance of one region and the appearance of another. It seems more likely that the observed variation must be due to changes in the same emission region, i.e. the region initially cools and then emission is increased, perhaps by isothermal compression. Alternatively, if the emission occurs by synchrotron emission the electron acceleration mechanism could be varied to fit the observed X-ray spectrum behaviour.

APPENDIX A

LEAST SQUARES FIT TO SKYLARK COUNTRATE DATA

The collimators employed on the Skylark experiment had a triangular response function, 10.5^o full width at half transmission in rocket azimuth (i.e. along the scan direction) and 35° full width at half transmission normal to the scan direction. The Least Squares technique was used to fit the collimator response to the countrate data observed from a point source first on the individual scans, and then to the data observed on several consecutive scans. This enabled the position of the source and also the countrate corresponding to normal incidence to be determined.

The observed data consists of a series of countrates, $X(t_i)$, observed at times, t_i. If the collimator response is $g(t)$, with $g(0) = 1$, then the theoretical response from a point source will be of the form $Ag(t - t_o)$ where A is the strength of the source and t_o is the time of maximum response. In the least squares method the parameters A and T_o are chosen so as to make the sum of the squares of the deviations as small as possible, i.e.

$$E = \sum_i \left[X(t_i) - Ag(t_i - t_o) \right]^2 \qquad (A.1)$$

is minimised. Each point was weighted equally. At the minimum the
partial derivatives will be zero and so

$$\frac{\partial E}{\partial A} = \sum \left\{ \left[X(t_i) - Ag(t_i - t_o) \right] 2g(t_i - t_o) \right\} = 0$$

$$A = \frac{\sum X(t_i)g(t_i - t_o)}{\sum \left[g(t_i - t_o) \right]^2} \qquad (A.2)$$

The variance of A is given by

$$V(A) = \frac{\sum V[X(t_i)][g(t_i - t_o)]^2}{\left\{ \sum [g(t_i - t_o)]^2 \right\}^2}$$

For poisson statistics $V[X(t_i)] = X(t_i)$

$$V(A) = \frac{\sum X(t_i)[g(t_i - t_o)]^2}{\left\{ \sum [g(t_i - t_o)]^2 \right\}^2} \qquad (A.3)$$

Along a given scan the response function g(t) was a triangle with
a base equal to (21/360)T where T was the spin period. In the analysis
A, V(A) and E were computed for various values of t_o, the correct t_o
being that which minimised the error function, E. It was deemed
sufficient to determine t_o by this method rather than using the Taylor
expansion method (e.g. Deming 1943).

The variance of t_o is determined by considering the Least Squares fit of half of the triangle to the data, i.e.

$$g(t_1 - t_o) = A \left[1 - (t_o - t_i)/B \right] \qquad \text{(A.4)}$$

This expression is used in equation A.1 and the partial derivative with respect to t_o is set to zero. This gives

$$t_o = \frac{1}{N} \left[t_i - \frac{B}{A} \sum X(t_i) \right] + B \qquad \text{(A.5)}$$

where N is the number of data points. Then

$$V(t_o) = \left[\frac{B}{NA} \right]^2 \sum V \left[X(t_i) \right] \qquad \text{(A.6)}$$

where A is known from equation A.2. Since the triangular response is effectively two straight lines, equation A.6 was sufficiently accurate to give the variance of the triangular fit directly.

Hence the maximum intensity, the variance in the intensity, the time of the maximum on the scan, and the variance in the time have been determined. The Least Squares fit of the data from consecutive scans was performed in an almost identical manner. The times of sightings of the source were used as the independent variable and the calculated time of maximum response was used to interpolate between the two nearest sightings. The response function from scan to scan

was determined from the attitude solution. It was found to be triangular for the sightings of Sco XR-1 on Flight I and Cen XR-2 on Flight II. However, for Sco XR-1 on Flight II and Cen XR-2 on Flight I deviations from a triangular response became noticeable after the maximum countrate. This was due to the phasing between the precession and scan motion of the rocket. The deviation was approximated by using a different width triangle after the maximum. The rest of the analysis followed the procedure outlined for the Least Squares fit to the data observed on one scan.

APPENDIX B

PUBLICATIONS

The following papers have been published on the work described in this thesis:

A Strong X-ray Source in the Vicinity of the Constellation Crux,
J. R. Harries, K. G. McCracken, R. J. Francey, and A. G. Fenton,
Nature, 215, 38-40, (1967).

Variability of Centaurus XR-2, R. J. Francey, A. G. Fenton, J. R. Harries,
and K. G. McCracken, Nature, 216, 773-774, (1967).

Thermal Models of Centaurus XR-2, P. J. Edwards and J. R. Harries,
Proc. Astron. Soc. Aust., 1, 109-111, (1968).

The X-ray Albedo from the Earth, J. R. Harries and R. J. Francey,
Proc. Astron. Soc. Aust., 1, 111-112, (1968).

Variability of Centaurus XR-2, R. J. Francey, A. G. Fenton, J. R. Harries,
and K. G. McCracken, Proc. Astron. Soc. Aust., 1, 108-109, (1968).

Observations of Cen XR-2, Sco XR-1 and Terrestrial X-rays, J. R. Harries,
and R. J. Francey, Aust. J. Phys., (in press).

Impulsive X-ray Emission by the Sun, J. R. Harries, Proc. Astron. Soc.
    Aust., 1, 51-52, (1967).

Solar X-ray Bursts Observed on IMP-F, J. R. Harries, Proc. Astron. Soc.
    Aust., (in press).

REFERENCES

Acton, L. W., 1968, Astrophys. J., 152, 305.

Acton, L. W., Chubb, T. A., Kreplin, R. W., and Meekins, J. F., 1963
J. Geophys. Res., 68, 3335.

Andrews, B. H., and Purton, C. R., 1968, Nature, 218, 855.

Arnoldy, R. L., Kane, S. R., and Winckler, J. R., 1968a, Astrophys. J.,
151, 711.

Bahcall, J. N., and Wolf, R. A., 1965, Phys. Rev., 140, B1452.

Barkas, W. H., and Berger, M. J., 1964, 'Tables of Energy Losses and
Ranges of Heavy Charged Particles', NASA Special Publication
SP-3013.

Bartley, W. C., McCracken, K. G., and Rao, U. R., 1967, IEEE Trans.,
Aerospace Electronic Systems, AES-3. 230.

Bergamini, R., Londrillo, P., and Setti, G., 1967, Nuovo Cimento,
52B, 495.

Blake, R. L., Chubb, T. A., Friedman, H., and Unzicker, A. E., 1963,
Astrophys. J., 137, 3.

Blake, R. L., Chubb, T. A., Friedman, H., and Unzicker, A. E., 1965
Astrophys. J., 142, 1.

Blanco, V., Kunkel, W., Hiltner, W. A., Lynga, G., Bradt, H., Clark, G.,
Naranan, S., Rappaport, S., and Spada, G., 1968a, Astrophys. J.,
152, 1015.

Blanco, V., Kunkel, W., Hiltner, W. A., Chodil, G., Mark, H.,
Rodrigues, R., Seward, F., and Swift, C. D., 1968b, Astrophys. J.,
152, L135.

Bless, R. C., Fischel, D., and Stecher, T. D., 1968, Astrophys. J.,
151, L117.

Bowen, P. J., Norman, K., Pounds, K. A., Sanford, P. W., Willmore, A. P.,
1964, Proc. Roy. Soc., 281A, 538.

Bowyer, S., Byram, E. T., Chubb, T. A., and Friedman, H., 1964, Science,
146, 912.

Bowyer, C. S., Field, G. B., and Mack, J. E., 1968, Nature, 217, 32.

Boyd, R. L. F., 1965, Space Sci. Rev., 4, 35.

Bradt, H., Mayer, W., Naranan, S., Rappaport, S., and Spada, G., 1967,
Astrophys. J., 150, L199.

Bradt, H., Naranan, S., Rappaport, S., and Spada, G., 1968, Astrophys. J., 152, 1005.

Brecher, K., and Morrison, P., 1967, Astrophys. J., 150, L61.

Broadfoot, A. L., 1967, Astrophys. J., 149, 675.

Burbidge, G., 1966, Proc. International School of Physics, 'Erico Fermi', course 35, Academic Press, N. Y., p115.

Burgess, A., 1964, Astrophys. J., 139, 776.

Buselli, G., 1968, Proc. Astron. Soc. Aust., (in press).

Byram, E. T., Chubb, T. A., and Friedman, H., 1966, Science, 152, 66.

Cameron, A. G. W., and Mock, M., 1967, Nature, 215, 464.

Cazzola, P., Lucaroni, L., and Scarini, C., 1967, Nuovo Cimento, 1967, 52B, 411.

Chang, C. H., Cook, C. S., and Primakoff, H., 1953, Phys. Rev., 90, 544.

Charles, M. W., and Cooke, B. A., 1968, Nuclear Instrum. and Methods, 61, 31.

Cheng, C. C., 1967, Nature, 215, 1035.

Chiu, H. Y., 1966, in Space Research VI, Spartan Books, Washington, D. C., p.101.

Chiu, H. Y., and Salpeter, E. E.,1964, Phys. Rev. Letters, 12, 413.

Chodil, G., Jopson, R. C., Mark, H., Seward, F. D., and Swift, C. D.,
1965, Phys. Rev. Letters, 15, 605.

Chodil, G., Mark, H., Rodrigues, R., Seward, F. D., and Swift, C. D.,
1967a, Astrophys. J., 150, 57.

Chodil, G., Mark, H., Rodrigues, R., Seward, F., Swift, C. D.,
Hiltner, W. A., Wallerstein, G., and Mannery, E. J., 1967b, Phys.
Rev. Letters, 19, 681.

Chodil, G., Mark, H., Rodrigues, R., and Swift, C. D., 1968a, Astrophys.
J., 151, L1.

Chodil, G., Mark, H., Rodrigues, R., Seward, F. D., Swift, C. D.,
Turiel, I., Hiltner, W. A., Wallerstein, G., and Mannery, E. J.,
1968b, Astrophys, J., (in press).

Chodil, G., Mark, H., Rodrigues, R., and Swift, C. D., 1968c, Astrophys.
J., 152, L45.

Chubb, T. A., Kreplin, R. W., and Friedman, H., 1966, J. Geophys. Res.,71, 3611.

Cline, T. L., Holt, S. S., and Hones, E. W., 1968, J. Geophys. Res.,
73, 434.

Colgate, S. A., and White, R. H., 1966, Astrophys. J., 143, 626.

Compton, A. H., and Allison, S. K., 1935, 'X-rays in Theory and
Experiment', Van Nostrand, N.Y.

Connor, J. P., Evans, W. D., Montgomery, M. D., Singer, S., and
Stogsdill, E. E., 1965, in Space Research V, North-Holland,
Amsterdam, p546.

Cooke, B. A., Pounds, K. A., Stewardson, E. A., and Adams, D. J., 1967,
Astrophys. J., $\underline{150}$, L189.

Culhane, J. L., Willmore, A. P., Pounds, K. A., and Sanford, P. W., 1964,
in Space Research IV, North-Holland, Amsterdam, p741.

Curran, S. C., and Wilson, H. W., 1965, 'Alpha-, Beta-, and Gamma-Ray
Spectroscopy', p303, Ed K. Siegbahn, North-Holland, Amsterdam.

David, F. N., 1938, 'Tables of the Correlation Coefficient', The
University Press, Cambridge, England.

de Jager, C., 1959, 'Handbuch der Physik', $\underline{52}$, 80, Springer-Verlag, Berlin.

de Jager, C., 1964, 'Research in Geophysics', (ed. by H. Odishaw), MIT
Press, Massachusetts, p1.

Deming, W. E., 1943, 'Statistical Adjustment of Data', Wiley, New York.

Edwards, P. J., 1968, Nature, $\underline{217}$, 43.

Eggen, O. J., and Lynga, G., 1968, Astrophys. J., (in press).

Eggen, O. J., Freeman, K. C., and Sandage, A., 1968, Astrophys. J.,
    (in press).

Elwert, G., 1961, J. Geophys. Res., 66, 391.

Evans, K., and Pounds, K. A., 1968, Astrophys. J., 152, 319.

Fazio, G. G., Stecker, F. W., Wright, J. P., 1966, Astrophys. J., 144, 611.

Feast, M. W., 1967, Nature, 215, 1158.

Feldman, U., and Cohen, L., Astrophys. J., 151, L55.

Felten, J. E., 1967, Nature, 216, 775.

Felten, J. E., and Morrison, P., 1966, Astrophys. J., 146, 686.

Fink, R. W., Jopson, R. C., Mark, H., and Swift, C. D., 1966, Rev.
    Mod. Phys., 38, 513.

Finzi, A., 1965, Phys. Rev., 137, B472.

Fisher, P. C., Johnson, H. M., Jordan, W. C., Meyerott, A. J., and
    Acton, L. W., 1966, Astrophys. J., 143, 203.

Fisher, P. C., Jordan, W. C., Meyerott, A. J., Acton, L. W., and
    Roethig, D. T., 1968, Astrophys. J., 151, 1.

Friedman, H., 1963, Annual Rev. Astron. and Astrophys., 1, 59.

Friedman, H., 1967, Annual Rev. Nuclear Science, 17, 317.

Friedman, H., Byram, E. T., and Chubb, T. A., 1967a, Science, 156, 374.

Friedman, H., and Byram, E. T., 1967b, Science, 158, 257.

    See also: Argyle, E., 1968, Science, 159, 747.

Fritz, G., Kreplin, R. W., Meekins, J. F., Unzicker, A. F., and

    Friedman, H., 1967, Astrophys. J., 148, L133.

Frost, K. J., 1965, Space Research, 5, 513.

Giacconi, R., 1967, Scientific American, 217 Dec., 36.

Giacconi, R., Gursky, H., Paolini, F. R., and Rossi, B. B., 1962, Phys.

    Rev. Letters, 9, 439.

Giacconi, R. and Gursky, H., 1965, Space Sci. Rev., 4, 151.

Giacconi, R., Reidy, W. P., Zehnpfennig, T., Lindsay, J. C., and

    Muney, W. S., 1965, Astrophys. J., 142, 1274.

Giacconi, R., Gursky, H., Waters, J. R., Rossi, B., Clark, G., Garmire, G.,

    Oda, M., and Wada, M., 1966, Proc. International School of Physics,

    'Erico Fermi', Course 35, Academic Press, N. Y. p73.

Giacconi, R., Gorenstein, P., Gursky, H., and Waters, J. R., 1967a, Astrophys. J., 148, L119.

Giacconi, R., Gorenstein, P., Gursky, H., Usher, P. D., Waters, J. R., Sandage, A., Osmer, P., and Peach, J. V., 1967b, Astrophys. J., 148, L129.

Ginzburg, V. L., and Syrovatskii, S. I., 1964, 'The Origins of Cosmic Rays', Pergamon Press, London.

Ginzburg, V. L., and Syrovatskii, S. I., 1965a, Space Sci. Rev., 4, 267.

Ginzburg, V. L., and Syrovatskii, S. I., 1965b, Annual Rev. Astron. Astrophys., 3, 297.

Goldberg, L., 1967, Annual Rev. Astron. Astrophys., 5, 279.

Gorenstein, P., Giacconi, R., and Gursky, H., 1967, Astrophys. J., 150, L85.

Gould, R. J., 1967, Amer. J. Phys., 35, 376.

Grader, R. J., Hill, R. W., Seward, F. D., and Toor, A., 1966, Science, 152, 1499.

Grader, R. J., Hill, R. W., and Seward, F. D., 1968, 'An X-ray Airglow in the Daytime Sky', submitted to J. Geophys. Res.

Gregory, B. N., and Kreplin, R. W., 1967, J. Geophys. Res., 72, 4815.

Gursky, H., Giacconi, R., Gorenstein, P., Waters, J. R., Oda, M.,
Bradt, H., Garmire, G., and Sreekantan, B. V., 1966, Astrophys.
J., 146, 310.

Gursky, H., Gorenstein, P., and Giacconi, R., 1967, Astrophys. J.,
150, L75.

Hansen, C. J., and Tsuruta, S., 1967, Canad. J. Phys., 45, 2823.

Hayakawa, S., and Matsuoka, M., 1964, Suppl. Progr. Theor. Phys., 30, 204.

Hayakawa, S., Matsuoka, M., and Sugimoto, D., 1966a, Space Sci. Rev.,
5, 109.

Hayakawa, S., Matsuoka, M., and Yamashita, K., 1966b, Rep. Ionosphere
Space Res. Japan, 20, 480.

Hendrick, R. W., 1957, J. Opt. Soc. Amer., 47, 165.

Henry, R. C., Fritz, G., Meekins, J. F., Friedman, H., and Byram, E. T.,
1968, Astrophys. J., 153, L11.

Herbert, P. J., 1967, 'Determination of the Attitude of the Skylark
Rocket in Free Space', presented to AIAA Sounding Rocket Vehicle
Technology Specialist Conference, Williamsburg, Virginia, U.S.A.

Hudson, H. S., Peterson, L. E., and Schwartz, D. A., 1968, Science,
(in press).

Hurwitz, L., Knapp, D. G., Nelson, J. H., and Watson, D. E., 1966,
J. Geophys. Res., 71, 2373.

Jesse, W. P., and Sadaukis, J., 1957, Phys. Rev., 107, 766.

Johnson, H. M., 1966, Astrophys. J., 146, 960.

Johnson, H. M., 1967, Astrophys. J., 147, 1213.

Kawabata, K., 1960, Rep. Ionosphere Space Res. Japan, 14, 405.

Kawabata, K., 1966, Rep. Ionosphere Space Res. Japan, 20, 118.

Kreplin, R. W., Chubb, T. A., Friedman, H., 1962, J. Geophys. Res.,
67, 2231.

Kreplin, R. W., and Gregory, B. N., 1966, in Space Research VI,
Spartan Books, Washington, D. C., p1011.

Kundu, M. R., 1965, 'Solar Radio Astronomy', Interscience, New York.

Landini, M., Russo, D., and Tagliaferri, G. L., 1966, Nature, 211, 393.

Landini, M., Russo, D., and Tagliaferri, G. L., 1967a, Planet. Space
Sci., 15, 231.

Landini, M., Russo, D., and Tagliaferri, G. L., 1967b, in Space
Research VII, North-Holland, Amsterdam, p1281.

Lewin, W. H., Clark, G. W., and Smith, W. B., 1968a, Astrophys. J.,
152, L49.

Lewin, W. H., Clark, G. W., and Smith, W. B., 1968b, Astrophys. J.,
152, L55.

Lewin, W. H., Clark, G. W., and Smith, W. B., 1968c, Nature, 219, 1235.

Mandelshtam, S. L., 1965a, Ann. Astrophys., 28, 614.

Mandel'stam, S. L., 1965b, Space Sci. Rev., 4, 587.

Manley, O. P., 1966, Astrophys. J., 144, 1253.

Manley, O. P., 1967, Phys. Rev. Letters, 19, 1144.

Manley, O. P., 1968, Nature, 219, 1236.

Maraschi, L., Perola, G. C., and Schwarz, S., 1968, Nuovo Cimento, 53B,
443.

Meltzer, D. W., and Thorne, K. S., 1966, Astrophys. J., 145, 514.

Morrison, P., 1967, Annual Rev. Astron. Astrophys., 5, 325.

Morton, D. C., 1964, Astrophys. J., 140, 460.

Neupert, W. M., 1967, Solar Phys., 2, 294.

Neupert, W. M., Gates, W., Swartz, M., and Young, R., 1967, Astrophys. J., 149, L79.

Neupert, W. M., 1968, Astrophys. J., 153, L59.

O'Brien, B. J., 1964, J. Geophys. Res. 69, 13.

Oda, M., Bradt, H., Garmire, G., Spada, G., Sreekantan, B. V., Gursky, H., Giacconi, R., Gorenstein, P., and Waters, J. R., 1967, Astrophys. J., 148, L5.

Overbeck, J. W., and Tananbaum, H. D., 1968a, Phys. Rev. Letters, 20, 24.

Overbeck, J. W., and Tananbaum, H. D., 1968b, Astrophys. J., (in press).

Prendergast, K. H., and Burbidge, G. R., 1968, Astrophys. J., 151, L83.

Pounds, K. A., 1965, Ann. Astrophys., 28, 132.

Pounds, K. A., and Russell, P. C., 1966, in Space Research VI, Spartan Books, Washington, D. C., p38.

Reidy, W. P., Vaiana, G. S., Zehnpfennig, T., Giacconi, R., 1968, Astrophys. J., 151, 333.

Rieser, L. M., 1957, J. Opt. Soc. Amer. 47, 987.

Rossi, B. B., and Staub, H. H., 1949, 'Ionization Chambers and Counters, Experimental Techniques', McGraw-Hill, New York.

Roy, A. E., 1965, 'The Foundations of Astrodynamics', MacMillan, New York.

Rugge, H. R., and Walker, A. B. C., 1968, in Space Research VIII, North-Holland, Amsterdam, p439.

Russell, P. C., 1965, Nature, 205, 684.

Russell, P. C., and Pounds, K. A., 1966, Nature, 209, 490.

Sakashita, S., 1968, Progr. Theor. Phys., 39, 235.

Sandage, A. R., Osmer, P., Giacconi, R., Gorenstein, P., Gursky, H., Waters, J., Bradt, H., Garmire, G., Sreekantan, B. V., Oda, M., Osawa, K., and Jugaku, J., 1966, Astrophys. J., 146, 316.

Sartori, L., and Morrison, P., 1967, Astrophys. J., 150, 385.

Seward, F., Chodil, G., Mark, H., Swift, C., and Toor, A., 1967, Astrophys. J., 150, 845.

Shklovsky, I. S., 1967, Astrophys. J., 148, L1.

Silk, J., 1968, Astrophys. J., 151, L19.

Sofia, S., 1967, Astrophys. J., 149, L59.

Solar Geophysical Data, 1967, Environmental Science Services Administration, U. S. Dept. of Commerce.

Somogyi, G., and Body, Z. T., 1965, Brit. J. Appl. Phys., 16, 1285.

Symon, K. R., 1960, 'Mechanics', Addison-Wesley, Massachusetts.

Thomas, L., Venables, F. H., and Williams, K. M., 1965, Planet. Space
    Sci., 13, 807.

Tsuruta, S., and Cameron, A. G. W., 1966a, Canad. J. Phys., 44, 1863.

Tsuruta, S., and Cameron, A. G. W., 1966b, Canad. J. Phys., 44, 1895.

Tucker, W., 1967a, Astrophys. J., 148, 745.

Tucker, W., 1967b, Astrophys. J., 149, L105.

Tucker, W. H., and Gould, R. J., 1966, Astrophys. J., 144, 244.

Underwood, J. H., 1968, Science, 159, 383.

Underwood, J. H., and Muney, W. S., 1967, Solar Phys., 1, 129.

U. S. Standard Atmosphere, 1962, U. S. Government Printing Office,
    Washington, D. C.

Van Allen, J. A., 1967, J. Geophys. Res., 72, 5903.

Van Allen, J. A., Frank, L. A., Maehlum, B., and Acton, L. W., 1965,
    J. Geophys. Res., 70, 1639.

Verma, S. D., 1968, Astrophys. J., 152, 537.

Victoreen, J. A., 1949, J. Appl. Phys., 20, 1141.

Wallerstein, G., 1961, Pub. Astron. Soc. of the Pacific, 74, 153.

Wallerstein, G., 1968, Astrophys. J., 151, L121.

White, M. L., 1965, 'Handbook of Geophysics and Space Environments',
    p 18.1, Ed S. Valley, McGraw-Hill, New York.

White, W. A., 1964, Space Research, 4, 771.

Wilkinson, D. H., 1950, 'Ionization Chambers and Counters', Cambridge
    University Press, London.

Williams, A., and Sara, R. I., 1962, Internat. J. Appl. Radiation and
    Isotopes, 13, 229.

Wolf, R. A., 1966, Astrophys. J., 145, 834.

Zhitnik, I. A., Krutov, V. V., Maljavkin, L. P., Mandelstam, S. L.,
    and Cheremukhin, G. S., 1967, in Space Research VII, North-Holland,
    Amsterdam, p1263.